INFORMATION TO USERS

This manuscript has been reproduced from the microfilm master. UMI films the text directly from the original or copy submitted. Thus, some thesis and dissertation copies are in typewriter face, while others may be from any type of computer printer.

The quality of this reproduction is dependent upon the quality of the copy submitted. Broken or indistinct print, colored or poor quality illustrations and photographs, print bleedthrough, substandard margins, and improper alignment can adversely affect reproduction.

In the unlikely event that the author did not send UMI a complete manuscript and there are missing pages, these will be noted. Also, if unauthorized copyright material had to be removed, a note will indicate the deletion.

Oversize materials (e.g., maps, drawings, charts) are reproduced by sectioning the original, beginning at the upper left-hand corner and continuing from left to right in equal sections with small overlaps. Each original is also photographed in one exposure and is included in reduced form at the back of the book.

Photographs included in the original manuscript have been reproduced xerographically in this copy. Higher quality 6" x 9" black and white photographic prints are available for any photographs or illustrations appearing in this copy for an additional charge. Contact UMI directly to order.

Order Number 9211590

The directional solidification of salt water

Wettlaufer, John Scott, Ph.D.

University of Washington, 1991

The Directional Solidification of Salt Water

by

John S. Wettlaufer

A dissertation submitted in partial fulfillment
of the requirements for the degree of

Doctor of Philosophy

University of Washington

1991

Approved by _____
(Chairperson of Supervisory Committee)

Program Authorized   Geophysics
to Offer Degree_____

Date_____23 August, 1991_____

Doctoral Dissertation

Signature

Date   23 August, 1991

University of Washington

Abstract

The Directional Solidification of Salt Water

by

John S. Wettlaufer

Chairperson of the Supervisory Committee: Professor Norbert Untersteiner
Geophysics Program

A sodium chloride solution is used as a model for the natural solidification of seawater.
A linear perturbation theory is used to show that the one-dimensional steady state describing
the unidirectional solidification of a dilute H_2O-NaCl solution is morphologically unstable.
This instability breaks the translational symmetry of the steady state, resulting in the transi-
tion from a planar to a cellular solid-liquid interface. The cellular interface represents a state
with a different translational symmetry; parallel arrays of ice platelets. Consistent with other
studies, for fixed far-field solute concentration C_∞, it is found that there is a range of
solidification velocity $V_c < V < V_a$ for which the system is linearly unstable to a range pertur-
bations. Naturally occuring sea ice grows at rates between theses limits, so it will always
have a cellular solid-liquid interface. The system exhibits weak wavelength selection near
critical, that is, the wavelength of the instability is only weakly dependent on V near V_c, At
low values of the segregation coefficient k, the predicted value of V_c is so small that it invali-
dates a continuum theory. At higher values of k the theory predicts realistic values of V_c.

A weakly non-linear Landau analysis reveals that, during natural solidification, the tran-
sition to a cellular interface occurs via a subcritical bifurcation. That is, there is a 'jump'
transition to cells for V close to V_c. A physical explanation is offered to explain the suppres-
sion of subcritical bifurcations that occurs when the temperature gradient in the solid
increases for a fixed mean velocity.

For restricted ranges of the control parameters, we investigate the asymptotic behavior
of the solidification equations. In three cases we derive scaling laws that relate the

wavelength to the mean growth velocity of the interface: In the long wavelength limit (a) for V close to V_c (b) for V close to V_a, and in the short wavelength limit for velocities between V_c and V_a.

The linear theory provides a characteristic equation relating the disturbance growth rate to wavelength, mean growth velocity and other control variables. An equivalence transformation of the characteristic equation reveals several new aspects of the linear theory: (a) The characteristic equation can be viewed as a one-parameter unfolding f of a cuspoid normal form $N = x^m$ where $m = 3$. (b) The bifurcation problem for f defines a trajectory on a cusp surface which is defined by the bifurcation problem of a two-parameter unfolding f_2 of N. (c) The values V_c and V_a parametrize degenerate singular points. (d) Relative to the standard neutral curves, wavelength selection is enhanced in the neutral curves of the system, and there is a particular curve for which this behavior is most pronounced. (e) The bifurcation set, or locus of singular points, of $f_2 = 0$, demarcates stability regions solely in terms of observables. (f) A neutral curve will be open or closed depending on how the solution trajectory determined from $f = 0$ crosses the bifurcation set. (g) It is observed that the origin of weak wavelength selection is related to a high order degeneracy in the vicinity of the bifurcation point associated with V_c.

For parameters relevant to natural solidification, the fluid layer adjacent to the solid-liquid interface is found to be hydrodynamically unstable for mean growth velocities between V_c and $V \approx 10^{-4}$ cm s^{-1}.

The main results point to the need for careful experiments on this system. It is recommended that the critical point of instability be investigated for temperature gradients one or two orders of magnitude greater than, and solute concentrations one or two orders of magnitude less than, the geophysical values. Interferometry can be used to detail the solute field adjacent to the interface and to assess the role of convection.

TABLE OF CONTENTS

LIST OF FIGURES

ACKNOWLEDGEMENTS

CHAPTER 1

INTRODUCTION

1.1 *Cellular Substructure and the Natural Ice Cover*

Naturally occurring sea ice has a lamellar/cellular solid - liquid interface (Weeks, 1958). Mature Arctic sea ice has a substructure consisting of horizontal c-axes, with pure ice platelets extending into the water, separated by regions of highly concentrated seawater (Figure 1.1). As the ice sheet grows downward, the substructure is embedded in the material. Therefore, at every level sea ice is a mixture of pure ice and concentrated seawater (Figure 1.1). We are interested in the physics responsible for the appearance of this substructure. In particular, we wish to determine the range of conditions that determine the existence of substructure.

A review of the growth and structure of naturally occurring sea ice can be found in Weeks and Ackley (1986), but a brief review is also in order here. During winter cracks in the perrenial sea ice cover expose the ocean ($T \approx 271.16$ K) to a relatively cold ($T \approx 243$ K) atmosphere. A surface skim of the ocean is slightly undercooled so that the abundance of ice crystals (supplied by the local snowcover) that enter the layer grow by dissipation of latent heat into the surrounding fluid. The crystals are initially small spheres that quickly form discs with the crystallographic c-axis and perpendicular to the ocean surface (Figure 1.2). The crystals grow more rapidly in the direction perpendicular to the c-axis; parallel to the ocean surface. Therefore, since the crystals float at various angles from vertical, some will grow into the fluid more rapidly than others. In the absence of mechanical agitation, a

transition from vertical to horizontal c-axis orientation is observed within the top few centimeters of the ice cover (Figure 1.1b). Ice growth then proceeds by molecular attachment to the existing ice. The underside of perrenial sea ice is always characterized by horizontal c-axes. Initially, a small region the size of an individual grain has a macroscopically smooth interface, but a cellular interface forms as freezing progresses. This type of interface morphology is the focus of the present study.

During the directional solidification of seawater, salt and other impurities are rejected by the solid and build up in front of the advancing interface. This results in the coexistence of solute C, and thermal T_L, diffusion fields in the melt; C decays and T_L increases with distance from the interface. The dynamics of a macroscopically planar interface depends on these fields, the thermal field in the solid (T_S), microscopic effects at the interface, and under certain conditions the momentum field in the melt. We do not treat the momentum field explicitly, but it's qualitative effects are discussed later. The diffusion fields are sketched in Figure 1.3, a schematic of the system under study. A planar ice - saltwater interface described solely in terms of these diffusion fields is subject to shape instabilities giving rise to a regular spatial pattern along the phase boundary (Figure 1.1c). The structure of the interface is determined by surface tension and thermal gradients which tend to flatten out solid protuberences. The solute field, which by depressing the freezing point, creates a local undercooling in the liquid, is responsible for enhancing the growth of solid protuberences (Mullins and Sekerka 1963, Langer 1980, Coriell et al., 1985, Langer 1987). The shape instabilities resulting from these competing effects are generally referred to as *morphological instabilities*. The bulk of this work focuses on explaining the presence of cellular substructure resulting from the interaction of surface tension with the diffusion fields (C, T_L, T_S).

In laboratory experiments a variety of platelet orientations have been observed (Harrison and Tiller, 1963). Experiments reveal (Weeks and Lofgren, 1967; Lofgren and Weeks, 1969) that, as the growth rate increases, the cell spacing decreases, thereby increasing the solute per unit volume. The two phase structure observed in the growing solid influences the bulk mechanical (Weeks, 1962) and thermophysical (Schwerdtfeger, 1963) properties of sea ice in much the same way as in binary alloys. This influence depends on the amount of solute per unit volume as well as its distribution within the ice lattice. Malmgren (1927) was the first to consider the effects of seawater on the thermophysical properties of sea ice. As the ice grows, the planar interface breaks down, and cellular substructure appears. As a result, small cells of seawater are trapped within the lattice at the ice-water interface and act to retard changes in the temperature of the material. For example, when the temperature decreases, the fractional salt content of the seawater within the cells increases, since the fresh water in the cells must solidify to maintain phase equilibrium (see Fig. 1.4). When the fresh water in the cell freezes, the release of latent heat warms the ice surrounding the it. Thus, compared to fresh ice, in the bulk, it takes more energy to cool and warm sea ice. Because of this process, the thermal conductivity and heat capacity of sea ice depend sensitively on the solute concentration and temperature. For temperatures close to the bulk freezing point of seawater, the heat capacity can increase two orders of magnitude when the solute concentration increases one order of magnitude (Schwerdtfeger, 1963).

In studies of the dependence of the platelet spacing on growth parameters, the only approach has been to assume that the stable interfacial growth form is cellular (Weeks and Lofgren, 1967 and Lofgren and Weeks, 1969). Qualitatively, this approach is useful in the study of the transition from cells to dendrites, (Karma and Pelce', 1990) or for long time

simulations of bulk properties in growth from an impure melt (Huppert, 1990), but will not be helpful in uncovering the essential mechanisms responsible for the initial appearance of substructure.

1.2 *Crystal Growth Regimes*

The formation of cellular substructure is one of the pattern formation problems in crystal growth. The spontaneous formation of patterns from a disordered environment is an example of self-organization. It is observed in a variety of physical and biological systems and yet is still not well understood (Langer 1987, Nicolis and Prigogine 1977,1989). The process of crystal growth is an inherently non-equilibrium phenomenon, since a gradient in one of the thermodynamic variables (e.g., chemical potential) is necessary to drive molecules toward the solid - liquid or solid - vapor interface. The stable phase will grow at the expense of the metastable phase at a rate that depends on the magnitude of the gradient(s). For the case where a crystal starts with its equilibrium shape, and then a growth drive is imposed, Elbaum and Wettlaufer (1991) define three growth regimes: 1) "thermodynamically slow", in which the equilibrium shape would be maintained, 2) "reversibly slow", where details of the shape may change, but the system will still relax to the equilibrium shape on an experimentally observable time scale if the growth drive is removed, and 3) a "kinetically dominated" regime, such as dendritic growth, where the shape no longer relates to the minimization of the total surface free energy. It is the third regime that is treated here. In this regime the advance of the phase boundary is limited by the diffusion of nutrient molecules and the efficiency with which the latent heat of fusion and/or chemical impurities are removed. The molecular scale forces have an influence on the interfacial dynamics which is parameterized

through anisotropic surface tension and growth kinetics. A conclusion of the study of Elbaum and Wettlaufer (1991) is that the hexagonal symmetry of a snowflake has a microscopic origin in the lattice of the seed crystal that emerges from the reversibly slow regime. In the case of crystal growth in the kinetically dominated regime, the interplay between microscopic interfacial kinetics and externally imposed macroscopic forces determines the growth shape. The relationship between micro-and macroscopic processes which underlies this class of problems is not clear. Progress has been made in understanding the microscopic behavior of equilibrium transitions (see e.g., Haymet 1987a,b and Oxtoby 1990) and macroscopic pattern formation in non-equilibrium transitions (see e.g., Langer 1980 and Ben-Jacob and Garik 1990). The work presented here draws from this latter pool of knowledge, but to elucidate the nature of the scale interaction mentioned above, their results are discussed briefly below.

1.2.1 Thermodynamically Slow

Equilibrium crystallization and spontaneous magnetization are characterized by the breaking of a spatial symmetry (Landau and Lifshitz, 1969). When a volume of liquid freezes, the isotropic distribution of molecules or atoms is replaced by the anisotropic structure of a crystal in which not all positions in space are equally accessible to a particle. Interfacial 'dynamics' are dominated by atomic and molecular interactions, and close to the transition point they coordinate over a long range to modify the liquid structure. This has been shown theoretically, experimentally, and with molecular dynamics simulations (Oxtoby 1990). Equilibrium or near-equilibrium crystallization is a first-order transition, that is, the thermodynamic variables (e.g., chemical potential, volume) undergo a discontinuous change at the transition point. Equilibrium crystallization is viewed as a 'non-universal' phenomenon

(Oxtoby 1990) since all diagnostics; the freezing temperature, changes in the state variables

and the symmetry properties of the stable lattice depend on the nature of the intermolecular

forces. This is the most acute difficulty in the microscopic investigations since, in some

instances (e.g., atomic metals), there are several crystal structures (face- and body-centered

cubic, and hexagonal close-packed) with similar free energies. Therefore, predictions of the

stable crystalline structure depend sensitively on the interaction potential chosen. The essen-

tial mechanisms of crystal growth and the structure of equilibrium crystal surfaces were

described by Burton et al., (1950), and their work serves as the paradigm in this field.

1.2.2 Kinetically Dominated

Progress in the study of systems driven far from equilibrium has come from variety of

fields. The focus has been on the formulation of theories, and the performance of experi-

ments that investigate the stability of the crystallization front in a non-equilibrium situation.

Most of the progress (theoretical and experimental) in this problem has come from materials

scientists investigating phase boundary processes in binary alloys (Mullins and Sekerka

1963,1964 and Coriell et al., 1985). The ideas that have evolved are of use to surface physi-

cists growing thin films of material from the vapor phase as well as to those investigators

interested in understanding natural solidification phenomena (Huppert, 1990 and references

within). The coupling of large and small scales is accomplished by assuming that both

phases are a continuum, and by parameterizing the microscopic interactions through the boun-

dary conditions at the interface. In order to keep track of a free, moving phase-boundary one

must solve thermal and chemical (for binary melts) diffusion equations. There is a similarity

between the type of stability analysis that is necessary here and that which is used in the free

boundary problems of hydrodynamics. The key difference is that non-linearities enter the formalism through the boundary conditions rather than through the equations of motion themselves.

In recent years effort has gone into uncovering the physics responsible for the growth selection mechanism that nature employs in the creation of snowflakes. In the *kinetically dominated regime*, the mechanism of pattern formation is that of a morphological instability wherein the surface tension competes with the diffusion field to determine the shape. The deterministic approach (e.g., Langer 1980,1986) has been successful in producing patterns which qualitatively mimic real snowflakes (six crystal arms with symmetric sidebranching). While the overall features have been captured, the observed aperiodicity of the snowflake sidebranches (Dougherty et al., 1987) is not reproduced by the deterministic models even when anisotropy is included (Langer, 1986 and Sawada, 1986). In order to account for sidebranch aperiodicity, an approach based on the physics of random systems has been adapted for the snowflake class of problems (Nittmann and Stanley, 1986,1987ab). Here, I speak of a class of problems because some of the patterns observed in crystal growth resemble the those observed in viscous fingering experiments (Couder et al., 1986). The work of Nittmann and Stanley (see in particular Nittmann and Stanley 1987b) is strikingly successful at qualitatively and quantitatively reproducing features of real snowflakes, yet the mechanisms relating random molecular attachments to the growth selection process have not been clarified. In their diffusion-limited-aggregation models, there exists mass 'screening' of interfacial minima by maxima so that the minima eventually become the liquid or vapor 'fjords' in the crystalline structure. Similar work (Saito and Ueta 1989) simulates growth shapes with a lattice gas model that reproduces diffusive instabilities. Recently, it has been claimed that energy or

entropy calculations of crystal forms will not indicate the morphology assumed by a growing crystal. Rather, the form selected for a particular thermodynamic gradient is the one which will, during formation, release entropy at the highest rate, not that which is energetically the most stable (Hill 1990).

1.3 *Constitutional Undercooling*

Rutter and Chalmers (1953) first discussed constitutional undercooling in relation to phase boundary instability in unidirectional solidification of dilute tin alloys. They observed substructure at the solid-liquid interface (these had also been observed by Buerger [1934]) and offered an explanation in terms of the impurities in the system. They proposed that the impurities which could not incorporate themselves into the lattice as the solid grew, would build up ahead of the advancing interface. Since the equilibrium freezing temperature in the liquid depends on the impurity or solute concentration, the possibility exists that the freezing temperature ahead of the interface will be above the actual temperature. They postulated that if the impurities induced this local undercooling, any perturbation of the interface would tend to grow spontaneously. This was the first attempt at explaining the observations of interfacial substructure.

A more quantitative explanation of constitutional undercooling was offered by Tiller, et al., (1953). They argued that in order for constitutional undercooling to exist, the actual temperature gradient in the liquid just ahead of the interface G, must be less than the gradient of the equilibrium temperature, giving the first criterion for instability of such an interface. Generally, the equilibrium freezing point of a binary liquid is a linear function of its impurity content (Figure 1.5). The freezing point, T_f, of a binary solution with solute concentration C

(in parts per thousand (ppt)) can be approximated as

$$T_f = m\, C, \tag{1.1}$$

where m is the the slope of the solid-liquid coexistence line and has units K ppt^{-1} (see Figure 1.4). In the case where the solution is seawater, $m = -0.0548$ K ppt^{-1} (Fujino et al., 1974). Note that equation (1.1) is only relevant for a flat boundary between the solid and the liquid. If we define the solute gradient in the liquid adjacent to the interface as G_c then equation (1.1) gives

$$m\, G_c = m\, \frac{dC}{dz} = \frac{dT_f}{dz}. \tag{1.2}$$

Therefore, according to Tiller et al., (1953), in order for constitutional undercooling to exist the condition

$$\frac{G}{m\, G_c} < 1 \tag{1.3}$$

must be satisfied. This is shown schematically in Figure 1.5.

Rutter and Chalmers (1953) discovered that they could suppress the substructure by reducing the growth velocity and increasing the temperature gradient. The layer of high solute concentration adjacent to the interface falls off exponentially as

$$C \propto \exp\left[\frac{-V\, z}{D}\right] \tag{1.4}$$

where V is the growth velocity, and D is the impurity diffusion coefficient in the liquid. This allows one to write the constitutional undercooling criterion (Eq. 1.3) as a function of growth velocity (Tiller and Rutter, 1956)

$$G < \Theta\, V, \tag{1.5}$$

where $\Theta = \Theta\,(D,C,\text{thermophysical parameters})$. Therefore, for small growth velocities the condition for constitutional undercooling is relaxed, that is, close to the interface, the gradient

of the freezing point approaches the actual temperature gradient G. This is consistent with their observation that the substructure is depressed at small V.

For a given ratio of G/V the impurity concentration determines whether there will be constitutional undercooling. Tiller and Rutter (1956) rapidly separated the solid from the liquid during solidification and inspected the interface for substructure. They did this for a variety of materials, and by varying the parameters in Eq. (1.5) they separated substructure regimes graphically. This technique provides a plot of the ratio G/V versus the solute concentration in the melt which demarcates the conditions for planar and nonplanar interfaces. Precise determination of interface instability was well beyond the capacity of these experiments. The thermophysical parameters were not well known and the visual method of determining the presence of substructure was hardly precise.

The constitutional undercooling criterion has proved to be an excellent way to investigate a variety of systems. However, since it does not include the effect of surface tension, it gives little information as to exactly under what conditions a planar interface becomes unstable, and what the pattern and scale of the substructure will be. The criterion tells one the thermodynamic conditions of the liquid which may result in an unstable phase boundary; it tells one nothing about the heat transfer in the solid, or the effects of latent heat release and interfacial attachment kinetics. In short, constitutional undercooling is a necessary condition for interfacial instability, but it is not a sufficient one. We will see how this condition arises out of the formalism in the next chapter. An interface stability criterion based on the dynamics of the entire system and not simply the conditions of the liquid phase is necessary to extract this information. Theories with some of these ingredients appear to have been developed independently by four researchers; Wagner (1956) who was interested in the oxi-

dation of alloys of noble metals, and Mullins and Sekerka (1963) and Voronkov (1965), who were interested in the growth of crystals.

1.4 *Directional Solidification and the Planar Interface*

The directional solidification system (Wollkind and Segal, 1970) is used in a variety of approximate forms to examine the unidirectional solidification of dilute binary alloys. We adopt the same basic approach to investigate the solidfication of a sodium-chloride solution. The alloy is pulled with a constant speed V through an imposed thermal field and a mean position is established at which the planar solid - liquid interface is located. A planar phase boundary will be stable if the influence of the thermal fields and surface tension overcome the destabilizing effect of solute rejection at the interface (Langer, 1980 and Mullins and Sekerka, 1964). The thermal fields act to melt back the solid bulges (which encounter higher temperatures) and freeze back the depressions (which encounter lower temperatures, see Figure 1.3). The surface tension, acts to melt back a solid bulge by a local depression of the melting point. The solute field is compressed in the vicinity of a bulge, providing a steeper gradient there (Fig. 1.3). The interface can advance more easily behind a steeper solute gradient, which enhances the constitutional undercooling (Figure 1.5). Therefore, the solute field drives the instability. These mechanisms result in shape instabilities that break the translational symmetry of a planar ice - saltwater interface giving rise to a regular spatial pattern along the phase boundary (Figure 1.1c).

The planar state can be maintained for growth velocities V less than a critical velocity V_c or above an absolute velocity V_a. For $V_c < V < V_a$, a particular system will favor a phase boundary with nonzero curvature. The physics of this process is generic, in that any

planar interface separating a solid from its binary liquid during solidification will become unstable for growth velocities above the threshold, V_c, where the solute diffusion process is too slow to remove local solutal undercooling. At the upper limit, V_a, the stabilizing effect of surface tension becomes greater than the destabilizing effect of solutal undercooling. The analysis of Mullins and Sekerka (1964) identified these limits for the case in which an alloy is solidifying in a constant temperature gradient. Langer (1980) describes this type of instability in terms of the competition between kinetic and surface tension effects: In a typical range of growth conditions diffusion kinetics are more efficient when the solid phase can increase its surface area. This configuration favors a more complicated interfacial structure.

1.5 Outline of Theoretical Procedure

The solidification of seawater is approximated as that of a dilute H_2O - NaCl solution. The stability of the system is examined by perturbing the interface about a basic or stationary state, with an infinitesimal disturbance of the form $\exp(\sigma t + i\, a\, x)$, where σ is the complex growth rate, and a is a spatial wavenumber in the direction x, along the planar interface, and perpendicular to the mean growth direction. A linear stability analysis of the equations of motion for the fields C, T_L and T_S represented in Figure 1.3 is performed. The evolution of the fields is represented by a thermally nonsymmetric (thermal conductivities of both phases are allowed to differ), infinite one sided (solute diffusion in the solid is negligible) model. The effect of the latent heat liberated at the interface is accounted for and advective/convective transport of heat or solute is proscribed. Thermally symmetric, zero latent heat models (e.g., Langer, 1980 or Sivishinsky, 1983) do not allow the possibility of disturbances of the interface inducing disturbances in the thermal fields since the temperature

gradient across the entire solid-liquid system is constant and fixed.

The linear stability analysis results in in an eigenvalue problem for σ. This yields a characteristec equation $F[\sigma, a, M \; (V, C_\infty), \Gamma \; (V, C_\infty),$ thermophysical constants$]$ that is an implicit function of σ. The control parameters M and Γ (described below) are functions of the interface velocity V and far-field solute concentration C_∞. The demarcation between stability and instability is obtained by setting $\sigma = 0$, giving a neutral characteristic equation, $g(a, M, \Gamma,$ thermophysical constants$) = F(\sigma = 0, \cdot, \cdot, \cdot, \cdot)$. The analysis of g, leads to two neutral curves that are of particular interest, $V \; (C_\infty)$ and $V \; (a)$. The former curve is useful in laboratory studies, but the latter curve is of more interest in the examination of naturally solidifying seawater.

A subcritical instability refers to the case in which the infinitesimal disturbance undergoes a jump transition to a finite-amplitude state as $V \to V_c^-$. A supercritical instability refers to the case in which there will be a slow evolution of infinitesimal disturbances along the interface as $V \to V_c^-$ (Wollkind and Segal, 1970, Merchant and Davis 1989a,b). Merchant and Davis (1989a) examined the importance of latent heat in determining the nature (subcritical or supercritical) of the bifurcations by using the results of the weakly nonlinear analysis of Alexander et al., (1986). They showed that when latent heat is included in the nearly thermally symmetric SCN-acetone system (where SCN is succinonitrile), the region of supercritical bifurcation is extended into experimentally accessible parameter ranges. With the same approach we find that the entire range of H_2O - NaCl system is a region of subcritical bifurcation, but this range is reduced as the ratio of thermal conductivities of the two phases approaches unity.

The absence of horizontal boundary conditions results in normal modes that depend continuously on wavenumber. Constraining the horizontal dimension will result in a discretized spectrum in which several modes must be considered (Bennett and Brown, 1989). The system width can be used as an additional control parameter, effectively increasing the dimensionality of the problem. The width is not a variable in the natural solidification problem.

1.6 Scalings

The length and time scales are based on the solute diffusion scales D/V and D/V^2, respectively, where D is the solute diffusivity in the liquid. The advantage of this scaling is that standard dimensionless control parameters M, the morphological number, which is a measure of the degree of constitutional undercooling, and Γ, the surface energy parameter, will result when the thermal and solute field scales are correctly chosen. A disadvantage of this choice of scales is that both control parameters depend on the planar growth velocity V, and the far field solute concentration C_∞. The former dependence is relevant to the common observation of weak wavelength selection near the critical point of instability (Bennett and Brown, 1989). By weak wavelength selection for a system we mean that V_c, for the onset of morphological instability depends weakly on the critical wavelength. This is one of the difficulties in comparing the standard theory (Mullins and Sekerka, 1964) with experiment.

Merchant and Davis (1989b) chose scales that isolate the V and C_∞ dependence of the system's dimensionless numbers. They also predict weak wavelength selection near critical. Their goal in this choice of scales was to isolate control parameters that more closely reflect the link to the experimental process. Their control parameters were obtained by choosing different length and time scales. These scales are velocity independent under the assumption

that the liquid temperature gradient is linear near the interface. One result of this approach is that the nondimensional wavenumber a, is independent of planar interfacial growth velocity. As they have pointed out, this scaling may be invalid at high velocities where the curvature in the temperature field is not negligible. We show this to be the case for the seawater system, rendering this approach invalid close to absolute stability.

1.7 Relation of Linear Theory to Normal Forms

The mathematical features of the instabilities that arise in the planar solidification problem can be described using the techniques of catastrophe, singularity and bifurcation theories (e.g., Poston and Stewart, 1978 and Golubitsky and Schaeffer, 1985). With the help of these techniques the topological structure of the solutions of the problem is examined. The V (a) neutral plane is most relevant to the task at hand. With a simple coordinate transformation that removes the explicit dependence on thermophysical parameters, g (section 1.5) becomes a more useful function of control parameters $f(x,\alpha,\beta)$. We view f as a one-parameter unfolding of a cuspoid normal form $N = x^m$ (m = 3). The trajectories of f are subsets of the complete *neutral solution surface* determined by solving $f_2 = 0$, where f_2 is a two-parameter unfolding of N. The manner in which a trajectory intersects the *bifurcation set* of f_2, determines the structure of a neutral curve. The parameters α and β are more sensitive functions of the planar interfacial growth velocity than are M and Γ. This behavior, in combination with the geometry of the solution sets of f and f_2, enhances wavelength selection in the theoretical framework, extending the utility of this type of a linear analysis.

1.8 Related Phenomenon and Approaches

Theoretical treatments of the dynamics of interfacial motion have proceeded along two paths. One is that which is taken in this work, and the other treats the free energy of a nonuniform system (Cahn and Hilliard (1958)) in a diffusive process. For systems with isotropic surface tension and a nonconserved order parameter, such as density or solute concentration, a standard procedure (reviews are Hohenberg and Halperin 1977, and Gunton et al., 1983) models interfacial motion with a diffusion type equation (Ginzburg-Landau or Langevin equation) for the order parameter. The equation treats the dependence of the free energy on the order parameter in the vicinity of an interface with a specified geometry. Numerical simulation (Kessler et al., 1990) of this type of an equation has revealed interesting dynamics on isolated surfaces.

The same type of analysis has been brought to bear in the study of hydrodynamic fluctuations. A classic example is the Rayleigh-Benard system (Chandrasekhar, 1961) in which a horizontal layer of fluid is heated uniformly from below. At a critical value of the temperature gradient, cellular convective patterns immerge. Swift and Hohenberg (1977) find a second-order type of transition using the Ginzburg-Landau approach. The immerging asymmetric states have correlations that are macroscopic in range. In the body of this paper we will discuss the similarity between the breaking of the symmetry of spatial translations in the hydrodynamic Rayleigh-Benard instability and the instability of a planar solidification front.

Once the interface has broken down a new stable growth form may be maintained for a wide range of parameters. For some materials the new growth form will be cellular with the possibility of secondary and tertiary instabilities creating a dendritic structure (see e.g., Karma and Pelce' 1990 and Warren and Langer 1991).

For rapidly solidifying binary solutions a two phase region of cellular/dendritic solid with concentrated melt in the interstitial region can grow to a substantial thickness and necessitate consideration of fluid flow (Huppert 1990 and references within). The work of Huppert and his colleagues has been responsible for solving a number of important problems in geophysical and geological crystallization in which fluid flow occurs on many spatial scales. They have been successful in obtaining similarity solutions to the relevant thermal and concentration equations with a moving boundary and a finite two phase or "mushy" zone separating the bulk solid from the bulk melt.

These approaches as well as those which consider the details of interfacial kinetics for large and small growth rates can be brought to bear on problems related to H_2O-NaCl systems, and the natural solidification of seawater, and are the subjects of future work. In addition, the local interaction between hydrodynamic and morphological instabilities recently reviewed by Davis (1990) has particular relevance to these systems growing downward into their melts.

1.9 *Summary of Work*

In the next chapter the problem is formulated. The neutral curves $V(C_\infty)$ and $V(a)$ that result when evaluating the neutral dispersion function g, are presented in chapter 3. These curves demarcate the parameter ranges in which the interface is stable from those in which it is unstable, when the only parameters varied are V and C_∞ and V and a respectively. We also present the results of a Landau type weakly non-linear analysis in the third chapter. Chapter 4 is a brief comparison with the linear analysis based on velocity independent length and time scales. In chapter 5 we examine the *neutral solution surface* determined from $f_2 = 0$, and a trajectory of f. The topological origin of weak wavelength selection in

the linear theory is shown in this chapter. We show the strengthening of wavelength selection which results from this transformation, and the condition which dictates the closedness of the neutral curve. The results apply to any binary alloy for which this formulation of the solidification system is valid. In chapter 6 we discuss hydrodynamic effects during solidification, and theories for the relation between interfacial attachment kinetics and solute segregation. Finally, we discuss a method for studying bulk solute trapping during rapid solidification of seawater. Chapter 7 is a summary of the work presented here and a discussion of related problems and future work.
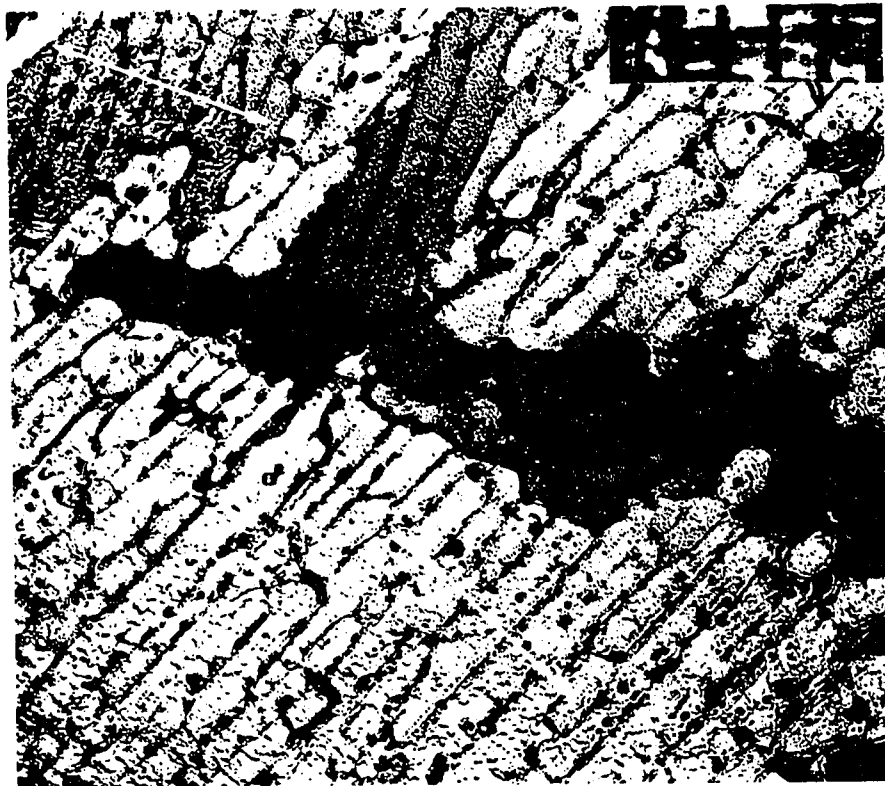
Fig. 1.1a Horizontal thin section of Arctic sea ice exhibiting substructure consisting of pure ice platelets regularly spaced within single crystal grains. The crystallographic c-axis (see arrow) is in the plane of the section and oriented perpendicular to the platelet structure of individual crystals. Bulk seawater is trapped between the platelets. The scale in the upper right hand corner is in mm. (Adapted from Gow et al., 1987).
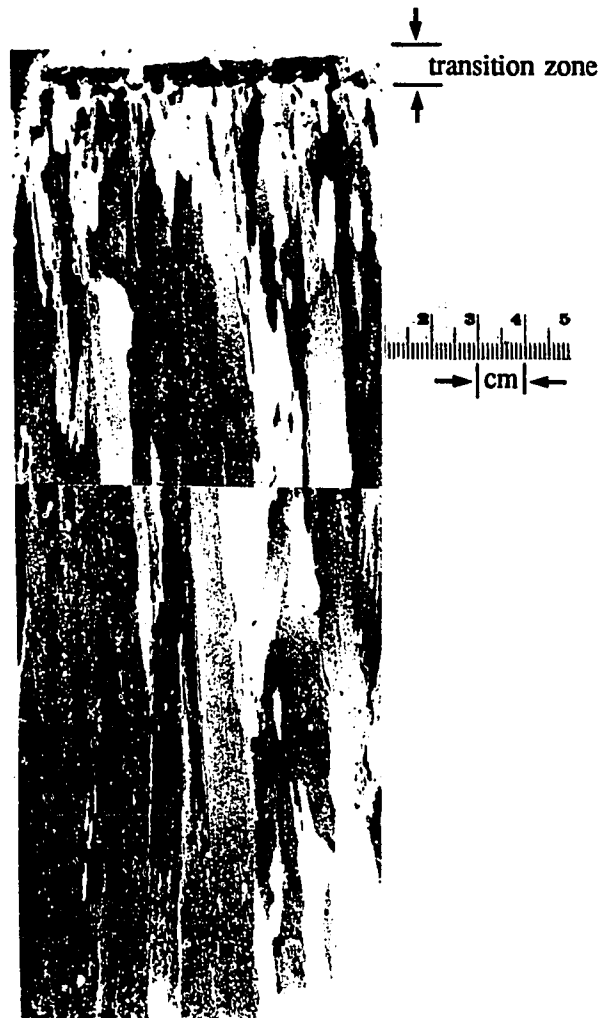
Fig. 1.1b Vertical thin section, showing the transition from vertical to horizontal c-axis orientation in the upper 2 cm of the ice sheet, and the columnar structure in the remainder of the section. As the ice sheet thickens, the growth velocity decreases. Note the uniformity of the structure and the increase in crystal grain size moving down into the ice sheet. The smallest scale subdivisions are in mm, and the entire section is about 20 cm thick. (Adapted from Gow et al., 1987).
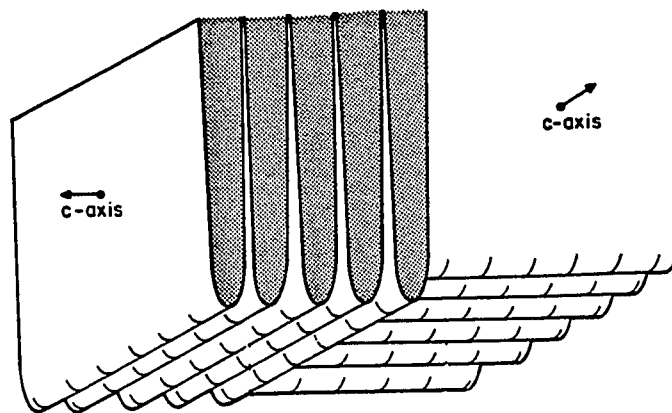
Fig. 1.1c Schematic of the cellular substructure (from Weeks and Ackley 1986)
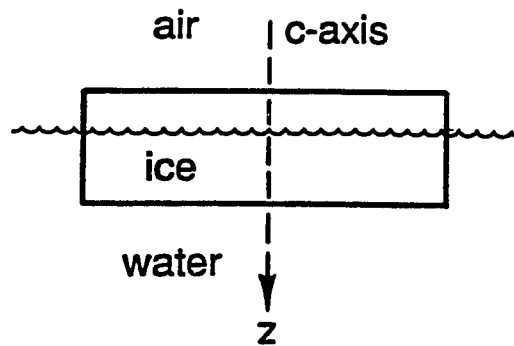
Fig. 1.2 Schematic of a single ice disc on the surface of the ocean. This is the observed growth form after nucleation in which the c-axis is vertical. The fast growth direction is perpendicular to the c-axis, so those crystals with c-axes oriented with a slight angle from vertical have a growth advantage. In the absence of mechanical agitation, the transition from vertical to horizontal c-axis orientation occurs early in the creation of the ice sheet (see Fig 1.1b).
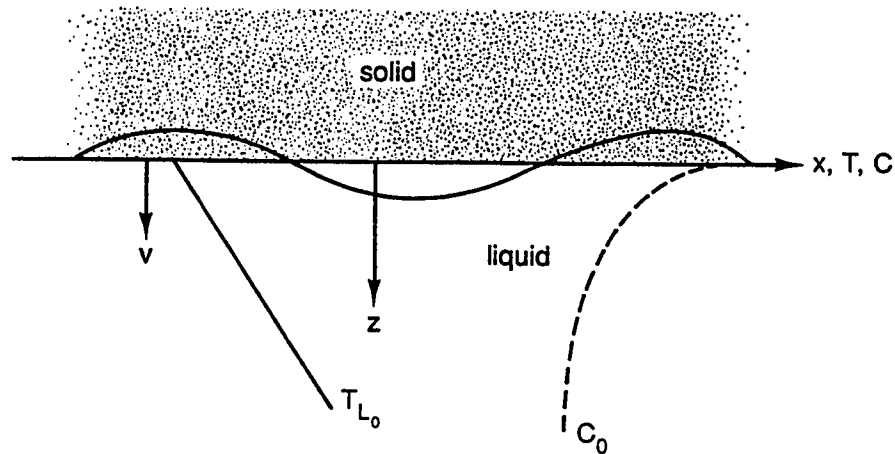
Fig. 1.3 Schematic of the solidification system in which the phase boundary is moving downward into the liquid. The steady state temperature T and concentration C fields are represented and there are no horizontal boundaries.
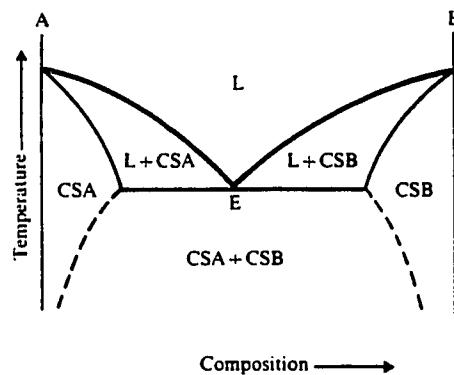
Fig.1.4 A typical equilibrium binary phase diagram for a two component system A and B. The heavy solid line is the liquidus, the light solid line is the solidus and the dashed line separates purely solid phases. L is the liquid, and CS denotes crystalline solid. For example, in regions denoted CSA the crystal is dominated by molecules of A. Molecules of B are not favored in the crystal because of steric and energetic considerations. For this study consider A to be H_2O and B to be NaCl. Therefore, the system is operating in the region where the liquidus and solidus approach each other. (Adapted from Worster, 1986).
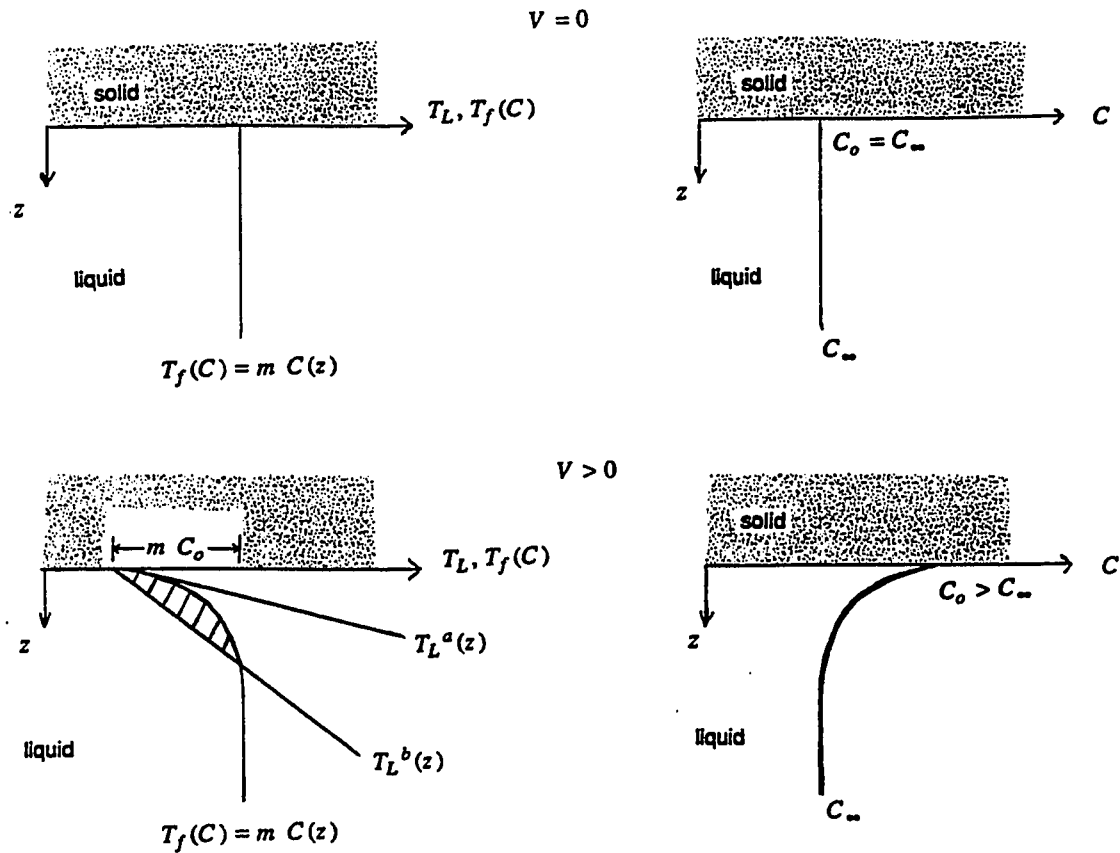
Fig.1.5 A schematic of constitutional undercooling. For $V = 0$ (top), the solute concentration in the water C is uniform, plotted on the right. The equilibrium temperature $T_f(C)$, being pinned to the solute concentration, is uniform, plotted on the left. There is no externally imposed temperature gradient, $T_L(z) = 0$. For $V > 0$ (bottom), we consider two cases. Since NaCl has a very low solubility in ice, it is rejected by the ice causing a local increase in the solute concentration adjacent to the interface. The external temperature gradient represented by $T_L{}^a(z)$ is greater than the gradient of equilibrium temperature, so a solid disturbance will melt back. The external temperature gradient represented by $T_L{}^b(z)$ is less than the gradient of equilibrium temperature, so there exists a region of water (hatched) that is undercooled, and therefore metastable. In this situation, a solid disturbance will grow. (See equation 1.3).

CHAPTER 2

FORMULATION

2.1 *The Dimensional Solidification Equations*

The approach used here is to specify the thermodynamic situation that gives rise to solidification, and to describe the conditions under which an imposed perturbation grows or decays. The system (Mullins and Sekerka 1964, Wollkind and Segal 1970) is a continuum description of heat and mass transfer, so the basic ingredients are the diffusion fields through both phases. The momentum field is not considered.

We are considering a disturbance of the planar interface $z' = h'(x',t')$, where all primed quantities are dimensional. One might also consider perturbing one of the diffusion fields. The reference frame is attached to the mean position of the planar interface at $z' = h'(x',t') = 0$ moving at a constant speed V into the liquid, at time $t' = 0$ (Figure 1.3). The thermal (T') and chemical (C') diffusion fields in the liquid $T'_L(x',z',t')$, $C'(x',z',t')$, and the solid $T'_S(x',z',t')$ obey the following two-dimensional equations:

For $z' > h'(x',t')$

$$\kappa_L \nabla^2 T'_L + V\, T'_{L_{z'}} = T'_{L_{t'}}, \qquad (2.1a)$$

$$D \nabla^2 C' + V\, C'_{z'} = C'_{t'}, \qquad (2.1b)$$

for $z' < h'(x',t')$

$$\kappa_S \ \nabla^2 \ T'_S + V \ T'_{S_{z'}} = T'_{S_{t'}},$$ (2.1c)

where the subscripts z', t' denote partial differentiation. The dimensional temperatures $T'_{L,S} = T^*_{L,S} - T_m$ are measured relative to bulk melting temperature T_m of the pure substance. Along the interface $z' = h' \ (x',t')$, we neglect effects of crystalline anisotropy such as the orientational dependence of the surface tension and anisotropic heat flow. Since the solution is dilute, the system is operating near the intersection of the liquidus and the solidus, that is, on a locally linear phase diagram (Figure 1.4). Therefore, we can expand the concentration dependent equilibrium freezing temperature for the planar interface in a Taylor series about the value for a pure solvent ($C' = 0$)

$$T'(C') = T'(0) + \frac{dT'(0)}{dC'} \ C' \equiv T_m + m \ C',$$ (2.2)

keeping the first two terms where m is the liquidus slope (cf., Eq. 1.1 and Fig. 1.4) and T_m is the melting point of a planar, pure ice water interface. Under these assumptions, the thermodynamic boundary condition at the interface is a form of the Gibbs-Thomson relation, corrected (as in 2.2) for the solute depression of the bulk melting point;

$$T^*_L = T^*_S = T_m + m \ C' + T_m \ \frac{\gamma}{L} \ h'_{x'x'} [\ 1 + (h'_x)^2 \ ]^{-3/2} - \frac{L}{c_p} \ \beta_o \ \overset{..}{h'}.$$ (2.3)

The subscript x' denotes partial differentiation and γ is the solid - liquid interfacial surface tension averaged over all crystallographic orientations, and we drop the standard subscript $s \ l$ in this study. We will come back to the orientational average presently.

The third term of (2.3) represents the Gibbs - Thomson effect which accounts for the excess interfacial free energy required to accommodate an increase in interfacial area during

the solidification of a curved surface. To demonstrate this we discuss the common model of a small spherical crystal in equilibrium with its melt (e.g., Woodruff 1973, or Langer 1987).

The Gibbs free energy of the crystal has a contribution from the particles in the volume, and from the particles in the surface. In equilibrium, the solidification of dn moles will change the free energy by an amount $(\mu_S - \mu_L)\, dn$, where μ_S (μ_L) is the chemical potential of the solid (liquid). The formation of interfacial area dA in which the bonds are distorted from those in the bulk solid results in an increase in free energy $\gamma\, dA$ that must be balanced to maintain the equilibrium. If the sphere of radius r increases in area by an amount dr, where $dr \ll r$, then we have $dA = 8\,\pi\,r\,dr$ and $dn = d\tilde{V}/v = 4(\pi\,r^2\,dr)/v$, where $\tilde{V}$ (v) is the volume (molar volume). Therefore,

$$\mu_S - \mu_L = \frac{2\,\gamma\,v}{r},$$

(2.4)

implying that solidification will not proceed unless the temperature of the liquid is depressed below the bulk melting point. The depression is necessary because the presence of the spherical interface increases the chemical potential of the solid phase relative to the liquid which implies that the liquid phase is favored for the molecules (or atoms) in the volume $4\,\pi\,r^2\,dr$. In order for these particles to remain part of the crystal, an undercooling of the liquid by an amount δT that decreases the free energy of the crystal volume by an amount $(\tilde{V}\, L\, \delta T)/T_m$, must offset the free energy increase due to the presence of the curved surface. By balancing these contributions, $n\,\mu_S - \mu_L = (\tilde{V}\, L\, \delta T)/T_m$, the equilibrium undercooling obtained is a form of the Gibbs - Thomson relation for a spherical crystal

$$\delta T = \frac{\gamma T_m \kappa}{L}; \quad \kappa = 2/r. \tag{2.5}$$

In this case the interfacial curvature κ is that of a sphere but one is free to express this relation for a more general interfacial configuration. When the interfacial deflection is in two lateral dimensions the curvature is given by $\nabla h' \cdot \nabla h' [1 + (\nabla h')^2]^{-1/2}$, where ∇ denotes the two dimensional lateral gradient. In one lateral dimension the curvature is as given in Eq. (2.3). If the effects of crystalline anisotropy are important, the orientational average represented by the γ we consider in this derivation will not correctly determine the depression δT because the equilibrium crystal shape will not be a sphere (Herring, 1951). The surface energy is different from the surface tension because the former depends on the local effects of the underlying lattice. Thus, the surface energy will depend on the angle θ, between the normal to the surface and some fixed orientation is space. In order to model crystalline anisotropy, one ascribes a θ-dependence to the surface tension as follows; $\gamma_\theta = \gamma [1 - d_1 \cos (m \theta)]$, where d_1 is the anisotropy strength and m specifies the crystalline symmetry. This is a perturbation to the isotropic surface tension γ. Therefore, when neglecting crystalline anisotropy we must interpret γ as the surface tension (Herring, 1951). The inclusion of anisotropy requires a more detailed derivation of (2.5).

The last term of Eq. (2.3) parametrizes the microscopic interfacial kinetics (see e.g., Ben-Jacob et al., 1984; Langer 1987) where $\dot{h}'$ is the normal velocity at the interface and β_o is a kinetic coefficient. For near equilibrium growth, the mechanisms of attachment on facets are different than they are on the rounded regions of the crystal (Burton et al., 1950); the nucleation barrier being much larger on the facets. This is the basis of the orientational preference for growth, and is intimately tied to the anisotropy in γ. The extension of this

concept to diffuse interfaces is embodied in the coefficient β. Preferred growth directions can be mimicked by ascribing an orientational dependence to the surface tension (as above) or the kinetic attachment process, or to both. As with γ, the kinetic coefficient takes the form $\beta = \beta_o$ [1 − cos (m θ)]. This enhances diffusive instabilities in the desired orientations, typically coinciding with the symmetry chosen for the surface tension. The velocity dependence of the kinetic term is tantamount to the statement that at higher velocities the assumptions of local equilibrium and diffusion control at the interface may become invalid. The relationship between these terms and the equilibrium crystal shape is discussed by Elbaum and Wettlaufer (1991). For a detailed description of orientational and kinetic properties of the crystal-melt interface, the reader is referred to Burton et al., (1951) and Woodruff (1973).

The conservation of thermal energy and solute at the interface, $z' = h' (x',t')$, are expressed as

$$L \ (V + h'_t) = k_s \ \left[T'_{S_{z'}} - h'_{x'} \cdot T'_{S_{x'}} \right] - k_l \ \left[T'_{L_{z'}} - h'_{x'} \cdot T'_{L_{x'}} \right] \tag{2.6}$$

$$(V + h'_t) \ C' \ (k - 1) = D \ \left[C'_{z'} - h'_{x'} \cdot C'_{x'} \right]. \tag{2.7}$$

Here, k_s and k_l are the thermal conductivities of the solid and liquid respectively. The unit normal to the interface is $\hat{n} = (- h'_{x'}, 1) \ [1 + (h'_{x'})^2]^{-1/2}$, which results in the horizontal flux terms in Eqs. (2.6) and (2.7). In the linear theory, only small amplitude disturbances are considered, so that when integrating along the interface there may be locations at which the horizontal gradients are larger than the vertical gradients, however, over one period, the flux must be consistent with a positive mean growth rate. These expressions are exact, and for small amplitudes the derivative $h'_{x'}$ will not diverge.

Eq. (2.6) can be interpreted as follows: If heat conduction through the solid, away from the interface, is greater than that through the liquid, toward the interface, then the solid will grow at the expense of the liquid at a rate that depends on the latent heat of fusion, L. The segregation coefficient $k = C_S/C_L$, is the ratio of the solute in the solid C_S, to that in the liquid C_L. The low solubility of NaCl in the ice lattice results in solute rejection at the interface. The H_2O-NaCl solution is dilute, and the discontinuity of solute across the interface is accounted for by k. Eq. (2.7) represents the mass conservation: the build up of solute at the interface balances that diffusing away. The segregation coefficient has a more physical interpretation which we will develop in a later chapter.

We expect that far from the interface the influence of the deflection $h'(x',t')$ on the diffusion fields will be negligible. Therefore, the steady state planar solutions T'_{Lo}, C'_o, and T'_{So} will adequately describe them:

$$T'_L \to T'_{Lo} \, , \qquad C' \to C'_o; \quad z' \to \infty \tag{2.8}$$

$$T'_S \to T'_{So}; \quad z' \to -\infty . \tag{2.9}$$

Equations (2.1) along with conditions (2.3) and (2.6) through (2.9) completely describe the mathematical problem for the unknown functions $C', T'_{L,S}$, and h'.

2.2 Scaling and the Basic State

The lengths and times in the problem are scaled on the solute diffusion scales $z, x = (z', x') V/D$ and $t = t' V^2/D$, where the primed quantities have dimensions, and the unprimed quantities do not. The temperature and solute scales are similar to those of Merchant and

Davis (1991). The dimensionless temperatures are

$$T_S = \frac{T'_s - T'_o}{G^* \, D/V} \, , \qquad (2.10a)$$

$$T_L = \frac{T'_L - T'_o}{G^* \, D/V} \, , \qquad (2.10b)$$

where the subscripts L, S denote the liquid and solid phases, and T'_o is the temperature depression at the planar interface due to solute. Recall that the dimensional temperatures $T'_{L,S} = T^*_{L,S} - T_m$ are measured relative to the dimensional bulk melting temperature T_m of the pure substance. The quantity $G^* = \dfrac{2 \, G'_L + L \, V/k_l}{(1 + n)}$ is the average temperature gradient in the liquid at the interface. The dimensional temperature gradient in the liquid is G'_L, the latent heat per unit volume is L, and the ratio of the thermal conductivity of the solid to that of the liquid is $n = k_s/k_l$. The dimensionless solute concentration in the liquid is

$$C = \frac{C' \, k - C_\infty}{(k - 1) \, C_\infty} \, , \qquad (2.11)$$

where C_∞ is the far-field solute concentration, and $k = C_S/C_L$, as defined above.

Using the scales (2.10) and (2.11), the equations (2.1) transform to dimensionless field equations for temperature and solute in the liquid T_L, C and the solid T_S:

For $z > h \, (x, t)$

$$\nabla^2 T_L = 0, \qquad (2.12a)$$

$$\nabla^2 C + C_z = C_t; \qquad (2.12b)$$

for $z < h\ (x,t)$

$$\nabla^2 T_S = 0, \tag{2.12c}$$

where the subscripts z, t denote partial differentiation. Equations (2.12a,c) represent the limit as D/κ_L and D/κ_S approach zero. The approximation is reasonable because the thermal diffusivities are much larger than the solute diffusivity; $D/\kappa_L \approx 10^{-3}$ and $D/\kappa_S \approx 10^{-4}$. Along the interface $z = h\ (x,t)$, the conditions (2.3), (2.6), and (2.7) become

$$T_L = T_S = M\ C + M\ \Gamma\ h_{xx}\ (1 + h_x^2)^{-3/2}, \tag{2.13}$$

$$l\ (1 + h_t) = n\ \left[T_{Sz} - h_x\ T_{Sx}\right] - \left[T_{Lz} - h_x\ T_{Lx}\right], \tag{2.14}$$

$$(1 + h_t)\ [1 + C\ (k - 1)] = C_z - h_x\ C_x, \tag{2.15}$$

respectively. The equilibrium condition (2.13) for the dimensionless system does not include the microscopic kinetics term because there is no nucleation barrier on a molecularly diffuse interface (e.g., Cahn, 1960, Woodruff 1973), and we assume the interface is diffuse on this scale. The latent heat parameter, $l = \dfrac{L\ V}{G^*\ k_l}$, is commonly set to zero (Wollkind and Segal, 1970; Merchant and Davis, 1989b,1991) in the limit of small velocity, giving symmetry to Eq. (2.14). We retain this parameter for all values of V. The far field boundary conditions, (2.8) and (2.9) become

$$T_L \rightarrow T_{Lo}\ , \qquad C \rightarrow C_o; \qquad z \rightarrow \infty \tag{2.16}$$

$$T_S \rightarrow T_{So}; \qquad z \rightarrow -\infty. \tag{2.17}$$

The dimensionless system (2.12) through (2.17) defines the mathematical problem that we

will analyze.

The morphological number M and surface energy parameter Γ are the nondimensional parameters appearing in (2.13);

$$M = \frac{m \, G_c}{G^*} = \frac{m \, C_\infty \, (k-1) \, V}{D \, k \, G^*},$$
(2.18)

$$\Gamma = \frac{T_m \, \gamma \, k \, V}{L \, D \, m \, C_\infty \, (k-1)},$$
(2.19)

in which G_c is the steady state solute gradient in the liquid at the interface. The nomencature, parameters, and values of the thermophysical constants are listed in the Appendix. It is important to recognize that in this formulation the velocity dependence of M is also implicitly represented in G^*, which is not the case in a model without latent heat.

The steady-state solution for the system (2.12) - (2.17) with a planar interface depends only on z, and is given by

$$T_{Lo}(z) = G_L \, z,$$
(2.20a)

$$C_o(z) = 1 - e^{-z},$$
(2.20b)

for the liquid, and in the solid

$$T_{So}(z) = \frac{(G_L + l) \, z}{n},$$
(2.20c)

$$h_o = 0.$$
(2.20d)

The linear stability analysis is performed by perturbing this basic state. For a constant liquid

temperature gradient and $l = 0$ this basic state reduces to that of Wollkind and Segal (1970).

2.3 Linear Stability of the Basic State

The basic states, (2.20), which represent the planar interface are perturbed as $\exp(\sigma_a t + i a x)$ and we keep track of their temporal behavior. The choice of one horizontal dimension is dictated by the observation that, in the absence of external fluid flow in the melt, there is random c-axis orientation in the horizontal plane, and there is only orientational preference in individual grains (Fig. 1.1).

The configuration of the interface is given by $h(x,t) = h(x) + h_a(x,t)$, where we are perturbing about the steady state configuration $h(x)$ and the subscript a emphasizes the wavenumber dependence of the perturbation. The perturbation we introduce into the plane has an infinitesimal amplitude at time $t = 0$. In order to simplify the problem, the steady state configuration is planar $[h(x) = 0]$, but this is not a necessary condition (Langer 1987). An interfacial perturbation of arbitrary shape can be Fourier decomposed and the evolution of the Fourier components or normal modes can be computed (e.g., Chandrasekhar 1961, Sekerka 1967). We assume the perturbation is separable and can be expanded as

$$h_a(x,t) = \frac{1}{\sqrt{2\pi}} \int_{-\infty}^{\infty} da\ e^{i a x}\ \bar{h}_a(a,t) \tag{2.21}$$

with the inverse Fourier spectrum being,

$$\bar{h}_a(a,t) = \frac{1}{\sqrt{2\pi}} \int_{-\infty}^{\infty} dx\ e^{-i a x}\ h_a(x,t). \tag{2.22}$$

The stability of the interface will depend on the time dependence of the amplitude of the perturbation, so that $h(x)$ is linearly stable if *all* of the components of $h_a(x,t)$ are such that the disturbance decays in time and $h(x,t)$ approaches $h(x)$. The linear perturbation procedure

yields an expression for the time dependence of all Fourier components,

$$\sigma_a = \frac{d \, \bar{h}_a/dt}{\bar{h}_a}. \tag{2.23}$$

If σ_a depends only on a equation (2.23) has a solution

$$\bar{h}_a \, (a,t) = \bar{h}_{ao} \, (a) \, e^{\sigma_a \, t}. \tag{2.24}$$

Therefore, the interface perturbation evolves in time as

$$h_a \, (x,t) = \frac{1}{\sqrt{2 \, \pi}} \int_{-\infty}^{\infty} da \, \bar{h}_{ao} \, e^{\sigma_a \, t} \, e^{i \, a \, x}. \tag{2.25}$$

The Fourier components with $\sigma_a > 0$ will grow exponentially in time and those with $\sigma_a < 0$ will decay in time which we shall see presently. For the remainder of the discussion we drop the subscript a from the perturbation growth rate σ. Next, we outline the procedure by which an expression for σ is obtained.

The perturbed solutions to (2.10) are written as $X(x,z,t) = X_o(z) + X_1(z) \exp{(\sigma \, t + i \, a \, x)}$;

$$\begin{bmatrix} T_L(x,z,t) \\ C(x,z,t) \\ T_S(x,z,t) \\ h(x,t) \end{bmatrix} = \begin{bmatrix} T_{Lo}(z) \\ C_o(z) \\ T_{So}(z) \\ 0 \end{bmatrix} + \begin{bmatrix} T_{L1}(z) \\ C_1(z) \\ T_{S1}(z) \\ h_1 \end{bmatrix} \exp{(\sigma \, t + i \, a \, x)}. \tag{2.26}$$

The system of governing equations (2.12) - (2.17) is then linearized in the perturbed quantities using a procedure common in thermodynamics (Landau and Lifshitz, 1969) and hydrodynamics (Chandrasekhar, 1961 and Drazin and Reid, 1981).

First, the solution (2.26) is substituted into equations (2.12) retaining only the terms of $O(X_1)$ which results in

$$[\, Y + D \, - \sigma \,] \, C_1(\, z \,) = 0, \tag{2.27a}$$

$$Y \, T_{L1}(\, z \,) = 0, \tag{2.27b}$$

$$Y \, T_{S1}(\, z \,) = 0. \tag{2.27c}$$

Here, D is the operator d/dz and Y is the operator $D^2 - a^2$. We must substitute (2.26) into (2.13) - (2.15), linearize and then expand about $z = h = 0$, for the linearization about the basic state. After the initial linearization, each condition is a function $F(z)$ of z only so we Taylor expand them, $F(z) = F(0) + [F(0)_z] \, h_a$ and linearize again so that (2.13) - (2.15) become

$$T_{L1}(0) - M \, C_1(0) + [\, M \, \Gamma \, a^2 + G_L - M \,] \, h_1 = 0, \tag{2.28a}$$

$$T_{L1}(0) - T_{S1}(0) + \left[\, G_L - \frac{G_L + l}{n} \,\right] = 0, \tag{2.28b}$$

$$D \, T_{L1}(0) - n \, D \, T_{S1}(0) + \left[\, D \, G_L - n \, D \, \frac{G_L + l}{n} + \sigma \, l \,\right] h_1 = 0, \tag{2.29}$$

$$D \, C_1(0) - (k - 1) \, C_1(0) + [D - (k - 1) - \sigma \,] \, h_1 = 0, \tag{2.30}$$

upon taking (2.13) in two parts.

The equations (2.27) have constant coefficients and will have solutions of the form

$$\left[\, C_1, T_{L1}, T_{S1} \,\right](z) = \left[\, \Pi, \Phi, \Omega \,\right] \exp(\, - \, [\xi_C, \xi_L, \xi_S] \, z \,). \tag{2.31}$$

We substitute (2.31) into (2.27) along with a constant value for $h_1 = \chi$ and the requirement that C_1, T_{L1}, and T_{S1} be nontrivial (Wollkind and Segal, 1970) yields expressions for the exponential factors;

$$\xi_C = \frac{1}{2} \pm \left[\, \frac{1}{4} + [\, a^2 + \sigma \,] \,\right]^{1/2} \tag{2.32a}$$

$$\xi_L = \pm \, | \, a \, | \tag{2.32b}$$

$$\xi_S = \pm \mid a \mid. \tag{2.32c}$$

We recall that (2.16) and (2.17) require that far from the interface the influence of the interfacial disturbance is negligible so the signs of (2.32) are such that ξ_C, $\xi_L > 0$ and $\xi_S < 0$ giving

$$\xi_C = \frac{1}{2} + \left[\frac{1}{4} + [\, a^2 + \sigma \,] \right]^{1/2} \tag{2.33a}$$

$$\xi_L = + \mid a \mid \tag{2.33b}$$

$$\xi_S = - \mid a \mid. \tag{2.33c}$$

The solutions to (2.27) are

$$\left[C_1, T_{L1}, T_{S1} \right](z) = \left[\Pi, \Phi, \Omega \right] \exp(- [\xi_C, \mid a \mid, - \mid a \mid] \, z \,), \tag{2.34}$$

with ξ_C given by (2.33a).

The interfacial boundary conditions will define an equation for Π, Φ, and Ω. We substitute (2.34) into (2.28) - (2.30) which yields the system

$$\begin{bmatrix} -M & 1 & 0 & M \,\Gamma \, a^2 + G_L - M \\ 0 & 1 & -1 & G_L - (G_L + l)n^{-1} \\ 0 & a & na & -\sigma \, l \\ \xi_C + k - 1 & 0 & 0 & \sigma + k \end{bmatrix} \begin{bmatrix} \Pi \\ \Phi \\ \Omega \\ \chi \end{bmatrix} = 0, \tag{2.35}$$

of four equations and four unknowns. We can write this compactly as

$$\underline{A} \, X = 0, \tag{2.36}$$

where $\underline{A}$ is the 4 x 4 matrix of control parameters containing σ, and X is the column vector $[\Pi, \Phi, \Omega, \chi]^T$. The requirement that the equations allow non-trivial solutions is equivalent to the secular equation $\mid \underline{A} \mid = 0$. This condition gives the dispersion relation F (discussed in the last chapter) that is an implicit function of σ;

$$\sigma = \frac{a \ [M \ \underline{R} \ (1 + n) - (2 \ G_L + l) \ (\underline{R} + k) - a^2 \ M \ \Gamma \ (\underline{R} + k) \ (1 + n)]}{l \ (\underline{R} + k) + M \ a \ (1 + n)},$$

(2.37)

in which $\underline{R} = (1/4 + a^2 + \sigma)^{1/2} - 1/2$ is a wavenumber parameter. If $Re(\sigma) = 0$, then $Im(\sigma) = 0$, since there is an exchange of stabilities for the finite latent heat system (Alexander et al., 1986). A general discussion of the principle of the exchange of stabilities is given by Chandrasekhar (1961) and Drazin and Reid (1981). In this situation it means that when $Re(\sigma) > 0$ the planar interface loses stability to non-oscillatory perturbations, and when $Re(\sigma) < 0$ it is stable. By setting $\sigma = 0$, we obtain the condition that must be satisfied by stationary solutions,

$$R^3 Q + R^2 Q \ (1 + k) + R \ \left[(Q \ / \ \Gamma) \ (k \ \Gamma - 1) + 2 \ G_L + l \right] + k \ (2 \ G_L + l) = 0.$$

(2.38)

Here, $Q = M \ \Gamma \ (1 + n)$ and $R = \underline{R}(\sigma = 0)$, and is related to the wavenumber a by $R^2 + R = a^2$. Seidensticker (1967) showed that inclusion of an isotropic kinetics term (e.g., Eq. 2.3) is not a singular perturbation to the theory. In this case, it is tantamount to adding a positive term to the denominator of Eq. (2.37), having no effect on the neutral stability results. Using the identity $(2 \ G_L + l) \ (1 + n)^{-1} = 1$, the following cubic polynomial in R results

$$R^3 + R^2 \ (1 + k) + \frac{R}{\Gamma} \ \left[k \ \Gamma + \frac{1}{M} - 1 \right] + \frac{k}{M \ \Gamma} = 0.$$

(2.39)

The neutral function g referred to in the first chapter is defined by Eq. (2.39) and can be shown to be the same as that obtained by Coriell et al. (1985), who used different thermal

and concentration scalings. The locus of points $(R > 0$, M , $\Gamma)$, for a given segregation coefficient k, demarcates regions of stability from regions of instability, since $\sigma = 0$ at every point satisfying (2.39).

THE STANDARD NEUTRAL CURVES AND WEAKLY NON-LINEAR RESULTS

3.1 *The $V(\lambda)$ Neutral Curve*

We can think of Eq. (2.39) as a function of dimensional wavelength $\lambda = 2\pi/a'$, where a' is the dimensional wavenumber, and other variables; $f(\lambda, V, C_\infty, G_L', n, k, \cdot, \cdot)$. To investigate solidification at the underside of sea ice, we fix the values of C_∞, G_L', n, and k to the observed values and vary V. Therefore, we obtain the locus of points (λ, V) that are neutrally stable, that is, they correspond to solutions that do not grow or decay according to the linear theory. This is termed the $V(\lambda)$ neutral curve. We choose to investigate this first because our main interest is in the relationship between platelet spacing and mean growth velocity. This also allows a qualitative comparison with the existing data. Fig. 3.1(a) shows the entire neutral curve, and Fig. 3.1(b) shows the bottom of the neutral curve close to V_c for $C_\infty = 35$ ppt, $k = 0.3$, and $G_L' = 3.57$ K m^{-1}. Near critical, we see the weak dependence of V on λ noted by other investigators (Bennett and Brown 1989, Merchant and Davis 1989b). There are low and high λ cutoffs which bound the allowable scale of the substructure. The value λ_c associated with the critical point of instability is also referred to as the most dangerous mode, since the system is stable to disturbances of all other wavelengths and it will be the first mode to become unstable as the velocity is increased beyond V_c.

Recalling Eq. (2.37) we see that there are three terms in the numerator, each having a different physical origin, as first pointed out by Mullins and Sekerka (1964) in a similar

expression. The denominator is always positive so that the sign of the terms in the numerator determine the sign of the perturbation growth rate. The first term is positive and proportional to $M \dot{R} (1 + n)$. It depends on the solute field, determining the degree of constitutional undercooling, and always has a destabilizing effect. The second term is negative and proportional to $(2 G_L + l) (\underline{R} + k)$. It depends on the temperature gradient in the water which always melts back solid disturbances. The third term is also negative and proportional to

$a^2 M \Gamma (\underline{R} + k) (1 + n)$. The factor $M \Gamma = \dfrac{T_m \gamma}{L} \dfrac{V^2}{D^2 G^*}$ is a function of surface tension,

always stabilizing the interface through the Gibbs-Thomson effect. Note that this term is multiplied by the square of the wavenumber so it becomes large at small wavelengths. This term provides the lower wavelength cutoff for all velocities. All wavelengths less than the lower cutoff are stabilized by surface tension, and all wavelengths greater than the upper cutoff are unable to grow because the solute field has a finite interaction range, of about D/V. Lateral solute redistribution takes place by diffusion, and drives the instability. When V is large, the diffusion time and space scales are small, so lateral gradients in the solute field can only accompany small wavelength disturbances. However, the small waves are strongly stabilized by surface tension, as discussed above. The low velocity limit, close to the onset of instability is termed the constitutional undercooling limit, where $M = 1$; the freezing temperature gradient balances the imposed temperature gradient. The high velocity upper limit, where the stabilizing affect of surface tension balances the destabilizing affect of solute rejection, is termed the absolute stability limit. Here the behavior is $\Gamma = k^{-1}$. These limits were established by Mullins and Sekerka (1964). Combined, these effects limit the range of instability and close the neutral curve.

The most striking implication of Fig. 3.1 is that the interface will develop a platelet substructure over a large range of growth velocities. Naturally occurring sea ice typically grows in the range of approximately 10^{-10} - 10^{-6} m s^{-1} or 10^{-3} - 10^{2} mm day^{-1}. This explains the ubiquitous observation of the substructure (Weeks and Ackley, 1986). The points plotted in Fig. 3.1 are the platelet spacing as a function of growth velocity. The crosses are from the laboratory experiments of Lofgren and Weeks (1969), and the circles are from the fit to field data by Nakawo and Sinha (1984). These data represent the fully developed substructure, well beyond critical. The laboratory experiments were not designed to investigate the critical platelet spacing. Thus, the neutral curve shows that the linear theory bounds the observed substructure. The dashed curve is the fastest growing perturbation, that is, the one that corresponds to the maximum value of σ. Above critical, the slope of the curve exhibits the power law dependence $\lambda \propto V^{-1/2}$ that has been experimentally observed (Lofgren and Weeks, 1969). The laboratory data presented have an average $C_\infty = 37.21$ ppt, and the average number of platelets measured to obtain each data point was 223. These comparisons should be thought of in terms of $V \rightarrow V_c^-$, since mature sea ice will slowly develop an adverse temperature gradient. The lowest laboratory velocities are higher than is typically found in mature sea ice, and in all cases greater than critical. Naturally occurring sea ice will never obtain a $V > V_a \approx 21$ cm s^{-1}.

To compare theory with experiment close to critical, careful experiments with the correct geometry are needed so that the initial breakdown can be observed. The transparency of the H_2O-NaCl system, like the commonly studied organic SCN-acetone system, makes it appealing for such applications. The large range of morphological instability, compared with some binary alloys, makes the system more difficult to study when seawater solute

concentrations are used. Since the base of the neutral curve is so broad, we expect a strong interaction of the critical mode with adjacent modes. This is often referred to as mode softening or a soft instability, and is predicted to be the result of the interaction of microscopic and macroscopic length scales (e.g., Langer 1987 and Brattkus and Misbah 1990). The degree to which this occurs here is addressed in section 3.4. Assessing the role of weak wavelength selection is the primary problem encountered when comparing a linear theory with experiments near critical. Because, in this case, the geometry of laboratory experiments (Harrison and Tiller, 1963 and Lofgren and Weeks, 1969) differs, the role of convective transport of solute cannot be assessed.

3.2 The V (λ) Neutral Curve at Large G'_L

We know that the thermal field has the effect of stabilizing morphological instabilities in this system because increasing G_L decreases the undercooling. It is clear from the previous section that under conditions which are present during natural solidification, namely small temperature gradients and large concentrations, the system exhibits a large degree of instability. Laboratory experiments allow the freedom to stabilize the interface by either increasing the liquid temperature gradient or decreasing the solute concentration.

Consider an experiment which has as a goal to desalinate seawater through freezing. We can vary the salinity a negligible amount depending on where we obtain the seawater, so we consider it fixed at 35 ppt. We also assume that the laboratory has the capability to fix the value of C_∞. The low solubility of NaCl in ice is parametrized by the small value of the equilibrium segregation coefficient. We take advantage of this fact by realizing that the only mechanism through which a large concentration of impurity can become part of the solid

phase is via a breakdown of the planar interface, wherein bulk brine is trapped in the solid phase. We have just shown this to be the case for naturally solidifying seawater. Therefore, we can stabilize the interface solely by increasing the liquid temperature gradient, and the solubility gradient will drive the purification.

Neutral curves have been calculated from Eq. (2.39) in which we fix the liquid temperature gradient at two values several orders of magnitude greater than that used in the natural solidification study (Fig. 3.1). Figure 3.2 combines the neutral curves for $G'_L = 200$ K cm^{-1} and $G'_L = 3570$ K cm^{-1}. We realize that a gradient of greater than about 100 K cm^{-1} for a substance like water may be a practical impossibility, without some elaborate pressure control or laser annealing techniques. However, we are interested in examining the sensitivity of the system to this control parameter. For a substance like copper, in which there is about a 1200 K separation between the freezing and boiling points, these gradients are accessible. The high temperature gradient has the expected effect of reducing the range of instability but it does so primarily by delaying (meaning at higher V) the onset of instability; in both cases, the system restabilize at the same point. For $G'_L = 200$ K cm^{-1} we have $V_c = 1.09 \times 10^{-4}$ cm s^{-1}, $\lambda_c = 1.4 \times 10^{-2}$ cm, and $V_a = 20.9$ cm s^{-1}, $\lambda_a = 8.5 \times 10^{-6}$ cm. For $G'_L = 3570$ K cm^{-1} we have $V_c = 2.01 \times 10^{-3}$ cm s^{-1}, $\lambda_c = 2.0 \times 10^{-3}$ cm, and $V_a = 20.9$ cm s^{-1}, $\lambda_a = 8.5 \times 10^{-6}$ cm. In the natural solidification case shown in Fig. 3.1, $G'_L = 0.0357$ K cm^{-1} where $V_c = 1.91 \times 10^{-8}$ cm s^{-1}, $\lambda_c = 4.5$ cm, and $V_a = 20.9$ cm s^{-1}, $\lambda_a = 8.7 \times 10^{-6}$ cm. The higher temperature gradient sharpens the wavelength selection somewhat, and the point of absolute stability is not sensitive to this increase. An increase in the liquid temperature gradient of five orders of magnitude results in virtually no change in the location of absolute stability.

The insensitivity of the absolute stability limit to changes in G'_L can be seen by re-examining Eq. (2.39) in light of the limits discussed in section 3.1. We focus on the coefficient of the term that is linear in the wavenumber parameter R since it controls the root structure. At $V \leq V_c$, $M \leq 1$ and $\Gamma \ll 1$, so that until $M = 1$ there are only negative real roots of Eq. (2.39). This is the constitutional undercooling limit, and the effect of delaying the onset of instability by increasing G'_L is obvious when examining Eq. (2.18), the expression for the morphological number; $M = (m\ C_\infty\ (k - 1)\ V)/D\ k\ G^*$. An increase in G'_L results in an increase in G^*, requiring a higher value of V for the $M = 1$ limit to be reached. In other words, the increase in the liquid temperature gradient reduces constitutional undercooling (see e.g., section 1.3). In section 3.3 we will see that as $k \rightarrow 0$, the limit $M \rightarrow 1$ results. For $V \leq V_a$, $M \approx 70$ and $\Gamma \leq k^{-1}$ and the coefficient of the linear term in Eq. (2.39) is negative. Absolute stability is reached as $\Gamma \rightarrow k^{-1}$ and the the linear coefficient becomes positive. This limit does not vary as the value of G'_L increases, as can be seen by examining Eq. (2.19) the expression for the surface energy parameter Γ. Therefore, we can only restabilize the system at a lower velocity by decreasing the far field solute concentration C_∞ or increasing k, and k is not a laboratory control parameter in the strict sense of the word. (One may view k as a control parameter that is slaved to the interfacial velocity when growth is rapid. This is the point of the study by Merchant and Davis, 1991] but it assumes a particular theory for the velocity dependence of k that may actually depend on the details of the interaction potentials. We will return to this topic later.) The effect of increasing the liquid temperature gradient is to decrease the range of instability of the system by delaying the onset of instability to higher growth velocities. Some systems operate close to these stability limits and it has been the focus of the asymptotic work discussed in the next section to exploit this behavior.

From the point of view of the desalination experiment one desires a neutral curve with the minimum extent along the vertical axis, and the largest stable growth rate. If one operates at a velocity just below critical in the case where $G'_L = 3570$ K cm^{-1} then it would be possible to produce about 90 cm of ice per day.

In some areas of the Arctic Ocean values of G'_L an order of magnitude greater than that used in section 3.1 for the natural solidification study have been observed (Wettlaufer et al., 1990 and Wettlaufer, 1991), suggesting the possibility of a geophysical thermal stabilization of the substructure.

3.3 *Asymptotic Behavior*

There have been several investigations that have focused on long-wave instabilities in the frozen-field approximation to the solidification system, Eqs. (2.12) - (2.17), the most recent being Riley and Davis (1990). The frozen-field approximation assumes that the thermal conductivities, densities and specific heats of both phases are equal and that the effect of latent heat release at the interface is negligible. Therefore, this eliminates the possibility of disturbances of the interface inducing disturbances in the thermal fields since the temperature gradient across the entire solid-liquid system is constant and fixed. Long-wave phenomena are of interest because they are accompanied by long time scales, or slow modes of evolution. The long-wave limit has been examined in the absolute stability (Brattkus and Davis, 1988) and constitutional undercooling, small k (Sivashinsky, 1983) regions of parameter space. Riley and Davis (1990) review the former two analyses and examine the longwave behavior for small k, and large Γ and for small k near absolute stability, to exhaust the possibilites for the frozen-field system in which solute is rejected ($k < 1$).

If it is known that near a critical point, a system operates at a characteristic scale that is much larger than another intrinsic scale of the system, it may be possible to separate space variables, thereby lowering the dimensionality of the problem. The approach used in this problem is to examine the dispersion relation that results from a linear stability analysis of the frozen-field system, [a simplified version of Eq. (2.37)], and extract the scales suggested by the long-wave limit and other constraints of interest. For example, in a long-wave approximation, a disturbance may take longer to evolve than otherwise, this suggests an adjustment to the time scale used. Once the adjustments dictated by the approximation are assessed, one rescales the original system and obtains a new characteristic equation from a linear stability analysis, and derives a non-linear evolution equation for interface deflections. Theories that result from this approach are termed *local* since they are only valid for a restricted range of physical parameters. This type of asymptotic analysis is useful in extracting the essential qualitative features of a system in particular regions of a neutral curve. One such feature is the relationship between the interfacial growth velocity and the neutral wavelength. We identify this relationship and attempt to shed some light on the utility of deriving exponents that characterize long and shortwave behavior.

3.3.1 *Behavior Near Critical Instability*

The local theory of Sivashinsky (1983) predicts that as $k \to 0$ and $M \to 1$; $\lambda_c \to \infty$. We shall see that this is qualitatively consistent with the behavior of the H_2O-$NaCl$ system. He investigated the dispersion relation that results from a linear stability analysis of the frozen-field system, namely

$$\sigma = (1 - M^{-1} - a^2 \, \Gamma) \, (\underline{R} + k) - k, \qquad (3.1)$$

where we recall that $\underline{R} = (1/4 + a^2 + \sigma)^{1/2} - 1/2$ is a wavenumber parameter. This equation is analogous to Eq. (2.37), the relation obtained from the analysis of the full solidification system. The frozen-field system was described above, and it is important to note that the functional dependence of M on V is simplified in this case since G^* is no longer a function of V (see discussion following Eq. (2.10)). The long-wave behavior in the limit $k \ll a^2 \ll 1$, near critical, dictates a small parameter $\varepsilon = 1 - M^{-1}$, and leads to new scales as follows:

$$a = \varepsilon^{1/2} \, \bar{a} \quad , \quad \sigma = \varepsilon^2 \, \bar{\sigma} \quad , \quad k = \varepsilon^2 \, \bar{k}, \qquad (3.2)$$

where it is assumed that the barred quantities and Γ are $O(1)$ as $\varepsilon \to 0^+$. When rescaling the frozen-field solidification equations using Eq. (3.2), and performing a linear stability analysis, the following dispersion relation results,

$$\bar{\sigma} = \bar{a}^2 - \Gamma \, \bar{a}^4 - \bar{k}. \qquad (3.3)$$

At neutral stability Eq. (3.3) leads to

$$\Gamma = \frac{1}{\bar{a}^2} - \frac{\bar{k}}{\bar{a}^4} = \frac{1 - M^{-1}}{a^2} - \frac{k}{a^4}. \qquad (3.4)$$

We seek the $\lambda - V$ behavior in the vicinity of the global minimum λ_{*c}, V_{*c} of the surface defined by Eq. (3.4). The standard approach does not give consistent results in the case where the only real underlying control variable is V. That is, treating either Γ or M^{-1} as a bifurcation parameter and seeking minima in the $a - \Gamma$, $a - M^{-1}$ planes leads to ambiguous results when interpreted in the dimensional variables. The values a_Γ such that $\partial \Gamma / \partial a^2 = 0$,

and a_M such that $\partial M^{-1}/\partial a^2 = 0$ are

$$a_\Gamma = \sqrt{2\,k}\ (1 - M^{-1})^{-1/2},\tag{3.5a}$$

and

$$a_M = \left[\frac{k}{\Gamma}\right]^{1/4}.\tag{3.5b}$$

In the dimensional $\lambda - V$ plane these become

$$\lambda_\Gamma = f_\Gamma\,(V)\,V^{-1},\tag{3.6a}$$

and

$$\lambda_M = C_M\,V^{-3/4},\tag{3.6b}$$

where $f_\Gamma\,(V) = C_\Gamma\,(1 - A\,V^{-1})^{1/2}$, $C_\Gamma = 2\,\pi\,D/\sqrt{2\,k}$, and $A = D\,k\,G^*/m\,C_\infty\,(k - 1) = V/M$.

In addition, $C_M = 2\,\pi\,D\,(B\,k^{-1})^{1/4}$ and $B = T_m\,\gamma\,k/D\,L\,m\,C_\infty\,(k - 1) = \Gamma/V$. Within the validity of the approximation, the qualitative behavior of λ_Γ is correct since it is an increasing

function of V for a small range of V. Letting $V = \iota\,A$ in Eq. (3.6a) leads to

$$C_\Gamma^{-1}\,\frac{\partial\lambda_\Gamma}{\partial V} = \frac{3 - 2\,\iota}{(\iota\,A)^2\,2\,\iota\,\sqrt{(1 - \iota^{-1})}},\tag{3.7}$$

so that for $1 < \iota < 3/2$ we will have $\dfrac{\partial\lambda_\Gamma}{\partial V} > 0$. However, when V takes on a minimum value

of A ($\iota = 1$), then λ_Γ vanishes. We see from Eq. (3.6b) that λ_M exhibits a power law decay

which we would not expect for $V \geq A$. The discrepent behavior is due to the fact that M and

Γ are both functions of V and as such cannot be independently varied for fixed C_∞, k and

G^*. We see this by determining the point at which $a_\Gamma = a_M$. When substituting Eq. (3.5) into

Eq. (3.4) we get

$$M_{*_c}^{-1} = 1 - 2 \ (k \ \Gamma_{*_c})^{1/2}, \tag{3.8}$$

showing that the wavelength is not a uniquely determined function of V. Kurtze (1988) discusses wavelength selection in terms of (3.5b) but does not mention the ambiguity between Eq. (3.5a) and Eq. (3.5b) since he does not derive the former.

The problem is less opaque when considering the dimensional version of Eq. (3.4);

$$\lambda^4 \ V^3 - \lambda^2 \ V \ c_1 + \lambda^2 A \ c_1 + c_2 = 0, \tag{3.9}$$

where $c_1 = (2 \ \pi \ D)^2 \ k^{-1}$ and $c_2 = (2 \ \pi \ D)^4 \ B \ k^{-1}$ are both positive. If we rewrite Eq. (3.9) in terms of the variable $\hat{\lambda} = \lambda^2$, the resulting equation has solutions,

$$\hat{\lambda} = \frac{c_1 \ (V - A)}{2 \ V^3} \pm \frac{\sqrt{c_1^2 \ (V - A)^2 - 4 \ c_2 \ V^3}}{2 \ V^3}, \tag{3.10a}$$

that are real and distinct when the quantity under the radical sign is positive. When the quantity under the radical sign vanishes, the roots are real and equal. This occurs at the point λ_{*_c}, V_{*_c}, where $dV/d\lambda = 0$. Therefore,

$$\lambda_{*_c}^2 = \frac{c_1 \ (V_{*_c} - A)}{2 \ V_{*_c}^3}, \tag{3.10b}$$

which is equivalent to the result obtained from implicit differentiation of Eq. (3.9) and to what obtains when evaluating Eq. (3.6a) at $V = V_{*_c}$. However, the essential V dependence of the wavelength near the critical point is not determined from the leading term in Eq. (3.10a). The point at which $dV/d\lambda = 0$, occurs when the quantity under the radical sign vanishes. This is the condition

$$V^3 = \frac{c_1^{\,2}}{4\,c_2}\,(V - A)^2,$$

<div align="right">(3.11)</div>

and is equivalent to Eq. (3.8) when transformed into dimensional variables. The minimum

velocity sought is determined from the intersection of the functions V^3 and $\frac{c_1^{\,2}}{4\,c_2}\,(V - A)^2$.

The quadratic vanishes at $V = A$ and the cubic intersects the quadratic once for $V < A$ and

twice, or never, for $V > A$. From the previous discussion, we know that $V < A$ is physically

uninteresting, so the minimum V that we seek corresponds to the first intersection for $V > A$.

We nondimensionalize Eq. (3.11) and linearize the cubic in the neighborhood of A so that

$V^3 A^{-3} \approx 1 + 3\,(V/A - 1)$, which approaches unity as V approaches A. This gives the critical

velocity in the long-wave small k limit as

$$V_{*c} = A\,(1 + q_1^{1/2}),$$

<div align="right">(3.12)</div>

where $q_1 = \dfrac{4\,c_2\,A}{c_1^{\,2}} = 4\,k\,B\,A = O\,(10^{-8})$, and the approximation improves with decreasing

q_1. As $k \to 0$, $q_1 \to 0$ so that $V_{*c} \to A$.

Now we can investigate the wavelength behavior in the vicinity of V_{*c} by letting

$V = V_{*c} + \delta_V$ and $\lambda = \lambda_{*c} + \delta_\lambda$ in Eq. (3.10a), where $\delta_V \ll V_{*c}$, and $\delta_\lambda \ll \lambda_{*c}$. When lineariz-

ing in δ, using Eq. (3.10b), and noticing that $\delta^{1/2} \gg \delta$ we obtain

$$(\lambda - \lambda_{*c}) = C_c\,(V - V_{*c})^{1/2},$$

<div align="right">(3.13)</div>

where $C_c = \left[(16\,\lambda_{*c}^{\,2}\,V_{*c}^{\,6})/[2\,c_1^{\,2}\,(V_{*c} - A) - 12\,c_2\,V_{*c}^{\,2}]\right]^{-1/2}$. Therefore, the increase in

wavelength with velocity on this branch has a simple power law dependence. This depen-

dence does not derive from the V - dependence that appears in the leading term of Eq.

(3.10a), which has a negligible contribution. Therefore, expansion of Eq. (3.6a) about the point λ_{*c}, V_{*c} will not yield the same V-dependence.

Sivashinsky (1983) predicted that as $k \to 0$, $\lambda_{*c} \to \infty$. Because c_1 and c_2 depend on k, letting $k \to 0$ in Eq. (3.10a) when $V = V_{*c}$ results in $\lambda_{*c} \to \infty$. We can also observe the effect of small k behavior by letting k become small in the exact relation, Eq. (2.37), for the full solidification system. The V (λ) neutral curve for $k = 3.0 \times 10^{-3}$, where $\lambda_c \approx 1.1$m, is shown in Fig. 3.3. As k is decreased, the neutral curve flattens further and begins to take on a winged cusp shape close to V_c on this scale. This curve is also closed, and as $V \to V_a^-$ the cusp curves to the left. However, in this limit, the prediction that $V_c \approx 10^{-10}$ cm s^{-1} is not a physically realizable under the assumptions of a continuum diffusion theory. Such a value of V_c corresponds to the "diffusion" of 10^{-2} molecular layers of nutrient molecules toward the interface per second. In the full system, the $M = 1$, small k limit predicts unphysical velocities, which may also be the case in other systems suggesting a cautious application of local theories of this type.

Sivashinsky (1983) rescaled the frozen-field system using the new scales, Eq. (3.2), and derived a weakly non-linear evolution equation for the interface deflection. He predicted that the bifurcation to two-dimensional cells would be subcritical (see section 1.5 and 3.4). The arguments that led to Eq. (3.13) show that the range of subcritical bifurcation is restricted to a small velocity interval. Kurtze (1988) showed that the steady state solutions to Sivashinsky's evolution equation are themselves linearly unstable for velocities only slightly greater than the threshold V_c.

3.3.2 Behavior Near Absolute Stability

Brattkus and Davis (1988) investigated long-wave behavior near absolute stability. The appropriate small parameter in this situation is $\varepsilon = k^{-1} - \Gamma$, when $a^2 \ll 1$, from which the analysis of (3.1) suggested the scales

$$a = \varepsilon^{1/2} \bar{a} \quad , \quad \sigma = \varepsilon \, \bar{\sigma} \quad , \quad M^{-1} = \varepsilon^2 \, \bar{M}^{-1}, \tag{3.14}$$

where it is assumed that the barred quantities and k are $O(1)$ as $\varepsilon \to 0^+$. The asymptotic dispersion relation they obtain, after rescaling the solidification equations using Eq. (3.14), and performing a linear stability analysis is

$$\bar{\sigma}^2 + a^2 \, \bar{\sigma} \, (2 + k^{-1}) + [k \, \bar{M}^{-1} - k \, \bar{a}^2 + \bar{a}^4 \, (1 + k^{-1})] = 0. \tag{3.15}$$

At neutral stability Eq. (3.15) leads to

$$\bar{M}^{-1} = \bar{a}^2 - \bar{a}^4 \, \frac{(k^{-1} + 1)}{k}, \tag{3.16}$$

$$M^{-1} = a^2 \, (k^{-1} - \Gamma) - a^4 \, \frac{(k^{-1} + 1)}{k}.$$

As in the case of the long-wave limit close to critical instability, we seek the $\lambda - V$ behavior in the vicinity of the point of absolute stability λ_{*a}, V_{*a}, an extreme point of the surface defined by Eq. (3.16). The same ambiguity that resulted in the previous case when treating either Γ or M^{-1} as bifurcation parameters, and examining the $a - \Gamma$, $a - M^{-1}$ planes occurs in this limit when the results are interpreted in terms of the dimensional variables. The values a_Γ such that $\partial \Gamma / \partial a^2 = 0$, and a_M such that $\partial M^{-1} / \partial a^2 = 0$ are

$$a_\Gamma = \left[\frac{k}{k^{-1} + 1} \right]^{1/4} M^{-1/4}, \tag{3.17a}$$

and

$$a_M = \left[\frac{k}{2\,(k^{-1}+1)} \right]^{1/2} (k^{-1}-\Gamma)^{1/2}.$$ (3.17b)

In the dimensional $\lambda - V$ plane these become

$$\lambda_\Gamma = C_\Gamma\, V^{-3/4},$$ (3.18a)

and

$$\lambda_M = f_M\,(V)\, V^{-1},$$ (3.18b)

where $f_M\,(V) = C_M\,[(k\,B)^{-1} - V]^{-1/2}$, $C_M = 2\,\pi\,D\,\sqrt{2\,(k\,B)^{-1}\,(1+k^{-1})}$, and

$C_\Gamma = 2\,\pi\,D \left[\dfrac{k\,A}{k^{-1}+1} \right]^{-1/4}$. As before, $B = T_m\,\gamma\,k/D\,L\,m\,C_\infty\,(k-1)$. For brevity we use the

same subscript convention as in Eqs. (3.5) and (3.6) but do not wish to equate Eqs. (3.17)

and (3.18) with these expressions.

Here again, it appears that we cannot determine the operating behavior for wavelength

selection but as we shall see presently it will be useful to know the velocity range in which

this approximation is valid. For $V^* < V < V_{*_a}$, λ_M increases with V with a decay factor as in

the other limit for λ_Γ (Eq. (3.6a)). For $V < V_2^*$, this curve is invalid in the chosen small

parameter. To determine V^*, we set $\partial\lambda_M/\partial V = 0$, giving $V^* = \frac{2}{3}\,(k\,B)^{-1}$. Here, it is λ_Γ that

exhibits the power law decay with the same exponent as did λ_M in the previous long-wave

limit, Eq. (3.6b). The point at which $a_\Gamma = a_M$ occurs when

$$M_{*_a}^{-1} = \left[\frac{k}{4\,(k^{-1}+1)} \right] (k^{-1} - \Gamma_{*_a})^2.$$ (3.19)

Consistent with the interpretation of Eq. (3.8), the wavelength selection is not a uniquely determined function of V.

We extract the essential qualitative behavior by analyzing Eq. (3.16) in the same manner as we did Eq. (3.4) and write the dimensional version;

$$\lambda^4 V^3 - \lambda^2 V^3 d_1 B + \lambda^2 V^2 d_2 + d_3 = 0, \tag{3.20}$$

where $d_1 = (2 \pi D)^2 A^{-1}$, $d_2 = d_1 k^{-1}$ and $d_3 = (2 \pi D)^4 (A k)^{-1} (k^{-1} + 1)$ are positive. If we rewrite Eq. (3.20) in terms of the variable $\hat{\lambda} = \lambda^2$, the resulting equation has solutions,

$$\hat{\lambda} = \frac{V^2 (d_2 - d_1 B V)}{2 V^3} \pm \frac{\sqrt{V^4 (d_2 - d_1 B V)^2 - 4 d_3 V^3}}{2 V^3}. \tag{3.21a}$$

As before, the point $\lambda_{\bullet a}, V_{\bullet a}$, where $dV/d\lambda = 0$ occurs when the quantity under the radical sign vanishes and is given by

$$\lambda_{\bullet a}^2 = \frac{V_{\bullet a}^2 (d_2 - d_1 B V_{\bullet a})}{2 V_{\bullet a}^3}. \tag{3.21b}$$

This result is equivalent to that obtained from implicit differentiation of Eq. (3.9), and to that obtained by evaluating Eq. (3.18b) at $V = V_{\bullet a}$. The condition that $dV/d\lambda = 0$ occurs when the quantity under the radical sign vanishes and is given by

$$\frac{4 d_3}{V} = (d_1 B)^2 [V - (k B)^{-1}]^2, \tag{3.22}$$

and is equivalent to Eq. (3.19) transformed into dimensional variables. Since we are examining the absolute stability region we seek the largest velocity determined from the intersection

of the functions $\frac{4 \, d_3}{V}$ and $(d_1 \, B)^2 \, [V - (k \, B)^{-1}]^2$. The quadratic vanishes at $V = (k \, B)^{-1}$ and the linear function intersects it twice in the vicinity of this point and once as it asymptotes to large values at small V. Therefore, the largest V occurs at the intersection to the right of the minimum of the quadratic. When $V \approx (k \, B)^{-1}$ we have $4/V \approx 10$ so we let the left hand side of Eq. (3.22) be $10 \, d_3$ and nondimensionalize the expression. The largest solution to the resulting quadratic equation gives the velocity at which the long-wave system restabilizes as

$$V_{*_a} = (k \, B)^{-1} (1 + q_2^{1/2}), \tag{3.23}$$

where $q_2 = k^2 \, 10 \, d_3 \, d_1^{-2} = 10 \, A \, (1 + k) = O \, (10^{-9})$. This approximation improves with decreasing q_2 which can happen by decreasing k or G^* or by increasing C_∞. Therefore, as $q_2 \to 0$ we have $V_{*_a} \to (k \, B)^{-1}$. We note the similarity of Eq. (3.23) to Eq. (3.12).

The wavelength behavior in the vicinity of V_{*_a} is investigated in the same manner as before. We let $V = V_{*_a} + \delta_V$ and $\lambda = \lambda_{*_a} + \delta_\lambda$ in Eq. (3.21a), where $\delta_V \ll V_{*_a}$, and $\delta_\lambda \ll \lambda_{*_a}$. When linearizing in δ, using Eq. (3.21b), and noticing that $\delta^{1/2} \gg \delta$ we obtain

$$(\lambda - \lambda_{*_a}) = C_a \, (V - V_{*_a})^{1/2}, \tag{3.24}$$

where $C_a = \left[(16 \, \lambda_{*_a}^2 \, V_{*_a}^4 \,)/[6 \, (d_2 \, B)^2 \, V_{*_a}^3 - 10 \, d_1 \, d_2 \, B \, V_{*_a}^2 + 4 \, d_2^2 \, V_{*_a} - 12 \, d_3 \,] \right]^{-1/2}$, and $C_a^2 < 0$. Therefore, the wavelength-velocity behavior near absolute stability has the same simple power law dependence as that near critical instability, Eq. (3.13), in the long-wave limit.

By rescaling the frozen-field system using Eq. (3.14) Brattkus and Davis (1988) derive a strongly non-linear evolution equation for the interface deflection which predicts supercriti-

cal bifurcation (sections 1.5 and 3.4) to cells near absolute stability. From the above analysis we have shown that the range of supercritical bifurcation is $2/3 < V /(k \ B)^{-1} < 1$ or $2/3 < k \ \Gamma < 1$. It is interesting to note that their evolution equation contains derivatives that are second order time which arise because Eq. (3.15) is quadratic in $\dot{\sigma}$.

The discrepency between the results obtained with the different sets of variables arises from the fact that when the only dimensional control variable is V, a three-dimensional surface in the nondimensional variables is a curve in the dimensional variables. Therefore, calculation of the extreme points of the nondimensional curves is tantamount to looking for maxima and minima with side conditions. The long-wave behavior near the critical and absolute stability points can be characterized by a relationship like

$$(\lambda - \lambda_*) = C \ (V - V_*)^{\eta}, \tag{3.25}$$

where $\eta = 1/2$, and the wavelength selection will in general be defined for a narrow range of the system control parameters.

3.3.3 Behavior in the Experimental Regime

In the NaCl-H$_2$O system, in terms of V, the experimental data lie 'between' the constitutional undercooling and absolute stability limits, in the short-wave region of the neutral curve (Fig. 3.1). Consider the dispersion relation for the full solidification system, Eq. (2.37), at neutral stability as follows;

$$0 = M \ R \ (1 + n) / (R + k) - (2 \ G_L + l) - a^2 M \ \Gamma \ (1 + n). \tag{3.26}$$

For $a^2 \gg 1$, $(1 + 4a^2)^{1/2} \approx 2 \ a$ giving

$$0 = a^2 (a + k) \Gamma + (a + k) M^{-1} - a. \tag{3.27}$$

Of the two short-wave limits; $a^2 \gg 1 \gg k$ and $a^2 \gg k \gg 1$, only the former is of physical interest for a system in which the magnitude of the solidus is greater than that of the liquidus, that is, when $k < 1$. The former limit results in

$$a^2 = \Gamma^{-1} (1 - M^{-1}), \tag{3.28}$$

In the experimental velocity range where the neutral curve (Fig. 3.1a) is straight we have M^{-1} = $O(10^{-2})$, so that $a^2 \approx \Gamma^{-1}$. This results in a velocity dependence of the dimensional neutral wavelength of

$$\lambda = S_1 V^{-1/2}, \tag{3.29}$$

where $S_1 = 2 \pi D \ B^{1/2} = $ $O(10^{-8})$ for $k = 0.3$. The power law dependence, $\lambda \propto V^{-1/2}$, is consistent with the experimental dependence (Weeks and Lofgren, 1969). We note that application of the long-wave limit $k \ll a^2 \ll 1$ to Eq. (2.37) gives the same scaling as that in Eq. (3.29) when $M^{-1} = O(10^{-2})$. Thus, on a qualitative level Eq. (3.29) is consistent with the parallel nature of the long and short-wave branches above critical.

3.3.4 Related Wavelength Behavior

For dilute systems above critical, pure systems and eutectics, the experimentally observed wavelength scales as $V^{-1/2}$ (Hunt and Chilton 1963, Langer 1987 and Kessler and Levine 1989, Kassner and Misbah 1991). Langer (1987) has shown that the symmetric model of directional solidification yields a characteristic stability length $\lambda_s = 2 \pi (d_o \ l_D)^{1/2}$ that is the geometric mean of the capillary length $d_o = \gamma c \ T_m / L^2$, where c is the specific heat,

and a diffusion length $l_D = 2D/V$. This results in the $\lambda \propto V^{-1/2}$, scaling. This mixing of two disparate length scales is thought to be at the root of the soft instability near critical.

Kassner and Misbah (1991) study eutectic growth and on the basis of scaling arguments they find

$$\lambda = f \ (l_D/l_T) \ V^{-\eta}, \tag{3.30}$$

where $\eta = 1/2$ and $l_T = m \ \Delta C/G_L'$ is a thermal length in which ΔC is the miscibility gap, which is the concentration difference between the two phases at the interface. As in the relations derived above (Eqs. 3.6 and 3.18) the actual behavior of the selected wavelength cannot be determined until the V dependence of f is determined. Kassner and Misbah (1991) were able to compute f as a function of V and found that it increases with V, and saturates at large V. Therefore, at large values of V, $\lambda \sim const \ V^{-1/2}$ which is consistent with experiments. At smaller V they found a steep value of $\partial f/\partial V$ giving significant deviation from the $\lambda \sim const \ V^{-1/2}$ behavior. They represent this as $\lambda \sim V^{-\eta(V)}$, where $\eta(V) < 1/2$. In their case, this is the easiest approach since f must be determined numerically.

It has been noted (Kessler and Levine 1989, and Brattkus and Misbah 1990) that on the long wavelength branch of the Eckhaus band, at sufficiently high velocities, the symmetric model scales as $\lambda \sim V^{-1/2}$, consistent with experiments and similar to the behavior of the hydrodynamic Taylor-Couette system. This is in the same regime as that for which Eq. (3.29) was derived.

If one desires a power law relation between V and λ in order to extract a more simple physical interpretation of wavelength selection, then one may be 'artificially' imposed on the theory. For curves like (3.6) and (3.18), where the functional form of λ is known, one may

determine the cofactor say c, and the exponent say η_c, such that $\partial I/\partial c = 0$ and $\partial I/\partial \eta_c = 0$ where

$$I = \int\limits_{V_1}^{V_2} dV \, (\lambda - c \, V^{-\eta_c})^2. \tag{3.31}$$

In case of Eqs. (3.6a) and (3.18b) the indefinite integral is nontrivial. In the case of (3.30) the integral cannot be performed since the functional form of f is not known, which is, of course, why Kassner and Misbah (1991) had to compute it numerically. Even in the case where the analytic form of f is known (as in Eqs. 3.6a and 3.18b) and the indefinite integral is tractable it must still be calculated for velocity ranges over which $\partial f/\partial V$ is large. Thus, it seems that theoretical situation is not much improved over that of Kassner and Misbah (1991) in that numerical tabulation is necessary in both cases.

It is worth noting at this juncture that an asymptotic theory that gives rise to a reduction of the dimensionality of the dispersion relation (as in the small k, $M \approx 1$ limit giving Eq. 3.3) will result in significant differences in the topological structure of the neutral solutions as compared to the exact theory. It is possible that a reduction in dimensionality can mediate mode softening so that the frozen-field system will present a different degree of 'softness' than the full system. This is the subject of chapter 5.

3.4 The V (C_∞) Neutral Plane and Weakly Nonlinear Results

Once the planar interface breaks down, cellular structure of *finite amplitude* will eventually appear. Therefore, it is possible that the cells observed will bear little resemblance to the infinitesimal disturbance that the linear theory predicts as being the most unstable. In order

to understand what happens to the interface after the onset of instability, it is necessary to perform a non-linear analysis. The approach used here is standard in hydrodynamics (e.g., Eckhaus 1965, Drazin and Reid 1981). It was first modified for the non-symmetric zero latent heat model (Wollkind and Segal, 1970), and has been used in other approximations to the directional solidification system (reviewed by Langer 1980, 1987). The inclusion of latent heat in the non-linear analysis of the non-symmetric system has important consequences which have been pointed out by Alexander et al., (1986) and Merchant and Davis (1989a). I outline the procedure here, and apply the central result to the H_2O-NaCl system.

We consider what happens to a disturbance that has the same spatial dependence as those of the linear theory, but an unknown amplitude, $A(t)$. This is done by positing solutions to equations (2.12)-(2.17) of the form

$$X(x,z,t) = X_o(z) + \sum_{m=1}^{\infty} X_m(x,z,t) , \qquad (3.32)$$

$$= X_o(z) + \sum_{m=1}^{\infty} \varepsilon^m A^m(t) X_m(x,z) ,$$

where $X(x,z,t) = [C(x,z,t), T_L(x,z,t), T_S(x,z,t), \varepsilon \, \hat{h}(x,t)]$, and the $X_0(z)$ are the base states, $[C(z), T_L(z), T_S(z), 0]$ (see Eq. (2.20)), of the linear analysis. The small parameter is $\varepsilon \equiv (max \mid \hat{h}(x,t) \mid) \, V/D$, and the complex disturbance amplitudes are $A^m(t)$. For $m \geq 1$, Alexander et al., (1986) write the $X_m(x,z,t)$ as

$$X_1(x,z,t) = A(t) X_{10}(z) \exp(i \, a \, x) + A^*(t) X_{01}(z) \exp(-i \, a \, x), \qquad (3.33a)$$

$$X_2(x,z,t) = A^2(t) X_{20}(z) \exp(2 \, i \, a \, x) + 2 \mid A(t) \mid^2 X_{11}(z) + \qquad (3.33b)$$

$$A^{*\,2}(t)\; X_{02}(z)\; \exp\left(-2\,i\;a\;x\right),$$

$$X_3(x,z,t) = A^3(t)\; X_{30}(z)\; \exp\left(3\,i\;a\;x\right) + A(t)\; |A(t)|^2\; X_{21}(z)\; \exp\left(i\;a\;x\right) + \qquad \text{(3.33c)}$$

$$A^*(t)\; |A(t)|^2\; X_{12}(z)\; \exp\left(-i\;a\;x\right) + A^{*\,3}(t)\; X_{03}(z)\; \exp\left(-3\,i\;a\;x\right),$$

where $X_{pq} = X^*_{qp}$. The first harmonic is represented by Eq. (3.33a), and describes the primary wave of the instability. The terms $A^n(t)\, X_{n0}(z)\, \exp\left(n\,i\,a\,x\right)$ and $A^{*\,n}(t)\, X_{0n}(z)\, \exp\left(-n\,i\,a\,x\right)$, for $n \geq 2$, are the second, third, etc., harmonics. The mean state response is given by the term $2\, |A(t)|^2\, X_{11}(z)$ and bears this name because it contains no dependence on the horizontal space variable, as is the case with the mean state.

Upon substitution of (3.32) into (2.12), for parameter values very close to critical, one sees that the amplitudes A, A^* obey Landau type equations of the form

$$\frac{\varepsilon}{2}\,\frac{dA}{dt} = \varepsilon\;\sigma\;A \;-\; \varepsilon^3\, b\; A\; |A|^2 + O(\varepsilon^5), \qquad \text{(3.34a)}$$

$$\frac{\varepsilon}{2}\,\frac{dA^*}{dt} = \varepsilon\;\sigma^*\;A^* \;-\; \varepsilon^3\, b^*\; A^*\; |A|^2 + O(\varepsilon^5). \qquad \text{(3.34b)}$$

Here, $\sigma = \sigma_r + i\,\sigma_i$ is the growth rate from the linear theory, and $b = b_r + i\,b_i$ is a coefficient. When multiplying Eq. (3.34a) by $\varepsilon\, A^*$ and Eq. (3.34b) by $\varepsilon\, A$ and adding the results the following equation obtains;

$$\frac{\varepsilon^2}{2}\,\frac{d}{dt}\, |A|^2 = \varepsilon^2\, \sigma_r\; |A|^2 - \varepsilon^4\, b_r\; |A|^4 + O(\varepsilon^6). \qquad \text{(3.35)}$$

This equation describes the weakly non-linear evolution of the primary wave with itself. In addition, expanding the interfacial boundary conditions (2.13)-(2.15) in a Taylor series about $z = \varepsilon\, \hat{h}(x,t)$ up to $O(\varepsilon^3)$ gives a set of differential equations and boundary conditions at each

order in ε. Solving the systems up to $O(\varepsilon^3)$ allows one to determine the coefficient b_r (Alexander et al., 1986). The terms of order ε^2 in Eq. (3.35) are the same order of magnitude as those of order ε^4, as can be seen from a change to the fast time scale $\tau = \varepsilon^2 t$. This results in a standard form of the Landau equation (cf., Eckhaus 1965, Drazin and Reid 1981),

$$\frac{d}{d\tau} \mid A \mid^2 = 2 \sigma_r \mid A \mid^2 - a_1 \mid A \mid^4, \tag{3.36}$$

a truncation of Eq. (3.35) after $O(\varepsilon^4)$. Here, the real part of the linear growth rate is σ_r, and $a_1 \equiv 2 b_r$ is the Landau coefficient. Equation (3.36) will reveal that the non-linear self-interaction of the most unstable mode may generate harmonics, and an altered mean state that can moderate slow exponential growth of that mode. For an initial amplitude of A_o, the solution of Eq. (3.36) is

$$\mid A \mid^2 = A_o^2 \left[\frac{a_1}{2 \sigma_r} A_o^2 + \left(1 - \frac{a_1}{2 \sigma_r} A_o^2 \right) e^{-2 \sigma_r \tau} \right]^{-1}. \tag{3.37}$$

When a_1 is zero, Eq. (3.36) is the evolution equation of the linear theory, so it is the second term on the right hand side that arises from the non-linearity, and the relative signs of σ_r and a_1 determine the manner in which an infinitesimal disturbance evolves. The analysis and derivation of Eqs. (3.36) and (3.37) has an interesting and varied history that is described by Drazin and Reid (1981) and originates from work by Landau in 1944. We detail the relevant behavior for the solidification problem.

If $a_1 > 0$ and $\sigma_r > 0$, then for small times τ, and small initial amplitudes A_o, the exponential term in Eq. (3.37) is very large and we have $\mid A \mid \sim A_o e^{\sigma \tau}$, as in the linear theory. As $\tau \to \infty$, the exponential term becomes very small and we have $\mid A \mid^2 \to 2 \sigma_r/a_1$,

independent of the size of the initial amplitude. Therefore, the system is linearly unstable to disturbances of amplitude A_o, but eventually obtains a cellular structure characterized by the amplitude $A_\epsilon \equiv (2\,\sigma_r/a_1)^{1/2}$, generally referred to as the *equilibrium* cell amplitude. So, the equilibrium cell amplitude, A_ϵ, will evolve slowly as $V \rightarrow V_c^-$, if $a_1 > 0$, when $\sigma_r > 0$. In this case the bifurcation to cells is termed *supercritical*. The basic state is linearly unstable for $V > V_c$, but the interface eventually obtains the equilibrium cell structure, so that the non-linear terms stop the exponential growth of the disturbance.

If $a_1 > 0$ and $\sigma_r < 0$, then as $\tau \rightarrow \infty$ for small initial disturbances A_o, Eq. (3.37) predicts that the perturbation will decay in accord with the linear theory, that is, as $|A| \sim A_o\, e^{\sigma_r \tau}$. This is because the non-linear term in Eq. (3.36) remains small for all time if it is initially small.

If $a_1 < 0$ and $\sigma_r > 0$, then both terms on the right hand side of Eq. (3.37) are positive and $|A|$ blows up, becoming infinite at time $\tau = (1/2\,\sigma_r)\ln[1 - 2\,\sigma_r/a_1\,A_o^2]$. Therefore, finite amplitude solutions do not exist in this case, calling attention to the need for higher order terms on the right hand side of the Landau equation.

If $a_1 < 0$ and $\sigma_r < 0$, then two things can happen, depending on the relative size of the terms on the right hand side of the Landau equation. If $A_o < A_\epsilon$ then $|A| \propto A_o\, A_\epsilon\, e^{\sigma_r \tau}$, vanishing as $\tau \rightarrow \infty$. If $A_o > A_\epsilon$ then $|A| \rightarrow \infty$ as $\tau \rightarrow \tau_* \equiv (-1/2\,\sigma_r)\ln[A_o^2/(A_o^2 - A_\epsilon^2)]$, so that the solution breaks down after finite time. The instability can occur with a finite amplitude greater than A_ϵ, for $0 < \tau < \tau_*$, even though all infinitesimal disturbances are stable. So, the cells will appear abruptly, as the disturbance jumps to a finite amplitude through a what is termed a *subcritical bifurcation*. The breaking of translational symmetry in this system, as

described above, is mathematically analogous to that which occurs in the Rayleigh - Benard system (Drazin and Reid, 1981).

Alexander et al. (1986) compute a_1 from a non-linear analysis of the non-symmetric system with finite latent heat. They found that the non-linear behavior of the disturbance is strongly affected by the inclusion of latent heat as $n \to 1$. Merchant and Davis (1989a) used these results to show that the latent heat effect for SCN-acetone is to extend the region of supercritical bifurcation into experimentally accessible parameter ranges. For $V \approx V_c$, Merchant and Davis (1989a) show that the Landau coefficient can be written in terms of Γ as

$$a_1 \sim \frac{1 - n + (1 + n)/I}{\Gamma\,(1 + n)\,(1 + I^{-1})} + O\left[(4\,k/\,\Gamma\,)^{2/3}\right], \tag{3.38}$$

where

$$I = \frac{(1 + n)\,k_l\,m\,C_\infty\,(k - 1)}{k\,L\,D}. \tag{3.39}$$

The seawater from which natural sea ice forms varies by only a few parts per thousand, so C_∞ is only a control parameter in laboratory experiments. There are two points of interest on the $V\,(C_\infty)$ neutral curve: the limit point and the transition point. The limit point $(V^*,\,C_\infty^*)$, is the minimum neutral C_∞, and the associated V at which the two branches of the curve meet. The transition point separates regions of subcritical and supercritical instability (Merchant and Davis, 1989a). The $V\,(C_\infty)$ neutral curves for $k = 0.3$ and $k = 3.0 \times 10^{-3}$ are shown in Fig. 3.4. The $k = 0.3$ curve is a cross section of Fig. 3.1 at $\lambda = \lambda_c$, and both curves follow from Eq. (2.39) as

$$C_\infty = \Gamma' \left[k + R (R + k + 1) \right] + \frac{1}{M'} (1 + k/R), \qquad (3.40)$$

where $\Gamma' = C_\infty \Gamma$ and $M' = M/C_\infty$. There are two branches to this curve; the high velocity upper branch, above which surface energy stabilizes the effects of solute rejection, corresponding to the absolute stability limit, and the lower branch, below which the thermal fields stabilize the effects of solute rejection, corresponding to the constitutional undercooling limit. Between the upper and lower branches of the curve defined by Eq. (3.40) the planar interface is unstable.

Merchant and Davis (1989a) define the transition point between subcritical and super-critical bifurcation as the point on the neutral curve where $a_1 = 0$. We present the neutral curve in Fig. 3.4 as they did for the SCN-acetone system. The solid curve denotes the region of supercritical bifurcation, and the dashed curve denotes the region of subcritical bifurcation. The value of $C_\infty = 35$ ppt, for which the $V (\lambda)$ neutral curve is drawn, is the vertical dotted line. The H_2O-NaCl system has $n = 3.572$, the neutral curves in Fig. 3.4 do not change when n changes from 3.572 to 1.286. The insensitivity of linear stability results to changes in n has been noted for metal and transparent organic systems (Merchant and Davis, 1989a and Alexander et al., 1986). In contrast, the non-linear results are very sensitive to this change in the value of n for the H_2O-NaCl system. For $n = 3.572$, the entire curve for both values of k is a region of subcritical bifurcation, implying that in naturally occurring sea ice the break-down of the interface will always evolve as a jump transition. Figure 3.4 shows the results when $n = 1.286$, for which the region of supercritical bifurcation extends well into the lower branch of the neutral curve. For $k = 0.3$, the transition point is located at $C_\infty = 8.28$ ppt, $V = 8.52 \times 10^{-8}$cm s^{-1}. For $k = 3.0 \times 10^{-3}$, it is $C_\infty = 5.81 \times 10^{-2}$ ppt, $V = 8.51 \times 10^{-8}$cm s^{-1}.

This is consistent with the observation that the range of stable, small amplitude cells is enhanced at small concentrations as $n \to 1$ in the Al-Cu system (Alexander et al., 1986). For $n = 1.1$, the entire V (C_∞) neutral curve is a region of supercritical bifurcation, where smooth transitions to cells will occur through the slow evolution of infinitesimal disturbances.

It is curious fact that there is a length scale dependence to the stabilizing effect of letting $n \to 1^+$ for the finite latent heat system. The effect of this is to increase the thermal gradient in the solid relative to $L = 0$ and $n > 1$, which is seen when Eq. (2.6) is written in the following form,

$$\frac{L V'}{k_l} = n \ G_S' \ (x',h',t') - G_L' \ (x',h',t'), \tag{3.41}$$

$V' = (V + h'_t)$, and G_S' (x',h',t'), and G_L' (x',h',t'), are the solid and liquid temperature gradients at the interface. For a fixed liquid temperature gradient, the inclusion of latent heat and the decrease in n steepens the thermal gradient in the solid. According to the Landau type of weakly non-linear analysis, this stabilizing effect only acts on the finite amplitude disturbances to suppress jump transitions, but infinitesimal disturbances are not damped (Alexander et al., 1986). This clearly suggests a scale dependence of the stabilizing effect of increasing G_S' at the interface. In examining the $n \to 1^-$, $L \neq 0$ case which has the same effect of steepening G_S', Alexander et al. (1986) also find that small amplitude cells close to critical are favored. When $n \to 1^+$ for fixed G_L', the increase in G_S' relative to its value at larger n has a stabilizing effect which tends to remove the disturbance minima by freezing.

In this case, the question Alexander et al. (1986) posed about the relation between thermal symmetry ($n = 1$ being the most symmetric) and weakly non-linear stability may be

stated as: Why is the steepening of the thermal gradient in the solid when $n \to 1^\pm$, in the finite latent heat system, only effective in suppressing subcritical bifurcations? The answer is based on the physical interpretation of the evolution of subcritical versus supercritical bifurcations. If we view subcritical bifurcations as true jump transitions from the planar state to a state of finite amplitude (A_e) cells, and supercritical bifurcations as a slow continuous evolution to this state from an infinitesimal disturbance, then we can qualitatively distinguish the two types of bifurcations based primarily on amplitude near $V = V_c$. The scale dependence is the result of the relative undercooling that is felt by various disturbances. At critical, the base state increase in G_S' associated with a decrease in n from n_1 to n_2 can be written as

$$\Delta G_S' = \left[\frac{L \, V_c}{k_l} + G_L' \right] \left[\frac{1}{n_2} - \frac{1}{n_1} \right]. \tag{3.42}$$

If $n_1 = 3.572$ and $n_2 = 1.286$, and if we fix $G_L' = 3.57 \times 10^{-2}$ K cm $^{-1}$ when $k = 0.3$, then $V_c = 1.907 \times 10^{-8}$ cm s^{-1} and $\Delta G_S' = 0.018$ K cm $^{-1}$. Therefore, a perturbation of amplitude $A_a = 0.1$ cm will experience a decrease in temperature of approximately $\delta T'_a = 0.002$ K at its minima, compared with the case when $n = n_1$. The total temperature depression from the planar state at the minima of A_a is $\delta T_a = 2.83 \times 10^{-3}$ K. A slowly evolving disturbance of amplitude $A_b = 0.001$ cm will experience a decrease in temperature of only about $\delta T'_b = 0.00002$ K at its minima. The total temperature depression at the minima of A_b is $\delta T_b = 2.83 \times 10^{-5}$ K.

If we view these temperature depressions as effective undercoolings from the planar $n = n_1$ state then we can construct a more intuitive interpretation of this scale dependent stabilization. We approximate the liquid region between the perturbation minima and $z = 0$ as a

sphere of fluid undercooled by the $\delta T_{a,b}$ computed above. Now we can compare the stabilization of different perturbation minima by examining the relative thermodynamic potential for freezing of this spherical region. The critical radius of nucleation for the region enclosed by the large amplitude perturbation is $R^*_a \simeq A_a/2$ and that for the small amplitude perturbation is $R^*_b \simeq A_b/2$. We ask how the undercooling $\delta T_{a,b}$ due to the steepening of the temperature gradient of the solid compares to that needed to freeze a sphere of radius $R^*_{a,b}$. The critical values are $\delta T^*_a(R^*_a) \simeq 1.18 \times 10^{-4}$ K $\ll \delta T_a$ and $\delta T^*_b(R^*_b) \simeq 1.18 \times 10^{-2}$ K $\gg \delta T_b$ so that the driving force to freeze back the large (small) amplitude minima is sufficient (insufficient). There is a crossover at which $R^* = R^*_c = O(10^{-2})$ cm and $\delta T = \delta T^*_c$ so that if $\delta T \gg \delta T^*_c$ ($\delta T \ll \delta T^*_c$), the planar interface will be stable (unstable) to perturbations with amplitude $A \gg R^*_c$ ($A \ll R^*_c$). This is one explanation of why the steepening of the thermal gradient in the solid has a negligible effect on the results of the linear theory.

The n-dependent stabilization suggests that in some systems there will be a crystallographically preferred stable growth direction. It is well known, for example, that ice has about a five percent greater thermal conductivity parallel to the c-axis which translates to a five percent decrease in n normal to the c-axis. Differences of a factor of about two would be necessary to result in a crystallographic/orientational supression or enhancement of subcritical bifurcations.
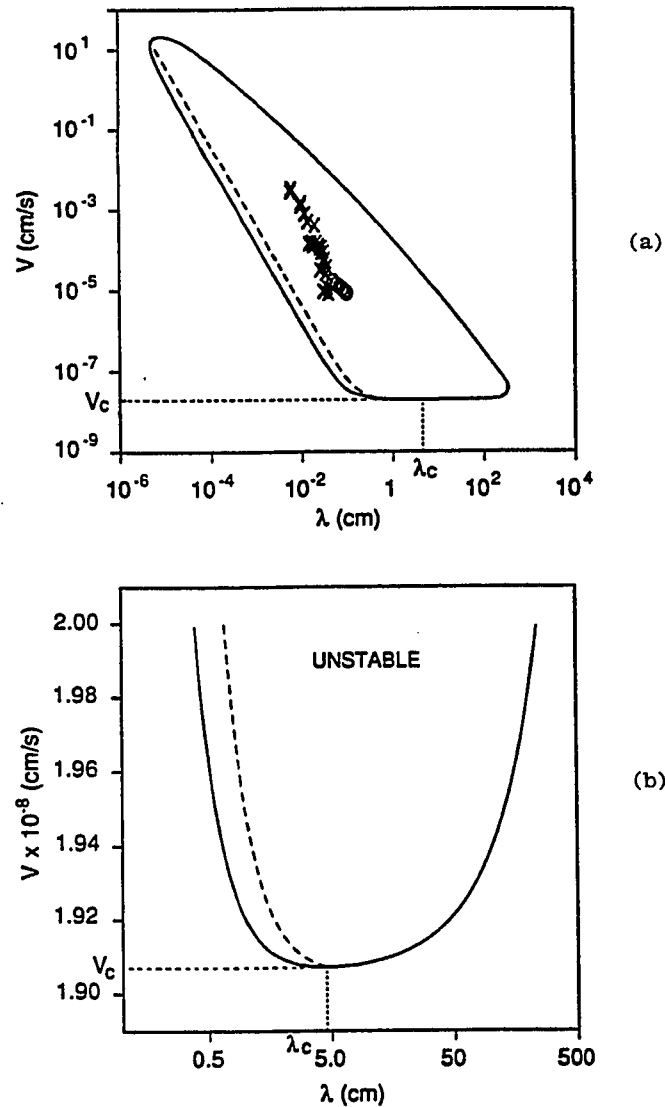
Fig. 3.1 The $V(\lambda)$ neutral stability curve, with $C_\infty = 35$ ppt and $G_L' = 3.57$ K m^{-1} for $k = 0.3$. The planar interface is unstable inside the curve. 3(a) has the full instability range of the system. The data points are the platelet spacing from Lofgren and Weeks (1969) and Nakawo and Sinha (1984) (see p. 41 for discussion). The dashed line is the low velocity approximation to the most unstable wavelength. A robust upper and lower bound on observable sea ice growth rates is 10^{-4} cm s$^{-1} \approx 10^{2}$ cm day^{-1}, and 10^{-7} cm s$^{-1} \approx 10^{-2}$ cm day^{-1}. 3(b) is the neutral curve near critical $V_c(\lambda_c)$.
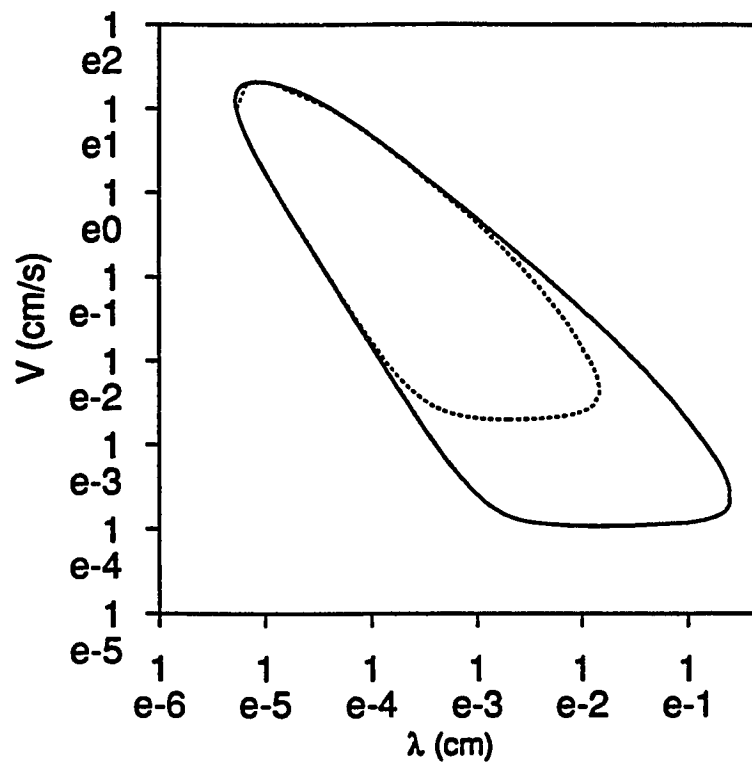
Fig. 3.2 Neutral stability curve in the $V(\lambda)$ plane for $G_L{}' = 200$ K cm^{-1} (solid line) and $G_L{}' = 3570$ K cm^{-1} (dotted line). $C_\infty = 35$ ppt and $k = 0.3$. Note the increase in the critical velocity with increasing $G_L{}'$ and the insensitivity of absolute stability to increasing $G_L{}'$. (See p. 42 - 45 for discussion).
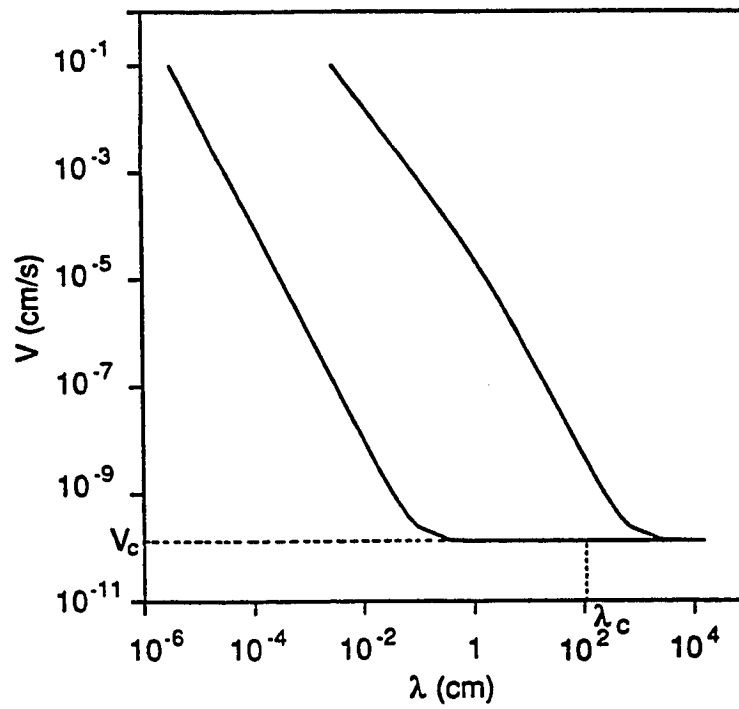
Fig. 3.3 Neutral stability curve in the $V(\lambda)$ plane for $C_\infty = 35$ ppt, $G_L' = 3.57$ K m^{-1} and k = 3.0 x 10^{-3}. The increase of λ_c with the decrease in k is qualitatively consistent with the local theory in this limit (Sivashinsky 1983), but for this system predicts an unphysical value of V_c. (See p. 51 for discussion)
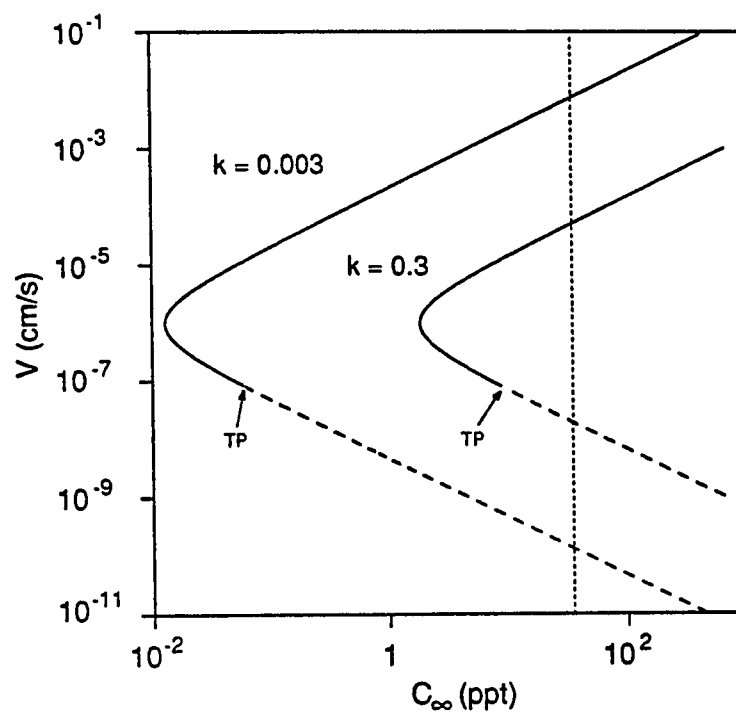
Fig. 3.4 Neutral stability curves in the $V(C_\infty)$ plane. The curve for $k = 0.3$ is a cross section of Fig. 3.1 at $\lambda = \lambda_c$ and is combined with the curve for $k = 0.3 \times 10^{-3}$. The dotted vertical line is $C_\infty = 35$ ppt and n = 1.286. The transition point (TP) divides regions of subcritical bifurcation (dashed line) from regions of supercritical bifurcation (solid line). (See pp. 59 - 68 for discussion).

CHAPTER 4

COMPARISON WITH DIFFERENT SCALES

In order to isolate the control parameters V and C_∞, Merchant and Davis (1989b) defined different length and time scales. These scales are $\delta_l = (\gamma\, T_m\, /\, L\, G_L')^{1/2}$ and $\delta_t = \gamma\, T_m\, /\, L\, G_L'\, D$, where all quantities are defined as previously, and the subscripts l, t denote length and time. When scaling the solidification system with these length and time scales the control parameters become

$$V_{md}^{\,2} = \frac{\gamma\, T_m\, V^2}{L\, G_L'\, D^2} \, ,$$

(4.1a)

$$C_{md}^{\,2} = \frac{m^2\, (k-1)^2\, L\, C_\infty}{k^2\, G_L'\, \gamma\, T_m} \, ,$$

(4.1b)

and

$$l_{md}^{\,2} = \frac{L^3\, D^2}{k_l^{\,2}\, G_L'\, T_m\, \gamma} \, ,$$

(4.1c)

which represent the mean velocity of the interface, the concentration of solute and the latent heat respectively. These parameters are the cursive V, C and l in Merchant and Davis (1989b). Their motivation in deriving these parameters was to construct a theory which more closely mirrors the underlying experimental situation. The dimensionless parameters M and Γ, measure the degree of constitutional undercooling and the importance of surface tension respectively. However, M and Γ contain both of the experimental control parameters V and C_∞, which does not allow an intuitive connection with experiment. The linear analysis of

Merchant and Davis (1989b) yields a characteristic equation (Eq. (2.4a) in Merchant and Davis (1989b)) which is an implicit function of the growth rate σ, and plays the same role as Eq. (2.37). At neutral stability, we derive the following expression similar to Eq. (2.39), which is a function of the parameters in Eq. (4.1),

$$\eta^3 + \eta^2 V_{md} (1 + k) + \eta \left[\frac{2 + l \, V_{md}}{(1 + n)} + V_{md} (k \, V_{md} - C) \right]$$

$$+ \frac{k \, V_{md} (2 + l \, V_{md})}{(1 + n)} = 0. \tag{4.2}$$

Here $\eta^2 + \eta \, V_{md} = a^2$ is a wavenumber parameter, and a is the spatial wavenumber of the perturbation. The entire V_{md} (η) neutral plane, and the region close to critical for the H$_2$O-NaCl system are shown in Fig. 4.1 and Fig. 4.2(a). The critical region of the $M(R)$ neutral plane is shown in Fig. 4.2(b) for comparison with the V_{md} (η) results. The full plane in Fig. 4.1 is qualitatively similar to the dimensional results shown in Fig. 3.1(a), with a mirror reflection since η is proportional to wavenumber. A comparison of Figs. 4.2(a) and 4.2(b) shows that in both systems there is weak wavelength selection near critical, but it is more pronounced in the V_{md} (η) plane. This is clearly a result of the sensitivity of these parameters to the mean interfacial velocity V. The parameter V_{md} is less sensitive to changes in V than the parameter M, primarily because V appears in the numerator of M and in the denominator as G^*. The difference in sensitivity can be seen explicitly by examining the behavior of these parameters near $V = V_c$. The first order term in the expansion of $\frac{\partial M}{\partial V}$ about $V = V_c$ is

$$\frac{\partial M}{\partial V} \sim \frac{m \, C_\infty \, (k - 1) \, (1 + n) \, 2 \, G_L{}'}{D \, k \, (2 \, G_L{}' + L \, V_c \, /k_l)^2} = O(10^9), \tag{4.3a}$$

and

$$\frac{\partial V_{md}}{\partial V} = \left[\frac{\gamma T_m}{L \ G_L{'} D^2}\right]^{1/2} = O(10^5).$$ (4.3b)

Therefore, $\frac{\partial M}{\partial V} \approx 10^4 \ \frac{\partial V_{md}}{\partial V}$, which is evident when one compares the horizontal axes of Fig. 4.2(a) and Fig. 4.2(b) close to critical. Of course, this is a theoretical sensitivity and ultimately only aids one in the choice of which theory to use when attempting to identify a critical wavelength. The experimenter must still measure V. For the case of $k = 0.3$, (Fig. 3.1) a change in velocity V, near critical of only 1 part in 10^{-11} cm s^{-1} results in a change in neutral wavelength of greater than an order of magnitude. Here, the sensitivity corresponds to growth rates of order μ m year^{-1}, making these effects experimentally inaccessible.

The problem of weak wavelength selection may of course be a more phenomenological one based on the inherent assumption, in a linear theory of this type, that there exists a unique, discrete, most unstable mode which manifests itself as λ_c. Since the normal modes are continuously dependent on a, the single mode picked by the linear theory is only infinitesimally more unstable than its neighbors. Thus, the flatness of the neutral curve may be a mask of critical behavior in which there is a wavepacket of most unstable modes rather than a single most unstable mode. This is common in the linear analyses of unbounded hydrodynamic stability problems (Drazin and Reid, 1981). Secondary bifurcations for V very close to V_c, which manifest themselves in terms of a flat neutral curve, can either be caused by mode interactions which arise when constraining the system in the horizontal or via nonlinear interactions between two adjacent linearly unstable wavelengths (Bennett and Brown, 1989).

Close to absolute stability, the linear theory which results from both scalings of the directional solidification system may be suspect. In both cases, the use of an equilibrium condition at the interface during rapid solidification may be invalid. The solute depression of the freezing point at high velocities may not be adequately accounted for by a locally linear phase diagram. A velocity dependence of the interfacial solute concentration may be needed to account for departures from equilibrium. By including a velocity dependent segregation coefficient in their linear stability analysis, with zero latent heat, Merchant and Davis (1991) showed that oscillatory instabilities can occur. The velocity independence of the scales $\delta_l = (\gamma\ T_m\ /\ L\ G_L{'})^{1/2}$ and $\delta_t = \gamma\ T_m\ /\ L\ G_L{'}\ D$, during rapid solidification may, for certain systems, also be suspect, as Merchant and Davis (1989b) point out. In order for both δ_l and δ_t, and therefore (4.1bc) to be independent of V, $G_L{'}$ must be independent of V. This assumption is equivalent to the assumption that there is no curvature in the liquid temperature field of close to the interface. In the case of a laboratory experiment, one has the freedom to remove the local curvature by decreasing the vertical dimension of the experimental box L, so that it is within the linear region of the thermal field, i.e., $L \ll \kappa_L/V$. For very high velocities, this may be an impossible experimental configuration. In the case of natural solidification one does not have the ability to vary L, so the assumption must be satisfied by some other constraint. If there is to be no curvature in the thermal field close to the interface, then thermal gradients must diffuse away in a time scale which is smaller than that associated with the advance of the interface itself, $\tau_d \ll \tau_i$. The subscripts d, i denote the diffusion field and the interface. The diffusion field decays a distance $\xi^d = \kappa_L/V$, in τ_d, and the interface advances a distance $\xi^i = \tau_i V$, at the same velocity V. Therefore, the constraint which must be satisfied for the capillary scales to be velocity independent is

$\xi^i \ll \xi^d$. We examine this condition at critical (c), and absolute (a) stability for the H$_2$O-NaCl system. At critical $\xi^i_c = O(10^{-13}\ \xi^d_c)$, but at absolute stability $\xi^i_a = O(10^8\ \xi^d_a)$, so that the quantitative predictions of Eq. (4.2) are of little use for this system operating near absolute stability. The violation of the curvature constraint at absolute stability is not this severe for the SCN-acetone system that Merchant and Davis[14] studied, in which $\xi^i_a = O(\ \xi^d_a)$. However, in an Al-Cu alloy in which $\kappa_a = 5.0 \times 10^{-5}\ cm^2\ s^{-1}$, and $V_a = 11.42\ cm\ s^{-1}$, we have $\xi^i_a = O\ (10^6\ \xi^d_a)$. Therefore, scaling a system with the capillary scales has the advantage of more closely mirroring the underlying experiment, but for some systems predictions close to absolute stability are not reliable.
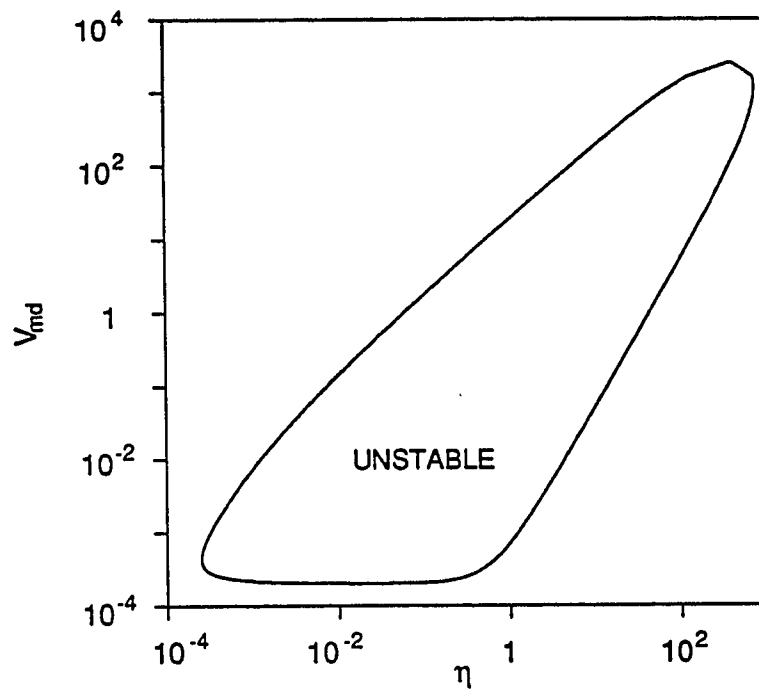
Fig. 4.1 The $V_{md}(\eta)$ neutral curve constructed from the linear theory of Merchant and Davis (1989b), in which the length and time scales are assumed to be velocity independent. Here $C_\infty = 35$ ppt and $G_L' = 3.57$ K m^{-1} for $k = 0.3$. The qualitative comparison is good with the exception of the region near absolute stability (see pp. 73 - 77 for discussion).
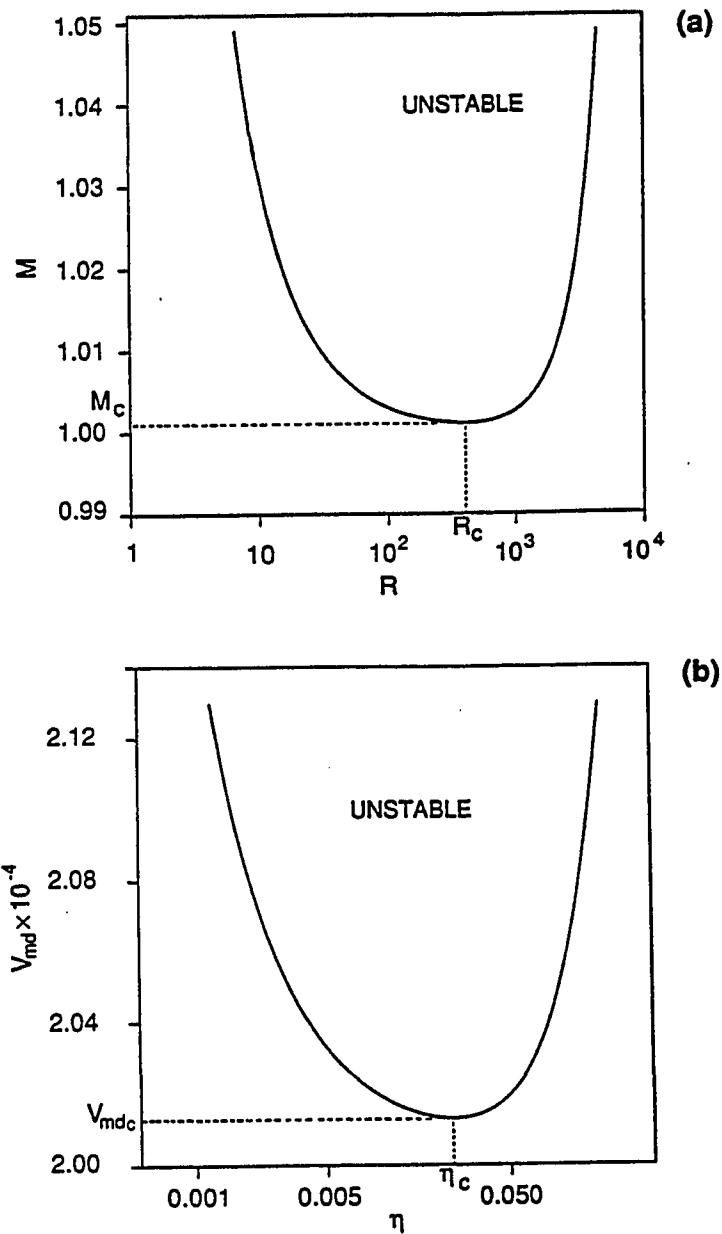
Fig. 4.2 The $M(R)$ (a) and $V_{md}(\eta)$ (b) neutral curves near critical. The former curve is sharper near critical due to the stronger dependence on the underlying control V (see discussion pp. 73 - 77).

CHAPTER 5

SURFACE OF NEUTRAL STABILITY

5.1 *The Bifurcation Problem and Unfoldings*

We have shown that the linear stability analyses based on two types of length and time scales exhibit weak wavelength selection in the nondimensional neutral curves. As discussed in the previous section, this effect can be thought of as either a diagnostic of the non-linear behavior of the system near critical, or as a different type of linear instability. For particular systems, (Bennett and Brown, 1989; Merchant and Davis, 1989a) the former argument has been made to point out the more limited utility of a linear analysis in making predictions near critical. In some systems, the predictions of linear theory may be enhanced if n is close to unity, so that the range of subcritical bifurcation is suppressed. Although wavelength selection is not strengthened in the limit $n \rightarrow 1^{\pm}$, the validity of linear results is extended. We will show (a) the origin of the wavelength selection problem within this type linear theory and (b) that even in systems in which weak wavelength selection is a prominent feature of the linear analysis, the predictive utility of the analysis can be extended by a transformation into a different neutral surface. The rudiments of the theory within which we view this problem are outlined briefly below.

The study of equations with multiple solutions is generally called bifurcation theory. (Golubitsky and Schaeffer 1985). A *bifurcation* occurs when the number of solutions changes as a parameter varies, as is the case when V passes through the values V_c or V_a. In

the third chapter we analyzed bifurcations in terms of a Landau equation, here we follow a different method; the singularity theory approach of Golubitsky and Schaeffer (1985). Using this approach, problems concerning multiple solutions can be reduced to an investigation of a single scalar equation of the form

$$g(x,\alpha) = 0. \tag{5.0a}$$

The investigation focuses on how the solutions x change as one varies the parameter α. The unknown x is the *state variable* and α is the *bifurcation parameter*. The set of (x,α) satisfying Eq. (5.0a) is called the *bifurcation diagram* or *solution set* of g. Of course, in many cases it is a non-trivial task to reduce the set of equations that describe a particular problem into the form of Eq. (5.0a). The technique employed is called Liapunov-Schmidt reduction. The Liapunov-Schmidt reduction shows that locally, the solutions to a system of n equations (n can be infinite) can be put in one-to-one correspondence with the solutions of a k-parameter family of bifurcation problems, $g(x,\xi) = 0$, where $\xi = (\xi_0, \ldots, \xi_k)$ is a vector of parameters. Generally, we think of ξ_0 as a bifurcation parameter α, and $\xi_1, \ldots, \xi_k$ as auxiliary parameters. Each of these equations has the form of Eq. (5.0a). In many systems this technique is required in order to make progress, fortunately it is not called for in our application. *Singularity theory* focuses on the qualitative properties of equations like (5.0a), defining precisely the conditions in which two such equations and their bifurcation diagrams are qualitatively similar.

The primary concept of singularity theory that we utilize is that of an *unfolding* of g. We generalize Eq. (5.0a) to a k-parameter family of equations of the form

$$G(x,\alpha,\beta) = 0, \tag{5.0b}$$

where $\beta = (\beta_0, \ldots, \beta_k)$ are auxiliary parameters. If for $\beta = 0$

$$G(x,\alpha,0) = g(x,\alpha), \tag{5.0c}$$

then G is defined as an *unfolding* of g. We may think of $G(x,\alpha,\beta)$ as a perturbation of $g(x,\alpha)$ since $G(x,\alpha,\beta) = g(x,\alpha) + [\ G(x,\alpha,\beta) - G(x,\alpha,0)\ ]$. A *universal unfolding* of g is a k-parameter family of functions, $G(x,\alpha,\beta)$, that satisfies Eq. (5.0c) and the following constraint; for any small perturbation p, there exists a value of β such that $g + p$ is equivalent to $G(x,\alpha,\beta)$. This is like saying that G contains all small perturbations of g. The *codimension* of g is defined as the number of parameters required in a universal unfolding of g. Here, we show how the neutral solutions to the solidification equations are equivalent to the bifurcation diagram of an equation of the form of Eq. (5.0a).

5.2 *The Neutral Solution Surface*

We can rewrite equation (2.39) as

$$g = R^3 + p\ R^2 + q\ R + r = 0, \tag{5.1}$$

where

$$p = (1 + k) \tag{5.1a}$$

$$q = \frac{1}{\Gamma}\left[\ k\ \Gamma + \frac{1}{M} - 1\right] \tag{5.1b}$$

and

$$r = \frac{k}{M\ \Gamma}.$$

<div align="right">(5.1c)</div>

This cubic polynomial has a finite positive intercept for all values of the coefficients. For $R > 0$, it is a monotonically increasing function of R for all k, M, Γ when $q > 0$. The quadratic term can be removed from the polynomial by letting $R = x - p/3$, which gives the bifurcation problem that defines the neutral trajectory mentioned in the first section,

$$f = x^3 + \alpha\ x + \beta = 0,$$

<div align="right">(5.2)</div>

where $\alpha = \frac{1}{3}(3\ q - p^2)$ and $\beta = \frac{1}{27}(2\ p^3 - 9\ p\ q + 27\ r)$ depend on the underlying control parameter V. The qualitative features of the bifurcation problems for f and g do not change under this equivalence transformation. The function f is a universal unfolding of the cuspoid normal form $N = x^m$ ($m = 3$), and has been studied in the context of catastrophe (Poston and Stewart 1978; Thorndike et al. 1978), singularity and bifurcation (Golubitsky and Schaeffer, 1985) theories.

In this context, we must consider two unfoldings of N; f as in Eq. (5.2) and $f_2(x, A, B)$, a more general two-parameter unfolding,

$$f_2 = x^3 + A\ x + B = 0,$$

<div align="right">(5.3)</div>

in which A and B are not slaved to one control parameter, and A is not to be confused with the complex amplitude of Eq. (3.36). The solution set of Eq. (5.3) forms the surface shown in of Fig. 5.1(a). We define $F_2 = \{(x, A, B) \text{ s.t. } f_2 = 0\}$ as the *neutral solution surface* since everywhere on the surface the base states, Eqs. (2.20), are neutrally stable. One might also refer to it as the perturbed neutral solution surface.

The various sheets of the surface illustrate the root structure of Eq. (5.3). In Fig. 5.1(b) the points of F_2 are projected onto the plane of control parameters $T(A, B)$,

$$\pi : F_2 \mapsto T \Leftrightarrow (x, A, B) \mapsto (A, B).$$

The points that satisfy $f_2 = \partial_x f_2 = 0$ are given by the equation

$$D = 4 A^3 + 27 B^2 = 0, \tag{5.4}$$

which is a semicubical parabola and defines the *bifurcation set S* of Eq. (5.3), where the tangent plane to the *neutral solution surface* is perpendicular to the control plane (Poston and Stewart 1978; Golubitsky and Schaeffer 1985). So, the projections of the folds in F_2 into T are the folds in T, defined by S. As (A, B) pass through S, into the interior of the cusp region (Fig. 5.1b), the root structure of Eq. (5.3) changes from one real and two complex conjugate roots, to three real roots. Two real roots meet along S and three real roots meet at the cusp point $A = B = 0$. Looking up in the x-direction, from a point (A', B') in T one might see three layers of the surface F_2, or just one, corresponding to the number of points on F_2 which have the value (A', B'). Each point defined by $D = 0$ is a *degenerate singular point*, since $f_2 = \partial_x f_2 = 0$ at these points (Poston and Stewart 1978; Golubitsky and Schaeffer 1985).

The problem that describes the solidification system proper, Eq. 5.2, results from the interpretation of f as a one-parameter unfolding of N; $f(x, \alpha, \beta)$ in which we have $(\alpha, \beta) = [A(V), B(V)] \subset (A, B)$ as parameters that depend on the same underlying control. We define $F = \{(x, \alpha, \beta) \text{ s.t. } f = 0\}$ as the *neutral solution trajectory* since everywhere along this path the base states are neutrally stable. F is a closed set, determined by the range

of growth velocity that is physically accessible to a particular system, so there are only a finite number of points in S where $f = \partial_x f = 0$. Simply put, F_2 is a surface; A and B vary independently, and F is a section of the surface that can be formed by the curve (α, β) in A,B space. We will see that the closedness of a neutral curve defined by $F \cap F_2$ depends on this number. Since $F \subset F_2$, then $F \cap F_2 = F$, so in practice, we are primarily interested in determining F. Here we are using V as the underlying bifurcation parameter, and fixing C_∞. By varying C_∞, we can obtain a family of trajectories F_k, which will form paths on F_2. The universal unfolding theorem and the recognition problem for the cuspoid normal form are presented in detail by Golubitsky and Schaeffer (1985), with a plethora of examples. They prove that the universal unfoldings of all bifurcation problems $G(x, A, B)$ that satisfy $G(x,0,0) = x^3$, may be written as parametrized families of paths through the cusp.

There is only one trajectory, for fixed C_∞ and thermophysical parameters, that is physically accessible to a particular system. This is obtained by determining F. For example, The velocity V constrains α and β to particular values and we can only allow $x > p/3$ since, in this formulation, the concept of a negative wavenumber is of no physical use. So, the surface in Fig. 5.1(a) can be thought of in terms of mathematically and physically allowable points; the entire surface is mathematically allowable given by the solution set F_2, and there are points which are physically accessible defined by the solution set F.

This approach can be used to investigate the qualitative behavior of the solidification equations themselves. The physical controls are the values of α and β that are obtained when varying V through the same range as in the previous examples. One may think of two observers, a mathematical observer that can walk anywhere in T and a physical observer that must remain on a specified path (α, β). In Fig. 5.2, we show the *neutral solution trajectory*

of the H_2O-NaCl system from $V < V_c \Leftrightarrow (\alpha > \alpha_c, \beta > \beta_c)$, to $V > V_a \Leftrightarrow (\alpha > \alpha_a,$ $\beta < \beta_a)$, both in the surface F_2 (Fig. 5.2a) and in the control plane T (Fig. 5.2b). We can think of the bifurcation diagram (in this case a neutral curve) as $F \cap F_2$ or as what is recovered by lifting the trajectory in T to the cusp surface F_2. The trajectory begins at ($\alpha >$ $\alpha_c, \beta > \beta_c$), on the right hand sheet where $x < 0$, so the solutions are unphysical here. At critical (α, β) = (α_c, β_c), the trajectory jumps up to the fold intersecting the surface where the tangent plane is perpendicular to the control plane. Therefore, (x_c, α_c, β_c) is the first bifurcation point in this evolution of the trajectory. As the trajectory moves into the pleated region only the upper fold is of physical interest. Here $x > p/3$ so for each (α, β) there are two x values. In this system it never occurs that $\beta < 0$ in the pleated region, which would result in a break of the neutral curve since $x \leq p/3$ is not allowed. Finally as $\alpha \rightarrow \alpha_a$ and $\beta \rightarrow \beta_a$ the roots coalesce at $x = x_a$ closing the neutral surface (and curve). The trajectory exits the pleated region through the right hand nappe S_1 of the bifurcation set S through which it entered. Then, the system stabilizes since $x \leq p/3$ in the region outside of S. Thus, if a solution trajectory enters the cusp region by crossing through the right hand nappe of the bifurcation set S_1, the neutral curve will be closed if it exits through S_1, and it will be open if it exits through S_2. We can see this by taking a slice of F_2 at constant A and moving B through $B = 0$ and finally through S_2 as shown in Fig. 5.3(a). Even if $x < p/3$ were allowed for a small range of A and B, the trajectory will run off on the upper left hand sheet leaving only one branch to the neutral curve. Two other trajectories and their bifurcation diagrams are shown in Fig. 5.3. If the system were formulated in such a way that only negative wavenumbers were allowed, then a neutral curve would be closed if the trajectory entered and exited through the left hand nappe as shown in Fig 5.3(c).

Near critical, the combination of the standard dimensionless control parameters in α and β results in the α-x neutral curve being sharper than the β-x neutral curve. One interpretation of this behavior is that it is due to the velocity dependences of α and β; $\partial_v |\alpha| > \partial_v \beta \gg \partial_v M$. Figure 5.4 shows the $|\alpha|$-x and β-x neutral curves superposed. Since both α and β are changing as one moves along the trajectory, each interval in one plane corresponds to an interval in the other, and the intervals are gradually approaching the cusp point of F_2 as the absolute stability limit is approached. Both curves are closed since the trajectory leaves the folded region by passing through S_1. Close to critical, the $|\alpha|$-x curve exhibits *relatively* strong wavelength selection, and folds back over itself on this scale. The β-x curve exhibits *relatively* weak wavelength selection at critical, and doesn't have the 'fishlike' structure of the $|\alpha|$-x plane. The curves are qualitatively similar for values of $|\alpha|, \beta < 10^5$. The $|\alpha|$-x plane is more revealing close to critical because α is changing very rapidly but β undergoes very little change for x ranging over more than two orders of magnitude. Since $|\alpha|$ reaches a maximum after its critical value and then turns around to approach α_a (cf., Fig. 5.2(b)), the critical wavenumber is flanked by bands of unstable modes, which are themselves flanked by the upper and lower cutoffs. The upper and lower cutoffs are the surface energy and finite solute interaction range stability limits, but the intermediate bands are an artifact of the turn around of α.

Combined, the following properties result in the the flatness observed in the standard neutral curves. First, the critical bifurcation point occurs on a part of the upper fold that has very little curvature. Second, although not apparent from Fig. 5.2(b) which is scaled for illustrative purposes, in the region very close to the critical bifurcation point, the trajectory is approximately tangent to the fold, or the right hand nappe S_1 of the bifurcation set. The

latter behavior points to weak wavelength selection as being due to a higher order degeneracy near critical. The question of whether this selection mechanism has a real physical origin, or is an artifact of the theory, may be addressed by unfolding the singularity at critical. This is the subject of future work. One suspects that it is the theory that is weak, not nature. After all, nature has no difficulty choosing a scale, and nature obeys the laws of physics.

If the experimenter could measure α directly rather than V, the wavelength selection problem near critical would be eliminated. Since a simple transformation does not remove the physical sensitivities no such victory can be claimed. Rather, this approach gives a qualitative method for investigating the behavior of different systems and extends the utility of the linear theory for predicting cellular structure close to critical. Once the results of a linear theory are cast in the form of Eq. (5.3), an entire rostrum of rich mathematical tools is made available (e.g., Poston and Stewart 1978; Golubitsky and Schaeffer 1985). The structure of the bifurcation points (α_c, β_c) and (α_a, β_a) is worthy of investigation using the techniques of singularity theory. This may provide a method to investigate new types of local asymptotic theories. The zero latent heat system results in trajectories with the same structure as F since excluding L does not change the codimension of the unfolding. In some approximations to the directional solidification system, the dimensionality of the system of equations changes, so the unfolding will be of a different normal form and the behavior of $F \cap F_2$ shown here cannot be reproduced. For example in some limits, the symmetric model of directional solidification does not admit a closed neutral curve since it contains no mechanism to stabilize long-wave perturbations (Langer 1980). The techniques of singularity theory yield the exact number of control parameters required to describe the most general perturbation of a bifurcation problem.
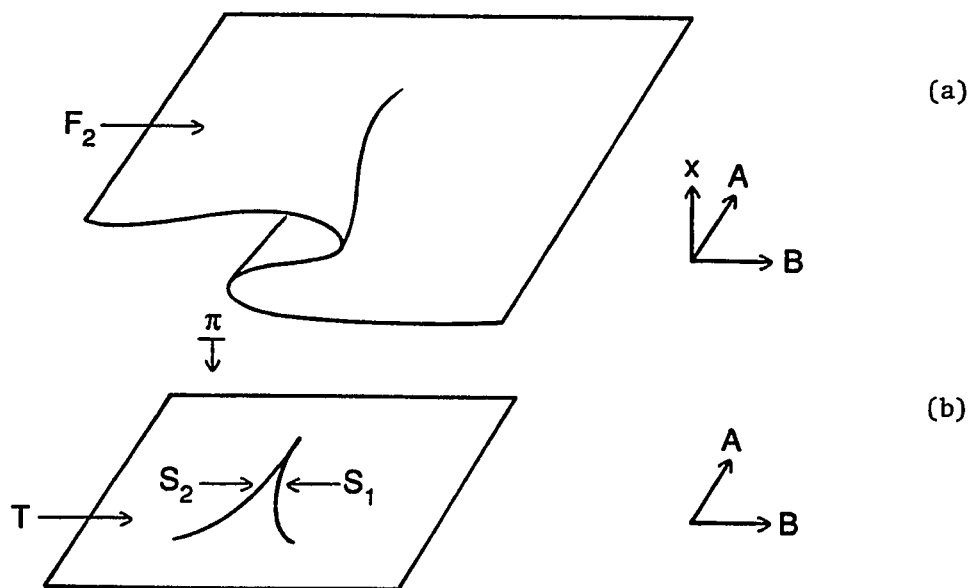
Fig. 5.1 (a) The *neutral solution surface* F_2; a two-parameter unfolding of the cuspoid normal form x^m, $m = 3$. (b) The projection π of the surface onto the control plane $T(A,B)$ where the cusp forms the *bifurcation set* S (with right and left hand nappes S_1 and S_2) along which the number and nature of the critical points of F_2 changes. Inside the cusp there are three real solutions to $f_2 = 0$, and outside there is one. (See pp. 80 - 88 for discussion).
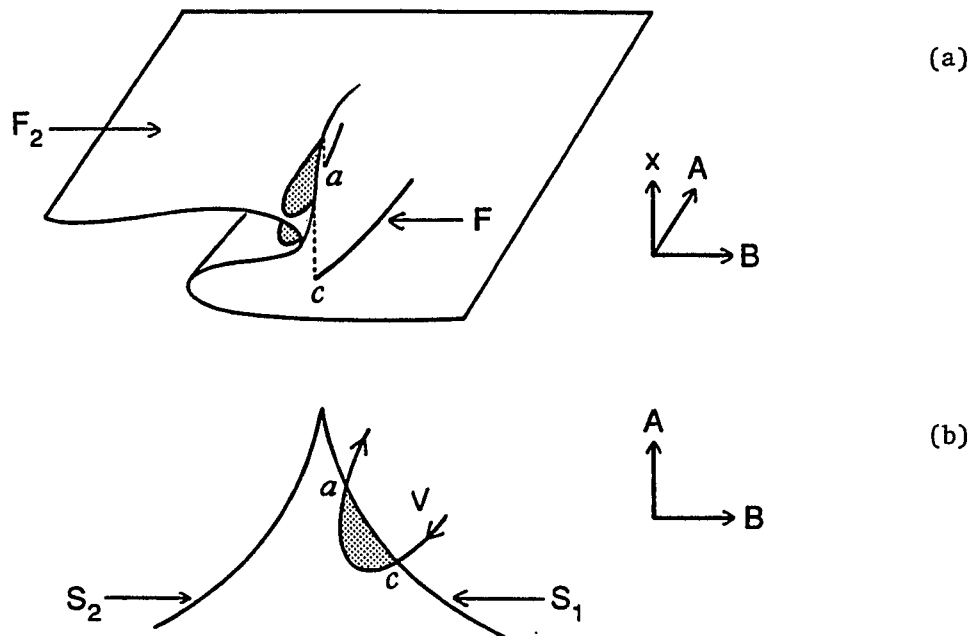
Fig. 5.2 (a) The *neutral solution trajectory* F on the surface F_2, (b) and in the control plane $T(A,B)$. The trajectory 'begins' on the lower right-hand sheet of F_2 where the solutions are unphysical (negative real wavelengths). The trajectory 'jumps' up to the right hand fold (see [a]) or crosses the right hand nappe of the *bifurcation set* S_1 (see [b]) when $(A,B) =$ (α_c, β_c), labelled by c. The system stabilizes after exiting the cusp region (see [b]) at $(A,B) = (\alpha_a, \beta_a)$, labelled by a. The shaded area is the region of instability. The trajectory is parametrized by the underlying control V and $C_\infty = 35$ ppt. A neutral curve is closed if the trajectory F enters and leaves S by crossing S_1. (See pp. 80 - 88 for discussion).
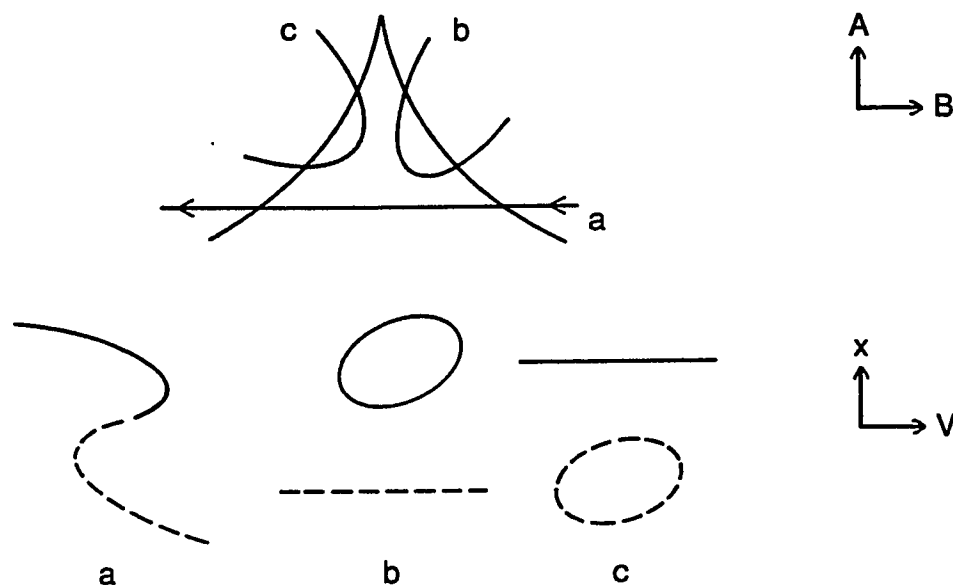
Fig. 5.3 Three trajectories a,b,c, (top) through the *bifurcation set S* in in the plane T (A, B) of observables. The bifurcation diagrams associated with these trajectories are drawn below and labelled a,b,c (here a and c are not associated with the absolute and critical bifurcation points). The horizontal coordinate is the underlying control parameter V, and the dashed lines refer to $x < p/3$. The direction of trajectory (a) is discussed in the text. The neutral curve is open in cases (a) and (c) and case (b) is similar to the trajectory F. If $x > p/3$ were not allowed, the neutral curve would be open in cases (a) and (b). (See pp. 80 - 88 for discussion).
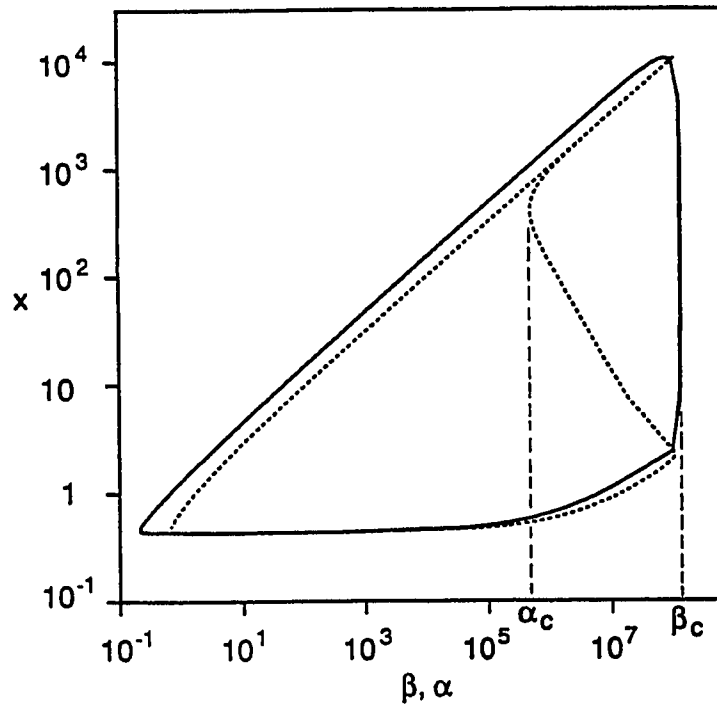
Fig. 5.4 The I α (x)I (dotted line) and β (x) (solid line) neutral curves from critical instability, (A,B) = (α_c, β_c) to absolute stability, (A,B) = (α_a, β_a). There is *relatively* strong wavelength selection in the α (x) plane due to the dependence on the underlying control V. Both planes exhibit strong wavelength selection compared with the standard neutral planes Figs. 3.1,4.1, and 4.2 but the β (x) curve is topologically similar to the standard curves at critical. (See pp. 80 - 88 for discussion).

CHAPTER 6

SOLUTE SEGREGATION AND CONVECTION

6.1 *Solute Segregation*

The stability analysis formulated in the second chapter accounted for the discontinuity of solute concentration across the solid-liquid interface by specifying a constant segregation coefficient k. This is the ratio of the solute concentration in the solid to that in the liquid. We recall from chapter three that some of the results were very sensitive to the value of k. In particular, for very small values of k, the theory gives unphysical predictions for V_c. During the formulation, the only physical motivation of k was that it accounted for the low solubility of NaCl in ice. In what follows we give a more physically based motivation for k, and distinguish two types of solute trapping that are relevant to this problem.

When solidification proceeds at sufficiently low rates, the interfacial undercooling is small and the advance of the interface is limited by the diffusion of heat and solute. In this case, the solid and the liquid adjacent to the interface are considered to be in local equilibrium. This is the situation represented by Eq. (2.13). Previously we mentioned that this local equilibrium assumption may, for some materials, be invalid at rapid solidification rates. When there is a substantial departure from equilibrium at the interface, we say that solidification is kinetically or interface controlled. That is, the advance may depend on the kinetic processes associated with the attachment of solvent (cf., Eq. 2.3) or solvent molecules. During rapid solidification of a planar phase boundary, larger than equilibrium solute concentrations in the solid can occur

(Aziz 1982). Thus, even though the total free energy of the system is reduced, as required during crystallization, the chemical potential of the solute is increased. This provides a mechanism of increasing the solute concentration of the solid that is different from the break-down of the planar interface.

Solute segregation can be viewed as a competition of two exchange processes: one exchanges solute atoms/molecules from the solid to the liquid, and the other does the opposite. The farther away the system is from equilibrium, that is, the larger the growth velocity, the less efficient the former exchange process. Solute molecules must diffuse away from the advancing interface in order to avoid being trapped. During solidification that involves only the short-range atomic/molecular redistribution, solute particles can escape being engulfed if their diffusive speed is greater than the solidification rate. Aziz (1982) has developed a theory for solute redistribution in this situation. Solute particles will be overtaken if growth exceeds the diffusive speed D/r_N, where r_N is a nearest neighbor spacing. For ice $r_N = O(10^{-10})$ m, so that $D/r_N \simeq 1$ m s^{-1}. Therefore, this type of trapping will not occur during natural solidification, but may be achievable with laser annealing techniques. The structure of the interface itself is an important factor in determining exactly how the trapping process will take place. The structure of the interface, diffuse or flat on a microscopic scale, depends on which crystal growth regime (section 1.2) is in operation. The theory presented by Aziz (1982) considers both cases, but does not consider how the trapping process affects the transition from one to the other, nor how the transition depends on driving force. For the case in which the interface is singular, and the growth proceeds by the propagation of steps, a trapping model is outlined below.

In equilibrium, each particle in both phases interacts with its nearest neighbors, vibrating about some mean position. Figure 6.1 is a schematic of the solute redistribution proposed by Aziz (1982). The solid is depicted as the ordered material on the left, consisting entirely of solvent particles. The monolayer of liquid, adjacent to the interface, is depicted by the numbered particles. The monolayer particle numbered 4 is the single solute particle B. The segregation coefficient k, used in our stability analysis, represents the ratio of B particles in the solid to those in the liquid. A small value of k has the physical interpretation that the lowest energy arrangement of bonds occurs with an $A-B-A$ bond angle of say 60°. The B particle is more likely to attain this configuration in the liquid. We view the passage of a step of height r_N in terms of the motion indicated by the arrows on particles 1,2,3, and 5. This motion has the effect of distorting the nearest neighbor minimum energy state of B, and dragging it toward the interface. If there is a nearby configuration, in the liquid, which allows B to attain a 60° $A-B-A$ bond angle, then it will reduce its energy and "roll" back into the liquid. Otherwise, it will be dragged into a higher energy state in the solid. If we view this rearrangement as instantaneous compared to the time it takes for the passage of a step, then the criterion for trapping is that B does not diffuse back into the liquid before another step passes. The continuous dynamics of this situation is extremely difficult since one must account for the fact that while B particles are being dragged toward the interface, they are trying to diffuse away.

A result of the Aziz model that is relevant to the morphological stability problem is a velocity dependent segregation coefficient for the growth of a diffuse interface,

$$K(v) = \frac{k + \beta_o v}{1 + \beta_o v},$$

(6.1)

where v is the local interfacial velocity, k is the equilibrium segregation coefficient, and β_o is the ratio of interatomic distance to diffusion coefficient, and has a value of about $1/2$ s m^{-1}. Merchant and Davis (1991) use this result in their zero latent heat, thermally symmetric linear stability analysis at rapid solidification rates. We know from chapter three, that the effect of a lower k is to increase the constitutional undercooling and increase the range of conditions under which the interface will break down. Thus, by encorporating Eq. (6.1) into the stability analysis of a planar interface, the actual undercooling at the interface can be explicitly accounted for at high V. At high velocity, when $K(v) \simeq 1$, The lack of latent heat in the Merchant and Davis (1991) study results in oscillatory instabilities, with infinite wavelength, reproducing commonly observed solute bands. Our analysis, with constant k, had a small wavelength cutoff because when V is large, the diffusion time is small, so lateral segregation can only accompany small wavelength disturbances. However, the small waves are strongly stabilized by surface tension. When k is allowed to vary with V, longer wavelength disturbances are allowed. By examining the case where $\sigma_r = 0$ and $\sigma_i \neq 0$, they explain the oscillatory instability as follows. The maxima of a given disturbance have a larger local growth rate v, and hence K, than do the minima. Since the increase in local K results in less local solute rejection, v decreases. As v decreases, the concurrent decrease in K increases the local solute gradient thereby enhancing the local growth rate again. This cycle will repeat itself. This approach presents a mechanism whereby solute trapping by both kinetic and interface breakdown processes may occur.

For planar interfaces, The segregation coefficient in Eq. (6.1) has a physical basis as just described. If one is interested in regimes where the planar interface does break down, then a different method of treating segregation exists. An empirical approach, which ignores the

physics of the microscopic trapping process, is that of defining an effective segregation coefficient k_{eff}. By measuring the concentration profile of a material solidified from a solution of known concentration, values of k_{eff} can be computed. For the case of sea ice, Cox and Weeks (1988) reanalyzed previous data, from radioactive tracer experiments, and obtained k_{eff} for a range of velocity V. These are

$$k_{eff} = 0.8925 + 0.0568 \, V; \qquad 2.0 \, x \, 10^{-6} < V < 3.6 \, x \, 10^{-5}, \qquad (6.2a)$$

$$k_{eff} = 0.26 \, [0.26 + 0.74 \exp(-7243 \, V)]^{-1}; \qquad V > 3.6 \, x \, 10^{-5}, \qquad (6.2b)$$

where V is in cm s^{-1}. They assume a constant value of $k_{eff} = 0.12$ for $V < 2.0 \times 10^{-6}$, since there were no data available for velocities less than this. For velocities greater than about 10^{-3} cm s^{-1}, k_{eff} becomes unity. Of course, Eqs. (6.1) and (6.2) are not ammenable to comparison because the former is treating the microscopic trapping and the latter measures the effect of bulk solute trapping. From the experiments we know this is the case for Eq. (6.2). In addition, the linear stability analysis with constant k tells us that the range of velocity for which Eq. (6.2) is valid is $V_c < V < V_a$. Once sodification begins, whatever the solute redistribution mechanism, a concentration profile like that pictured in Fig. 1.3, will be established. Such a profile leads one naturally to think of the possibility of convection, which is the focus of the section below.

6.2 Convection

Morphological instabilities of the solid-liquid interface can be affected by hydrodynamic interactions between the fluid and the molecular diffusion at interface. The flows that are of

interest are volume-change convection, due to the phase change expansion/contraction, buoyancy-driven convection, and externally forced flows. An excellent review of these cases is given by Davis (1990). A concern in the H_2O-NaCl system is whether or not the fluid adjacent to the interface transports heat and solute by diffusion only.

In a typical experiment, the distance between the cold contact and the bottom of the fluid container is fixed. At the interface, liquid of density ρ_L becomes solid of density ρ_S. If these densities are not equal, then the expansion or contraction of the material at the interface will drive a flow. In the case of seawater, $\rho_S/\rho_L \approx 0.9$, the expansion at the interface drives a weak flow away from the interface. This flow will stretch the solute concentration boundary layer thickness D/V, thereby decreasing the local concentration gradient G_c. From previous discussion, we know that this will suppress morphological instability. Therefore, expansion upon solidification is stabilizing and, by parity of reasoning, contraction is destabilizing. In the case of natural solidification, the ice sheet can rise in response to the expansion at the interface, eliminating the flow away from the interface.

As solidification progresses, the build up of solute adjacent to the interface creates a configuration in which highly concentrated colder melt lies above warmer, less concentrated melt (Fig. 1.3). Thus, the configuration is thermally and solutally unstable. This situation admits the possibility of a convective instability in the fluid phase. By way of illustration, consider a parcel of fluid near the interface; it is cold and concentrated. If a disturbance displaces the parcel downward, it encounters warmer, less concentrated fluid. The parcel will increase in temperature, but since the thermal diffusivity is much greater than the solute diffusivity, it maintains essentially the same solute concentration, during a small time increment. In this new location, it has nearly the same temperature as the environment but a greater solute

concentration. Since it is more dense than the surrounding fluid it will continue to descend if viscous forces are overcome. Therefore, the solute field drives the hydrodynamic instability. The formal approach to this stability problem is to couple the solidification system to the Navier-Stokes equations, thereby capturing the interplay between morphological and hydrodynamic instabilities.

For the case in which there is no volume change convection, Coriell et al. (1980) perform a linear stability analysis of the solidification equations, augmented by the Navier-Stokes equations. This analysis differs from standard double-diffusive convection because (a) the upper boundary is moving and has an unconstrained shape. (b) the solute gradient is not constant; it falls off exponentially. The perturbation equations obtained are equivalent to eight first order differential equations for a set of functions $X_i(z)$, $i = 1,2,...,8$, with far-field and interface boundary conditions. These must be solved numerically, and it is found that there are two neutral curves; one corresponding to convective modes, and one corresponding to morphological modes. In the systems studied to date, it is found that these modes are spatially uncoupled at critical so that $\lambda_c^{(C)} \gg \lambda_c^{(M)}$, where the superscripts C and M denote convective and morphological modes respectively. For a lead-tin system Coriell et al. (1980, see their table 2) found that $\lambda_c^{(C)} \approx 10^2 \lambda_c^{(M)}$ for low V. Thus, there is a small-scale morphological instability imbedded in a larger scale convective flow, and the morphological modes are unaffected by convective flow. The prominent role of non-linear interactions in the H_2O-NaCl system (chapter 3), and the fact that the data exists in a velocity range much greater than V_c, and for wavelengths much less than λ_c, preclude the coupled convective/morphological treatment as one amenable to comparison with data.

To study fluid flow adjacent to the solidifying interface, we can adapt the analytic solutions of the double-diffusive convection problem solved by Turner (1973). He solves (p. 255) the linearized two-dimensional Oberbeck-Boussinesq equations coupled to diffusion equations for temperature and concentration in a layer of thickness d. The layer is exposed to temperature and solute concentration differences of ΔT and ΔC respectively. The following neutral stability curve for non-oscillatory disturbances ($\sigma_i = 0$, where $\sigma = \sigma_r + i\,\sigma_i$ is the disturbance growth rate) results,

$$Ra = \frac{Rs\ \kappa_L}{D} + \frac{27\ \pi^4}{4},\tag{6.3}$$

where $Ra = g\ \alpha\ \Delta T\ d^3/\kappa_L\ \nu$ is the Rayleigh number, and $Rs = g\ \beta\ \Delta C\ d^3/\kappa_L\ \nu$ is the solute Rayleigh number. Here g is the acceleration due to gravity, κ_L is the thermal diffusivity of the fluid, and ν is the kinematic viscosity. The thermal and solute 'expansion coefficients' are defined for some mean values T^*, C^*, and p^* of temperature, solute and pressure as

$$\alpha = -\rho^{-1}\left[\frac{\partial \rho}{\partial T^*}\right]_{C^* p^*}, \qquad \beta = -\rho^{-1}\left[\frac{\partial \rho}{\partial C^*}\right]_{T^* p^*},$$

where ρ is the density of the fluid. For seawater, $\alpha = 2.54 \times 10^{-5}\ K^{-1}$ and $\beta = 7.92 \times 10^{-4}\ K^{-1}$, so that the fluid density is more sensitive to changes in solute concentration than temperature. The characteristic length scale over which the destabilizing solute gradient exists is D/V. Therefore, we choose this as the scale d in Eq. (6.3). For a constant k, C_∞, and G'_L, each growth velocity V is associated with a fluid layer of thickness D/V, and we evaluate its stability using Eq. (6.3). Therefore, we can examine the hydrodynamic stability of the diffusive layer at all states V of the solidification system assuming a *planar* solid-liquid interface.

In Fig. 6.2 we present the neutral curve (solid line) in the $Ra-Rs$ plane, and the Rayleigh and solute Rayleigh numbers (crosses) for a range of V, increasing from left to right. To the left of the neutral curve the fluid layer is unstable and to the right it is stable. The cross-over velocity, at which the layer is neutrally stable, is $V^c = 4.3 \times 10^{-4}$ cm s^{-1}. The Rayleigh number is proportional to $G'_L (D/V)^4$, and the solute Rayleigh number is proportional to $\Delta C (D/V)^3$. For constant G'_L, at small growth velocities, Ra and Rs are large. Here, the stability of the layer is determined by the competition between the destabilizing solute field and the stabilizing effect of viscosity. At growth velocities close to V_c for morphological instability, the magnitude of the solute Rayleigh number is large and instability prevails. At large growth velocities Ra and Rs become smaller, Rs being the larger of the two. Here again, the stability is determined by the competition between the stabilizing viscous forces and the destabilizing solute field; the latter losing for $V > V^c$.

Since both the solute and temperature fields have a destabilizing effect on the fluid layer, the behavior is more like that of a one component system. This is because the fluid density is more sensitive to changes in the solute concentration than to changes in the temperature. Since $\kappa_L \gg D$, the solute field is the rate limiting factor in the hydrodynamic stability problem. In the vicinity of V^c, $Ra = O(10^{-8})$, so the approximation $Ra = 0$ is quite accurate (see Fig. 6.2). Thus, Eq. (6.3) can be rewritten as $Rs = -27 \pi^4 D/4 \kappa_L \equiv Rs^c$. This is a useful result since it yields a cross-over point that depends only on the thermophysical parameters of the system. For the salt water system, $Rs^c = -2.66$. This approximation allows a simple estimate of $V^c = 4.7 \times 10^{-4}$ cm s^{-1}, which is within about nine percent of the previous result. The H_2O-NaCl system will be hydrodynamically stable for growth velocities V greater than about 5.0×10^{-4} cm s^{-1}.

It is interesting to note that $V^c = 4.3 \times 10^{-4}$ cm s^{-1} falls in the middle of the experimental velocity range. It is possible that convection played some role in the formation of the substructure in both the laboratory and field experiments, but there is no evidence of strong coupling in the vicinity of V^c (Fig. 3.1). If convection occurred at the lower velocities it should have manifested itself as a larger scale interfacial morphology, such as the two-dimensional rolls, rolls and polygons or hexagons observed in many systems (Davis 1990). However, the authors report no such observations. Weakly coupled and time-periodic instabilities have been predicted under some limited parameter ranges, but for most common materials studied it is found that $\lambda_c^{(C)} \gg \lambda_c^{(M)}$ (Davis 1990). Presently we mention two other situations of particular relevance to geophysical solidification.

Understanding the hydrodynamic interactions in solidification has obvious technological benefits. If one can control the solute boundary layer, crystals with well defined properties can be refined. This has been the impetus for studying the interaction of forced flows with a solidifying crystal (Davis 1990). It turns out that there is a geophysical phenomenon that lends itself to similar analysis. If there is a persistent directional current under growing sea ice, the substructure aligns perpendicular to the current direction (i.e., the c-axis is parallel to the current direction). Weeks and Ackley (1986) review the present hypotheses of c-axis/current alignment, from both field and laboratory studies. However, the answer must expose itself when coupling the solidification equations with a forced flow and perturbing the system in two horizontal dimensions. The suspicion is that the flow may mediate the directional selection of a preferred mode, and that the morphological stability criterion of some modes will be unaffected by the flow. This is the subject of future work.

There is a larger scale phenomenon that is also relevant. At very high growth rates some systems breakdown to form very deep grooves that undergo secondary and tertiary instabilities. Eventually, a bed of deep dendrites, separated by distances of order their width, will form. The interstices are filled with highly concentrated solution. This region of mixed phase, sometimes called a 'mushy zone' has been studied in a variety of geophysical situations (reviewed by Huppert 1990). The mushy zone is characterized by a *relatively* low solid fraction ϕ, the volume of pure solid in a unit volume of mush.

Because the entire region is a mixture, it will solidify at a rate that is different from that of a pure melt. Modeling the heat transfer through this layer as that through a material with constant thermal conductivity and heat capacity may result in a poor estimate of the growth rate (Huppert 1990). The approach is to treat the heat and mass transfer through the mixed phase, and the small region of liquid adjacent to the mixed phase as a continuum. Therefore, the basic ingredients are the diffusion fields through both phases averaged over a length scale larger than the typical cell/dendrite spacing.

The diffusion fields in the liquid T_L, C and the mixed phase T_m of constant solid fraction ϕ are modeled with one-dimensional equations (Huppert 1990). The major modification is that the thermophysical constants in the mixed phase vary as a function of ϕ. As a first approximation one writes

$$k_m = \phi \, k_S + (1 - \phi) \, k_L, \qquad (6.4)$$

and

$$(\rho \, c)_m = \phi \, (\rho \, c)_S + (1 - \phi) \, (\rho \, c)_L, \qquad (6.5)$$

where k_m and $(\rho \, c)_m$ are the thermal conductivity and specific heat of the the mixed phase.

In the simplest model it is assumed that the solute concentration in the crystalline interstices remains on the liquidus and that the density change upon solidification does not give rise to convection in the interstices or the melt (Huppert 1990). Another important feature, particularly relevant to sea ice work, is that the conservation of thermal energy and solute at the mush-liquid interface, $z = H$ (t) are expressed as

$$L \phi H_t = k_m T_{mz} - k_L T_{Lz},$$ (6.6)

$$H_t (1 - \phi) C = -D C_z,$$ (6.7)

where the subscripts z, t denote partial differentiation (cf., Eqs. (2.6) and (2.7) with $h = 0$) .

It has been shown (Huppert, 1990) that a more sophisticated model which takes into account that ϕ is not constant in the mixture phase (Worster, 1986) does not significantly improve results. In addition, Worster (1986) showed that for systems in which $\kappa_S \approx 10 \ \kappa_L$ a model with constant solid fraction may yield better predictions. The ice - seawater system system satisfies $\kappa_S \approx 10 \ \kappa_L$. The mushy zone approach would be particularly useful in the study of young sea ice that forms in an agitated environment, and contains a small solid fraction.
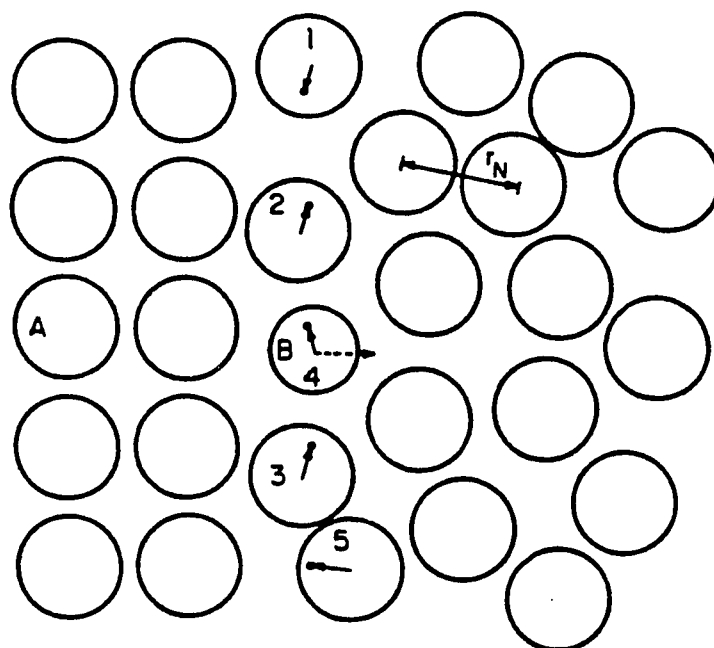
Fig. 6.1 A schematic of microscopic solute segregation. The solvent particles are labelled A and the solute particle is B. The ordered solid is on the left and the particles 1,2,3,4,5 represent the monolayer adjacent to the solid-liquid interface. The nearest neighbor spacing is $r_N \approx 10^{-10}$ m, and the diffusive speed is $D/r_N \approx 1$ m s^{-1}. For a cubic lattice, solute rejection is interpreted in terms of the low energy arrangement of A-B-A bonds being say $60°$. This configuration is achieved more readily in the liquid. See section 6.1 for discussion. (adapted from Aziz 1982).
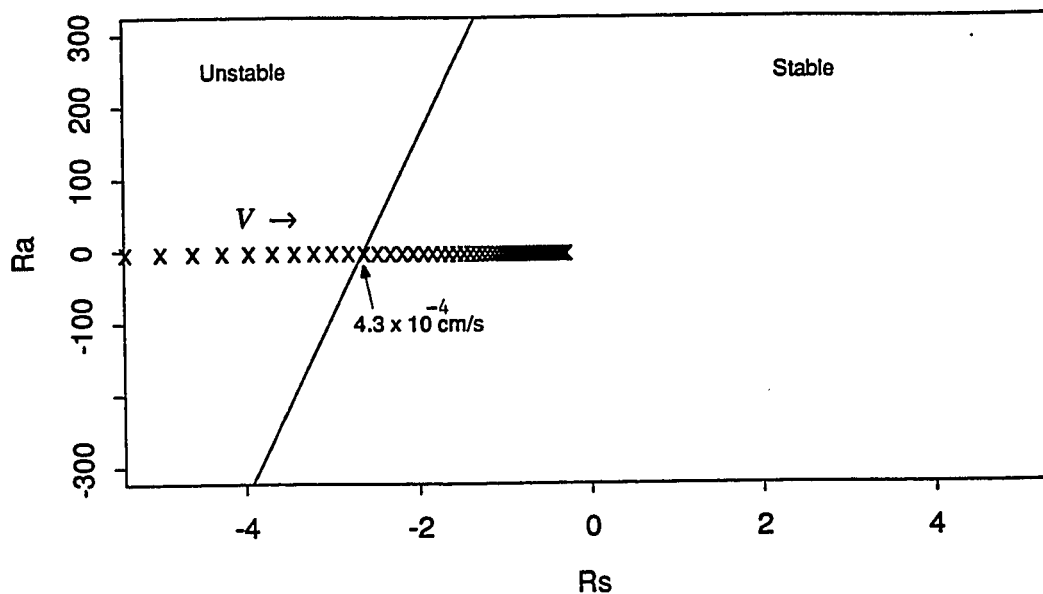
Fig. 6.2 The neutral curve (solid line) in the $Ra-Rs$ plane, and the Rayleigh and solute Rayleigh numbers (crosses) for a range of V, increasing from left to right. To the left of the neutral curve the fluid layer is hydrodynamically unstable and to the right it is stable. The cross-over velocity, at which the layer is neutrally stable, is $V^c = 4.3 \times 10^{-4}$ cm s^{-1}. The thermal and solute fields create an unstable density stratification in the fluid. At small growth velocities, close to V_c for morphological instability, the magnitude of the solute Rayleigh number is large, and an instability, driven by the solute field, prevails over the stabilizing effect of viscosity. At large growth velocities Ra and Rs become smaller, Rs being the larger of the two. Here, the stability is determined by the competition between the stabilizing viscous forces and the destabilizing solute field; the latter losing for $V > V^c$.

CHAPTER 7

DISCUSSION

We have studied the system of equations governing the directional solidification of an H$_2$O-NaCl system. Linear and weakly non-linear perturbation theory reveals that, over a wide range of growth conditions, the H$_2$O-NaCl system is morphologically unstable. The predictions of the theory are in good qualitative agreement with laboratory experiments on this system and field experiments on naturally solidifying seawater. In section 3.1 we focused on control parameters that are geophysically relevant, and consistent with conditions typically found at the underside of growing sea ice in the Arctic Ocean. Under these conditions there are approximately nine orders of magnitude between the critical point of instability V_c, and absolute stability V_a, for a fixed far-field solute concentration. This is shown in Fig. 3.1. Owing to the small value of the liquid temperature gradient used in this part of the study, the range between V_c and V_a is many orders of magnitude larger than that found in binary alloys. The implications are that for solidification of seawater in situations in which the solidification system is applicable, a planar phase boundary will not be the stable growth form. This explains the ubiquitous observations of platelet substructure in naturally occurring sea ice.

Consistent with other investigators (Bennett and Brown 1989, and Merchant and Davis 1989b), we observe weak wavelength selection close to critical on the $V(\lambda)$ neutral curve (Fig. 3.1). This weak wavelength selection manifests itself as an extreme sensitivity of neu-

tral wavelengths, near critical, to small changes in the interfacial velocity. This is a diagnostic for the non-linear behavior of this system, and a result of the continuous dependence of the normal modes on wavenumber. This is due to the absence of horizontal boundary conditions. The continuous dependence may be 'artificially' removed with the addition of a bifurcation parameter such as the experimental cell width (see e.g., Haug 1987). This discretizes the spectrum, leaving one with an arbitrary choice of interacting modes. The utility of a linear theory may be improved if one can formulate the problem in a way that will predict a most unstable wavepacket, rather than a single mode, as has been done in some hydrodynamic free boundary problems (Drazin and Reid 1981).

It is important to bear in mind that the data plotted in Fig. 3.1 are from experiments that measured the relationship between platelet spacing and mean growth velocity for a fully developed cellular interface. The goal of these experiments was not to determine the critical point of instability of a solidifying H_2O-NaCl solution. In addition, in neither case is the liquid temperature gradient known to any great degree of accuracy, and the role of convection was not assessed. These data appear in the figure primarily to show that the theory, in this regime, predicts the $\lambda \propto V^{-1/2}$ scaling observed experimentally. This was discussed in section 3.3.3 where we derived this relation (Eq. 3.29). Therefore, we should not interpret these experiments as validating or invalidating the theory for this system. Rather, the behavior of the theory should motivate careful experiments on H_2O-NaCl. For geophysical parameters, a careful laboratory experiment could assess the extent to which the system undergoes a subcritical bifurcation at critical, and shed light on the wavelength selection mechanism. Convection in the melt can be studied using interferometry. In terms of a model system, experiments with liquid temperature gradients from 10 to 100 K cm^{-1}, and solute concentrations

from 30 to 0.03 ppt will result in an interface that is unstable over about 3 to 4 orders of magnitude in velocity. This smaller range would allow direct observation, greater scrutiny of the stability boundaries, and detailed study of the role of kinetics and the orientational dependence of surface tension. For growth of ice cylinders, parallel to the c-axis, into very low concentration salt solution, some experiments have been performed (e.g., Hardy and Coriell, 1973), but none to investigate the situation that has been the focus here.

The range of instability is decreased as the liquid temperature gradient increases. However, this is not a control parameter in natural solidification (Wettlaufer et al., 1990, Wettlaufer 1991). We examined this sensitivity in section 3.2. It was found that if we use a liquid temperature gradient of 200 K cm^{-1} (common for metal alloys, Coriell et al. 1985), V_c increases to about 10^{-4} cm s^{-1} and V_a is unchanged. Since the absolute stability criterion does not depend on the liquid temperature gradient, we find that increasing this gradient decreases the range of instability by delaying its onset to higher velocities (see Fig. 3.2). When increasing the temperature gradient, the predicted range of substructure from λ_c to λ_a, decreases by about four orders of magnitude. Desalination through freezing may be practically impossible unless the interface can be stablilized by utilizing the convective/advective transport of solute, or by increasing the liquid temperature gradient to what appears to be inaccessibly large values. Laser annealing techniques may be helpful in this regard. The stabilization will eliminate the trapping of highly concentrated fluid in the ice matrix. If large temperature gradients can be maintained uniformly over a large area, growth rates of about 0.1 to 10 cm day^{-1} may allow the formation of relatively fresh ice.

In section 3.3 we investigated long-wave behavior close to the critical point of instability and at absolute stability. By transforming the neutral curves of Sivishinsky (1983) and Brattkus and Davis (1988) into dimensional variables, we found the following velocity-wavelength scaling relationship (Eq. 3.25): $(\lambda - \lambda_*) = C \ (V - V_*)^\eta$, where $\eta = 1/2$, (λ_*, V_*) is an extreme point, and C is a constant. In a short-wave approximation, for velocity values in the range of the experiments, we found the relationship (Eq. 3.29): $\lambda = S_1 \ V^{-1/2}$, where S_1 is a constant. This is consistent with the data for this system and qualitatively the same as that found in other systems (section 3.3.4).

Consistent with the predictions of the local theory of Sivashinsky (1983), when we decrease the value of k, the value of λ_c increases. The neutral curve is parabolic very close to critical, but exhibits a winged cusp shape for a larger range of velocity (Fig. 3.3). The value of V_c for this k is not consistent with the use of a continuum theory since it predicts 'velocities' of fractions of a molecular layer per second. Thus, caution must be exercised when one interprets the results of a local, asymptotic theory of this type.

In section 3.4 we investigated the $V(C_\infty)$ neutral curve by applying a Landau type of weakly non-linear analysis to the solidification equations. This showed that the transition to cells will occur through a subcritical bifurcation, so finite amplitude substructure will appear suddenly as $V \rightarrow V_c^-$. These results are shown in Figure 3.4. In agreement with alloy and transparent organic systems (Merchant and Davis 1989a, and Alexander et al, 1986), we find that as $n \rightarrow 1^+$, the range of subcritical bifurcation is suppressed. This limit corresponds to the steepening of the thermal gradient in the solid and does not affect the results of the linear theory. This has been pointed out previously, (Alexander et al., 1986) but no physical expla-

nation was provided. By ascribing large amplitude interface deflections to the case of sub-critical bifurcation, close to critical, we posited an explanation for why the steepening gradient has a stabilizing effect that is length scale dependent. The relative effect increases with the size difference between small (infinitesimal) and large (finite amplitude) perturbations. A somewhat heuristic physical argument ascribed the underlying scale difference to a difference between the undercooling δT, felt by a disturbance as a result of the gradient steepening, and the critical undercooling δT^* necessary to freeze the region of liquid created by the disturbance. There is a crossover at which $\delta T = \delta T^*_c$ so that if $\delta T \gg \delta T^*_c$ ($\delta T \ll \delta T^*_c$), the planar interface will be stable (unstable) to perturbations with amplitude $A \gg R^*_c$ ($A \ll R^*_c$), where the R^* are the critical radii of nucleation. Finite amplitude disturbances have $A \gg R^*_c$. This is offered as an explanation for the suppression of subcritical (finite amplitude) bifurcations while the linear results remain unaffected in this limit.

The non-linear extension of this approach is a spatially resonant theory which allows several modes to interact that are not restricted in the horizontal. The Landau approach, as presented here, only permits the investigation of the non-linear interaction of the most unstable mode with itself. The subject of future work is to investigate the non-linear interaction of a triad of incommensurate modes. This may allow us to identify the non-linear interactions responsible for the subcritical bifurcation identified near critical. The method will be that derived by Mourad (1987).

In the fourth chapter we compared the linear theory based on solute diffusion scales with that based on velocity independent scales derived by Merchant and Davis (1989b). Figure 4.1 shows that the qualitative behavior is similar over the whole range of instability. Both

theories exhibit weak wavelength selection, but it is more pronounced in the dimensionless neutral plane of the latter theory V_{md} (η). The dependence of the dimensionless velocity V_{md} on the underlying physical velocity V results in a neutral curve that is flatter than that in the $M(R)$ plane. This is shown in Figure 4.2.

To obtain velocity independent length and time scales, the assumption of negligible curvature in the liquid thermal field close to the interface must be valid. The violation of this condition is not severe in the SCN-acetone system to which the theory was first applied (Merchant and Davis 1989b), but we showed that this was not the case for the H_2O-NaCl and Al-Cu systems. Due to the presence of thermal curvature, predictions at rapid solidification rates are not valid for the two latter systems. However, there are other effects, such as nonequilibrium thermodynamics and attachment kinetics, which will also obscure the predictions near absolute stability, regardless of the scalings chosen.

Some mathematical observations were presented in the fifth chapter. We performed an equivalence transformation of the bifurcation problem for g (Eq. 5.1) to one that is a universal unfolding of a cuspoid normal form $N = x^m$, where $m = 3$. When viewed as a two-parameter unfolding f_2, of N, the *neutral solution surface* F_2 is the folded cusp surface which arises in the study of a variety of physical systems (Poston and Stewart 1978, Thorndike et al. 1978, Golubitsky and Schaeffer 1985). This is shown in Fig 5.1. This differs from what Haug (1987) has found, since he used the cell width as a bifurcation parameter, discretizing the normal modes of the frozen-field solidification equations. The solution of the solidification problem investigated here is equivalent to the solution of the bifurcation problem for the one-parameter unfolding of N, Eq. (5.2). This results in a *neutral*

solution trajectory F in the *neutral solution surface* F_2. There is an infinite set of *degenerate points* of the unfolding f_2, which form the *bifurcation set S* defined by the semicubical parabola (Eq. 5.4). Along S the nature and number of the real solutions to Eq. (5.3) change (Fig. 5.1). A neutral stability plane is drawn in terms of control parameters or observables by projecting the surface F_2 and $F \cap F_2$ onto the plane $T(A,B)$ (Fig. 5.2). We showed that if the *neutral solution trajectory* enters and exits the right-hand nappe S_1 of the bifurcation set S, then the neutral curve will be closed. Examples of two different open curves and a closed curve that result from three paths through S are given in Fig. 5.3.

We showed that the weak wavelength selection problem for theoretical predictions near critical can be bypassed by studying the structure of $F \cap F_2$. This is due to the underlying velocity dependence of the controls α and β. The neutral curve in the $\alpha - x$ plane is relatively sharper close to critical. These neutral curves are shown in Fig. 5.4. However, this is merely a surgical bypass of the underlying problem of a linear theory of this type, and we suggested possible solutions in previous chapters.

Combined, the following properties account for the wavelength selection predicted in the standard neutral curves. First, the critical bifurcation point occurs on a part of the upper fold that has very little curvature. Second, in the region very close to the critical bifurcation point, the trajectory is approximately tangent to the fold, or the right hand nappe S_1 of the bifurcation set. The latter behavior points to weak wavelength selection as being due to the presence of higher order degeneracy near critical. The extent to which this selection mechanism has a real physical origin, or is an artifact of the theory, may be addressed by unfolding the singularity at critical. We plan to pursue this in the future. The fact that nature has no

difficulty choosing a scale, points to a theoretical flaw, suggesting that the same conceptual problems haunting transitions in fields from turbulence to magnetism, are here too.

In the sixth chapter, we examined the physical basis for solute segregation for planar and nonplanar interface geometries. This revealed two mechanisms of solute trapping; microscopic and macroscopic, both of which can act simultaneously. This subject led to the consideration of the hydrodynamic stability of the fluid layer adjacent to the interface. We discussed volume-change convection, buoyancy-driven convection, forced flows, and the formation of mixed phases.

Treatments that couple the solidification equations to a momentum equation find bouyancy driven convection in the fluid layer of thickness D/V, adjacent to the interface (Davis 1990). It is found that, for most materials studied, the convective (C) instabilities are essentially uncoupled from the morphological (M) instabilities, so that at critical $\lambda_c^{(C)} \gg \lambda_c^{(M)}$. We chose a less complicated approach to this problem. In section 6.2, we adapted the neutral curve (Eq. 6.3), from Turner's (1973) analytic solution to the problem of double-diffusive convection, to the solidification problem. We based the length scale of Rayleigh Ra, and solute Rayleigh Rs, numbers on the solute boundary layer thickness D/V. It was found that the solute field drove an instability for $V < V_c$, where $V^c = 4.3 \times 10^{-4}$ cm s^{-1}. At $V > V_c$, viscous forces retard the solute driven instability and the fluid layer is stable. These results were presented in Fig. 6.2. The cross-over velocity V^c, at which the layer is hydrodynamically neutrally stable, lies in the middle of the experimental velocity range (cf., Fig. 3.1). We find no experimental evidence of strong coupling between morphological and convective modes. Increasing the liquid temperature gradient has a stabilizing affect on both

morphological and double-diffusive instabilities. It is interesting to note that when we chose

a liquid temperature gradient of 200 K cm^{-1}, the value of V_c was of order 10^{-4} cm s^{-1}, and

$V^c = \dot{V}_c$ for a temperature gradient two orders of magnitude smaller. We suspect that the

cross-over V^c would be much lower at this high temperature gradient. Thus, the system can

be stabilized with respect to both mechanisms of instability.

In section 6.2 we briefly discussed the coupling of forced flows with the solidification

system as a paradigm for the c-axis/current alignment problem observed in field and labora-

tory studies. We also outlined the theory for heat and mass transfer in a mixed phase and its

potential for application to sea ice problems.

In terms of other applications, it should be noted that acoustical scattering from the

interface is sensitive to the presence of cellular substructure (Stanton et al., 1986). Because it

appears that the cell depth and spacing are critical factors in the determination of the scatter-

ing properties of the material, the results presented here will be of use to researchers in this

field of acoustics.

It is natural to think that the interface might move in a manner that optimizes some

quantity, say growth rate, or entropy production. Langer (1987) has pointed out that no such

variational formulation exists for the symmetric solidification problem. Efforts to find some

free-energy-like functional that is minimized have not been successful, and he does not think

that one exists. Real physical systems operate in such a narrow range of wavelength that it is

hard to believe that such an explanation does not exist. Other possible approaches to this

problem are the Cahn-Hilliard formulation (outlined in Elbaum and Wettlaufer 1991), numeri-

cal simulations of the solidification equation themselves, Monte Carlo methods and diffusion

limited aggregation.

The long standing problems with linear stability theories and their weakly non-linear counterparts are in full evidence here. The lack of good experimental data for the H_2O-NaCl system, close to critical, precludes a thorough judgement of the linear theory results. The analysis presented here shows that the range of instability may be controlled in a laboratory setting, and the degree to which the bifurcation to cells is subcritical can be accurately assessed. The entire growth range of naturally occurring sea ice is unstable to a broad band of wavelengths. Thus, under normal conditions, we will always find substructure at the underside of growing sea ice. The presence of substructure, on scales of centimeters or less, is due to morpological instabilities. Since transparency has been the impetus to study systems such as SCN-acetone, it is hoped that the transparency of the H_2O-NaCl system would stimulate experiments with this material. Understanding the behavior of aqueous solutions, near phase transitions, has an aesthetic appeal, and biological, chemical, technological, physical, geophysical, and astrophysical implications.

LIST OF REFERENCES

Alexander, J. I. D., D. J. Wollkind, and R. F. Sekerka, J. Cryst. Growth, **79**, 849 (1986).

Aziz, M.J., J. Appl. Phys., **53**, 1158 (1982).

Ben-Jacob, E., N. D. Goldenfeld, J. S. Langer, and G. Schon, Phys. Rev. A, **29**, 330 (1984).

Ben-Jacob, E., P. Garik, Nature, **343**, 523 (1990).

Bennett, M. J. and R. A. Brown, Phys. Rev. B, **39**, 11705 (1989).

Brattkus, K. and S. H. Davis, Phys. Rev. B, **38**, 11452 (1988).

Brattkus, K. and C. Misbah, Phys. Rev. Lett., **64** (16), 1935 (1990).

Buerger, M. J., Z. Krist., **89**, 242 (1934).

Burton, W. K., N. Cabrera and F.C. Frank, Philos. Trans. Roy. Soc., A243, 299 (1950).

Cahn, J. W., Acta Metall., **8**, 554 (1960).

Cahn, J.W. and J.E. Hilliard, J. Chem. Phys., **28**, 258 (1958).

Chandrasekhar, S., *Hydrodynamic and Hydromagnetic Stability,* (Oxford University Press, 1961).

Coriell, S. R., M.R. Cordes, W.J. Boettinger and R. F. Sekerka, J. Cryst. Growth **49**, 13 (1980).

Coriell, S. R., G.B. McFadden and R. F. Sekerka, Ann. Rev. Mater. Sci., **15**, 119 (1985).

Couder, Y., O. Cardoso, D. Dupuy, P. Tavernier and W. Thom, Europhys. Lett., **2**, 437 (1986).

Cox, G.F.N. and W.F. Weeks, J. Geophys. Res., **93**, 12,449 (1988).

Davis, S. H., J. Fluid Mech., **212**, 241 (1990).

Dougherty, A., P.D. Kaplan and J.P. Gollub, Phys. Rev. Lett., **58**, 1652 (1987).

Drazin, P. G. and W.H. Reid, *Hydrodynamic Stability*, (Cambridge University Press, 1981).

Eckhaus, W., *Studies in Nonlinear Stability Theory*, (New York, Springer Verlag, 1965).

Elbaum, M. and J.S. Wettlaufer, Phys. Rev., submitted.

Fujino, K., E. L. Lewis and R.G. Perkin, J. Geophys. Res., **79**, 1792 (1974).

Golubitsky, M. and D. Schaeffer, *Singularities and Groups in Bifurcation Theory, Vol. I* (Springer, New York, 1985)

Gow, A. J., S. A. Arcone, and S. G. McGrew, CRREL Report 87-20, 36 pp., (1987).

Gross, G. W., A. Gutjahr, and K. Caylor, J. Phys. Coll. (Paris), **C1**, 527 (1987).

J.D. Gunton, M. San Miguel and P.S. Sahni, in *Phase Transitions and Critical Phenomena*, C. Domb and J., (Academic, London, 1983), Vol. 8.

Hardy, S. C. and S. R. Coriell, J. Crystal Growth, **20**, 292 (1973).

Harrison, J. D. and W. A. Tiller, J. Appl. Phys., **34** (11), 3349 (1963).

Haug, P., Phys. Rev. A, **35**, 4364, (1987).

Haymet, A. D. J., Science, **236**, 1076 (1987a).

Haymet, A. D. J., Ann. Rev. Phys. Chem., **38**, 89 (1987b).

Herring, C., Phys. Rev., **82**, 87 (1951).

Hill, A., Nature, **348**, 426 (1990).

Hohenberg P. C. and B.I Halperin, Rev. Mod. Phys., **49**, 435 (1977).

Hunt, J.D., and J.P. Chilton, J. Inst. Metals, **92**, 21 (1963).

Huppert, H. E., J. Fluid Mech., **212**, 209 (1990).

Jamieson, D.T., and J.T. Tudhope, Desalination, **8**, 393 (1970).

Karma, A. and P. Pelce', Phys. Rev. A, **41** (12) 6741, (1990).

Kassner, K. and C. Misbah, Phys. Rev. Lett., **66** (4), 445 (1991).

Kessler, D. and H. Levine, Phys. Rev. A., **39** (6), 3041 (1989).

Kurtze, D.A., Phys. Rev. B, **37**, (1), 370 (1988).

Landau, L. D. and E. M. Lifshitz, *Statistical Physics* (Addison-Wesley, Reading Mass., 1969).

Langer, J. S., Rev. Mod. Phys., **52** ,1 (1980).

Langer, J. S., Physica **A140** ,44 (1986).

Langer, J. S., *Chance and Matter* (Lectures on the Theory of Pattern Formation, Les Houches Summer School, 1986), J. Souletie, J. Vannimenus, R. Stora, Eds. (North-Holland, New York, 1987), p. 629-711.

Lofgren, G. and W. F., Weeks, J. Glaciol., **8**, (52), 153 (1969);

Malmgren, F., Scient. Results, Norweg. North Pole Exped. the "Maud" 1918 - 1925, **1**(5), p. 1-67, (1927).

Merchant, G. J. and S. H. Davis, Phys. Rev. Lett., **63** , 573 (1989a).

Merchant, G. J. and S. H. Davis, Phys. Rev. B, **40**, 11,140 (1989b).

Merchant, G. J. and S. H. Davis, Acta Metall., (to appear).

Mourad, P.D., Ph.D. dissertation, University of Washington, 190 pp. (1987).

Mullins, W. W. and R. F. Sekerka, J. Appl. Phys., **34** ,323 (1963).

Mullins, W. W. and R. F. Sekerka, J. Appl. Phys., **35** ,444 (1964).

Nakawo, M. and N. K. Sinha, Atmos.-Ocean, **22** (2), 193 (1984).

Nicolis, G. and I. Prigogine, *Self-Organization in Non-equilibrium Systems,* (Wiley-Interscience, New York, 1977).

Nicolis, G. and I. Prigogine, *Exploring Complexity,* (W.H. Freeman and Co., New York, 1989).

Nittmann, J. and H. E. Stanley, Nature, **321,** 663 (1986).

Nittmann, J. and H. E. Stanley, J. Phys. A: Math. Gen., **20,** L981 (1987a).

Nittmann, J. and H. E. Stanley, J. Phys. A: Math. Gen., **20,** L1185 (1987b).

Oxtoby, D. W., Nature, **347,** 725 (1990).

Poston, T. and I. Stewart, *Catastrophe Theory and its Applications,* (Pitman, Boston, 1978)

Riley, D. S. and S. H. Davis, SIAM J. Appl Math., **50,** 420 (1990).

Rutter, J. W. and B. Chalmers, Can. J. Phys., **31,** 15 (1953).

Saito, Y. and T. Ueta, Phys. Rev. A, **40,** 3408 (1989).

Seidensticker, R. G., in *Crystal Growth* (ed. H.S. Peiser, Oxford University Press, 1967)

Sekerka, R. F., J. Phys. Chem. Solids, **28** ,983 (1967).

Sawada, Y., Physica A**140** ,134 (1986).

Schwerdtfeger, P., J. Glaciol., **4** (36), 789 (1963).

Sivashinsky, G. I., Physica **D8** ,243 (1983).

Stanton, T.K., K.C. Jezek, and A.J. Gow, J. Acoust. Soc. Am., **80,** 1486 (1986)

Swift, J. and P. C. Hohenberg, Phys. Rev. A., **15,** (1), 319 (1977).

Tiller, W. A., K. A. Jackson, J. W. Rutter and B. Chalmers, Acta. Metall., **1**, 428 (1953).

Thorndike, A. S., C. R. Cooley and J. F. Nye, J. Phys. A: Math. Gen., **11**, 1455 (1978).

Turner, J.S., *Buoyancy Effects in Fluids*, (Cambridge University Press, London, 1973).

Voronkov, V. V., Soviet Phys. Solid State, **6**, 2378 (1965).

Wagner, C., J. Electrochem Soc., **103**, 571 (1956).

Warren, J. A. and J. S. Langer, Phys. Rev. A., (to appear).

Weeks, W. F., The structure of sea ice: A progress report. In *Arctic Sea Ice, U.S. National Academy of Sciences - National Research Council, Pub 598.*, 96-98, (1958).

Weeks, W. F., J. Glaciol., **4** (31), 25 (1962).

Weeks, W. F. and G. Lofgren, Physics of Snow and Ice, Vol. 1, Pt 1, edited by H. Oura, pp. 579-597, Inst. of Low Temp. Sci., Hokkaido, Japan, (1967).

Weeks, W. F., and S. F. Ackley, in *Geophysics of Sea Ice*, edited by N. Untersteiner, pp. 395-465, Plenum Press, New York, (1986).

Wettlaufer, J. S., N. Untersteiner, and R. Colony, Ann. Glaciol., **14**, 315 (1990).

Wettlaufer, J. S., J. Geophys. Res., **96**, 7215 (1991).

Wollkind, D. J. and L. A. Segal, Philos. Trans. R. Soc. London, **268**, 351 (1970).

Woodruff, D.P., *The solid-liquid interface*, (Cambridge University Press, 1973).

Worster, M.G., J. Fluid Mech., **167,** 481 (1986).

APPENDIX

NOMENCLATURE, PARAMETERS,
AND VALUES OF THE THERMOPHYSICAL CONSTANTS

Here we record for convenience, the main parameters and values of the thermophysical constants relevant to the H_2O-NaCl system.

V constant velocity of the planar interface in m s^{-1}

$\sigma = \sigma_r + i\,\sigma_i$ the dimensionless complex perturbation growth rate.

a the dimensionless perturbation wavenumber.

$\underline{R}$ a dimensionless wavenumber parameter; $(1/4 + a^2 + \sigma)^{1/2} - 1/2$, where $R = \underline{R}(\sigma = 0)$

Λ the dimensionless wavelength of the perturbation.

λ the dimensional wavelength of the perturbation.

T_m the bulk melting temperature of the pure ice, 273.16 K.

$T^*_L\ (T^*_S)$ dimensional temperature in the liquid (solid) in K.

$T'_L\ (T'_S)$ dimensional temperature in the liquid (solid) measured relative to T_m, e.g., $T'_L = T^*_L - T_m$.

T_L (T_S)	dimensionless temperature in the liquid (solid).

C' dimensional solute concentration in the liquid in parts per thousand; ppt.

C dimensionless solute concentration in the liquid.

n the ratio of the thermal conductivity of the solid s to the liquid l, $\dfrac{k_s}{k_l}$ = 3.572. (see e.g., Jamieson and Tudhope, 1970)

κ_L (κ_S) thermal diffusion coefficient in the liquid (solid) with a value of 1.37×10^{-7} m^2 s^{-1} (1.09×10^{-6} m^2 s^{-1})

c_p heat capacity of ice at constant pressure; 2.05×10^3 J kg^{-1} K^{-1}.

c_{pw} heat capacity of water at constant pressure; 4.22×10^3 J kg^{-1} K^{-1}.

L the latent heat of fusion per unit volume, 3.063×10^8 J m^{-3}.

D the diffusion coefficient of solute in water, 5.546×10^{-10} m^2 s^{-1}.

$D/V, D/V^2$ the length and time scales used for nondimensionalization.

γ the solid-liquid interfacial surface tension, 33.0×10^{-3} J m^{-2}.

k the segregation coefficient which is the ratio of the solute in the solid to that in the liquid. The range is from 0.003 to 0.30, the lowest value is the equilibrium value measured at very low solute concentration by Gross et al. (1987).

m	the slope of the liquidus line on the phase diagram (see Fig. 1.4). $m = -0.0548$ K ppt^{-1} (Fujino et al., 1974).

G'_L dimensional temperature gradient in the liquid, ranging from 3.57 to 3.57 x 10^5 K m^{-1}.

G^* average temperature gradient at the interface; $\dfrac{2\,G'_L + L\ V/k_l}{(1 + n)}$

G_c steady state dimensional solute gradient at the interface; $\dfrac{m\ C_\infty\,(k - 1)\ V}{D\ k}$ ppt m^{-1}.

M the morphological number, a dimensionless control variable; $\dfrac{m\ G_c}{G^*}$. The typical range is from 1 to 100.

Γ the surface energy parameter, a dimensionless control variable; $\dfrac{T_m\ \gamma\,k\ V}{L\ D\ m\ C_\infty\,(k - 1)}$. The typical range is from about 10^{-1} to 3.

δ_l the length scale used by Merchant and Davis (1989b); $(\,\gamma\ T_m\ /\ L\ G_L')^{1/2}$.

δ_t the time scale used by Merchant and Davis (1989b); $\gamma\ T_m\ /\ L\ G_L'\ D$.

$V_{md}{}^2$ the dimensionless control velocity used by Merchant and Davis (1989b); $\dfrac{\gamma\,T_m\ V^2}{L\ G_L'\,D^2}$

$C_{md}{}^2$ the dimensionless solute parameter used by Merchant and Davis (1989b); $\dfrac{m^2\,(k - 1)^2\,L\ C_\infty}{k^2\ G_L'\ \gamma\,T_m}$

$l_{md}{}^2$ the dimensionless latent heat parameter used by Merchant and Davis (1989b);

$$\frac{L^3 D^2}{k_l{}^2 G_L{}' T_m \gamma}$$

μ_L (μ_S)   the chemical potential per mole of the liquid (solid) in J mole^{-1}.

$\tilde{V}$ crystal volume in m^3.

v molar volume of crystal in m^3 mole^{-1}.

κ the average curvature of an interface in m^{-1}.

<div align="center">

Curriculum Vitae

J. S. Wettlaufer

</div>

Education

   May 1985   Bachelor of Science, Honors (Sigma Pi Sigma): Physics
                       University of Puget Sound, Tacoma, WA

   August 1991   Ph.D., Geophysics, University of Washington, Seattle, WA

Relevant Work Experience

   9/1987-present   APL Research Fellow, Polar Science Center
                           Applied Physics Laboratory, University of Washington, Seattle, WA

   1/1990 - 4/1990   Visiting Scientist, Norsk Polarinstututt,
                           Oslo, Norway

   9/1986 - 9/1987   Research Assistant, Geophysics Program,
                           University of Washington, Seattle, WA

Professional Activities

American Physical Society; Divisions of Chemical Physics and Fluid Dynamics
International Physics Group
American Geophysical Union

Publications

J. S. Wettlaufer, Heat Flux at the Ice - Ocean Interface, *J. Geophys. Res.*, **96**, 7215 - 7236, 1991.

A. Omstedt and J. S. Wettlaufer, Ice Growth and Oceanic Heat Flux: Models and Measurements, submitted, *J. Geophys. Res.*, 1991.

M. Elbaum and J. S. Wettlaufer, A Conjecture on the Growth Shapes of Crystals, submitted, *Phys. Rev. A*, 1991.

J. S. Wettlaufer, N. Untersteiner and R. Colony, Estimating oceanic heat flux from sea ice thickness and tempertature data, *Ann. Glaciol.* **14**, 315 - 318, 1990.

J. S. Wettlaufer, The Ice - Ocean Interface and the Variability in Oceanic Heat Flux, *Eos Trans.*, **71**, No. 2, p. 129, 1990.

J. S. Wettlaufer, Stability Analysis of the Directional Solidification of a Novel Aqueous Solution, *Eos Trans.*, **71**, No. 41, p.1144, 1990.

J. S. Wettlaufer and N. Untersteiner, Ice Thickness and Vertical Heat Flux in the Arctic Ocean, *International Conference on the Role of the Polar Regions in Global Change*, abstract, p.91, 1990.

R. S. Pritchard et al., CEAREX Drift Experiment, *Eos Trans.*, **71**, No. 40, p.1115-1118, 1990.

J. S. Wettlaufer, R. Colony and N. Untersteiner, Measurement of the Thermal Regimes in Perrenial Sea Ice, In *OCEANS 89, Proceedings of the 1989 IEEE International Conference for understanding the Global Ocean.* **4**, 1282 - 1286, 1989.

J. S. Wettlaufer, Sea Ice Thermodynamics in the Eastern Arctic, *Eos Trans.*, **70**, No 15, p. 371, 1989.

Personal

Born in the District of Columbia on 23 October, 1963. There was some early morning fog, but it cleared to expose sunny skies that afternoon; typical of D.C. during the fall.